CHEMICAL AND BIOMOLECULAR ENGINEERING

MATRIX MECHANICAL PROPERTIES AND THE INVASIVE POTENTIAL OF METASTATIC CANCER

NAZANIN SABINE RUPPENDER

Dissertation under the direction of Professor Scott Guelcher

Recent studies suggest that cancer cells undergo genotypic and phenotypic changes in response to the rigidity of the extracellular matrix (ECM). These studies have focused largely on non-mineralized tissues in the kPa range (corresponding to soft tissue), while many tissues important in the progression of cancer, such as mineralized bone ($O(10^9$ Pa)) and the basement membrane ($O(10^6$ Pa)), far exceed those values. In this work, we employed the use of *in vitro* culture systems spanning the entire range of tissue elasticity (10^3-10^9 Pa) to study the invasive potential of breast cancer. Here, we demonstrate that cancer cells can sense a wide range of rigidities, and show increased ECM degradation by invadopodia in response to rigidity. Furthermore, we show that the rigidity of bone, a preferential target for breast cancer, specifically induces changes in parathyroid hormone related protein (PTHrP) and its transcription factor Gli2 in the cancer cell to facilitate degradation and invasion of the bone matrix. We find that these genotypic changes are mediated by mechanotransduction, as bone-like matrix rigidity induced clustering of β_3 integrin and TGF-β receptor type II (TGF-βRII) to stimulate expression of PTHrP and Gli2 through Src, Rho-kinase (ROCK) and mitogen activated protein kinase (MAPK). These observations demonstrate the need for physiologically relevant *in vitro* culture systems and suggest a role for the differential rigidity of the mineralized bone microenvironment in early stages of tumor-induced osteolysis. These findings could lead to new clinical targets for the treatment of bone metastases, a major contributor in the lethality of metastatic cancer, for which no effective therapies exist to date.

Approved: Scott Guelcher Date: March 25th, 2011

MATRIX MECHANICAL PROPERTIES AND THE INVASIVE POTENTIAL OF METASTATIC CANCER

By

Nazanin Sabine Ruppender

Dissertation

Submitted to the Faculty of the

Graduate School of Vanderbilt University

in partial fulfillment of the requirements for the degree of

DOCTOR OF PHILOSOPHY

in

Chemical Engineering

Nashville, Tennessee

May, 2011

Approved:	Date:
Scott Guelcher	March 25th, 2011
Clare McCabe	March 25th, 2011
Jeffry Nyman	March 25th, 2011
Kane Jennings	March 25th, 2011

To my father. Thank you Papa, for everything.

ACKNOWLEDGEMENTS

This work was supported by the National Institutes of Health Breast Cancer SPORE (P50 CA098131), P01 CA040035, Tumor Microenvironment Network (TMEN) (U54 CA126505), 1R01GM075126 to AMW, U54CA113007 (PI, Quaranta), a pilot project on 2 P50 CA098131-06 (Arteaga) to SAG, and 1K25CA143412 to AP.

Thanks go to my wonderful husband Matt: I love you, you are my support, my best friend and a sea of calm in the most stressful of situations. I don't know where I'd be without you. Lastly, these studies would not have been possible without the pioneering mind and tireless support of Dr. Gregory Mundy. He always operated with the careers and education of his students in mind and advocated on my behalf when others did not. Thank you for all that you did, Greg. The world misses you.

LIST OF TABLES

LIST OF FIGURES

LIST OF ABBREVIATIONS

ADH – atypical ductal hyperplasia

BM – basement membrane

cDNA – complementary DNA

CTGF – connective tissue growth factor

DCIS – ductal carcinoma *in situ*

DMEM – dulbecco's modification of eagle's medium

E – Young's Modulus

ECM – extracellular matrix

EM – electron microscopy

FAK – focal adhesion kinase

FITC – fluorescin isothiocyanate

Fn – fibronectin

G – Shear Modulus

GFP – green fluorescent protein

Hh – hedgehog

HRP – horseradish peroxidase

IDC – invasive ductal carcinoma

IF – immunofluorescence

IGF-1 – insulin like growth factor 1

IHC – immunohistochemistry

IL – interleukin

IRMA – immunoradiometric assay

LDI- lysine diisocyanate

M-CSF – macrophage colony stimulating factor

MAPK – mitogen-activated protein kinase

MAT – mesenchymal to amoeboid transition

MDA-KDΔ4 - MDA-MB-231 cells expressing a dominant negative form of ROCK

MDA-TβRIIDcyt - MDA-MB-231 cells expressing a dominant negative form of the TGF-β Type II receptor

MDA-Δ4 – MDA-MB-231 cells expressing a constituently active form of ROCK

MLC – myosin light chain

MLCK – myosin light chain kinase

MMP – matrix metalloproteinase

MPI -- metalloproteinase inhibitor

mPP – myosin phosphatase

mRNA – messenger RNA

MSC – mesenchymal stem cell

OPG – osteoprotegerin

OPN- osteopontin

PAA – polyacrylamide

PTHrP – parathyroid hormone related protein

PUR – polyurethane

qPCR – quantitative real time PCR

QPP – quasiprepolymer

RANKL – receptor activator of nuclear factor kappa-B ligand

RGD - Arg-Gly-Asn peptide sequence

ROCK – rho-kinase

RT-PCR – see qPCR

SCP – single cell populations

SDF-1 – stromal derived factor 1

TCPS – tissue culture polystyrene

TGFβ - transforming growth factor beta

UBM – urinary bladder matrix

ρ - density

TABLE OF CONTENTS

CHAPTER I

INTRODUCTION

Breast Cancer Biology: Molecular Mechanisms of Invasion at the Primary Site

Breast cancer is by far the most common cancer among women, with 1.3 million women diagnosed worldwide annually [1]. Every year, approximately one third of these patients will die from breast cancer. The pathology of breast cancer is heterogeneous as it forms in both the mammary ducts or lobules, and as such, multiple pathways of invasion have been suggested [2]. Nearly 80% of all breast cancer diagnoses are ductal, and the suggested path of carcinogenesis has been through atypical ductal hyperplasia (ADH), followed by ductal carcinoma *in situ* (DCIS) resulting in invasive ductal carcinoma (IDC) and ultimately metastatic disease [3]. As the name suggest, DCIS is confined to the duct. Thus, development of IDC requires that cancer cells extravasate the ductal epithelial basement membrane to invade the surrounding tissue. Subsequently, cells are able to enter the vasculature and lymphatic system to metastasize to distant sites, which often ultimately results in patient fatality. Therefore, it becomes paramount to fully understand mechanisms of invasion and metastasis if science is to develop more effective cancer therapies that result in better patient prognosis.

The progression of breast cancer, beginning with the formation of ADH and its associated transformations, arises through multiple changes in gene expression that are both complex and varied and have been identified to have causal roles in

both initiation and progression of pathology [2]. While many studies have identified genes important in the transition from DCIS to ICS, there has been little overlap between these studies and as such, it has been difficult to identify a consensus genetic signature involved in the development of invasive ductal carcinoma [4-8]. Nevertheless, some of the most dramatic gene expression changes observed have been in genes directly involved in cell motility [9], suggesting that the mechanisms by which cells locomote and generate cytoskeletal tension play an important role in the progression of cancer.

Cell locomotion along a 2-dimensional surface (along the x-y plane) and invasion into a tissue (into the z-plane) involve various kinases, proteinases and intracellular signaling molecules. Single cell mesenchymal movement along a 2-dimensional surface is a four-step process, involving the formation of filopodia and lamellopodia protrusions in response to activation of Rho-family GTPases [10-12]. Subsequently, the cell forms focal adhesions with the extracellular matrix (ECM) via clusters of specialized transmembrane proteins (integrins) that bind to the ECM. This then stabilizes the cell-matrix interaction by means of a network of highly ordered F-actin filaments known as stress fibers. These fibers are linked to the motor regulatory protein non-muslce myosin II, whose regulatory light chain is phosphorylated to generate cytoskeletal tension and contract in the direction of movement and ultimately disassemble the F-actin linked focal adhesions at the rear of the cell, moving the cell forward [10-12].

In vivo, however, the cell must invade into a tissue (not merely along a surface), which requires the use of proteases to degrade the extracellular matrix. To

facilitate downward invasion of the ECM, cells recruit proteases to focal adhesions at particular actin-rich subcellular protrusions on the ventral surface of the cell known as invadopodia [13]. Various integrins have been identified in invadopodia, including $\alpha_3\beta_1$, $\alpha_5\beta_1$ and $\alpha_v\beta_3$ [14, 15]. Invadopodia secrete various matrix metalloproteinases (MMPs), including MT1-MMP, MMP2 and MMP9, as well as other proteases such as members of the ADAM family [16, 17] to break down matrix molecules like collagen, fibronectin and laminin. Co-localization of proteases and integrins is required in many instances for successful matrix deradation; MMP2 activation by MT1-MMP requires association with $\alpha_v\beta_3$ integrin [15], and MT1-MMP has also been shown to necessarily co-localize with various other proteases to degrade the ECM [13], demonstrating that adhesion and invasion mechanisms are closely linked.

In addition to secreted and membrane bound proteins, a number of intracellular molecules are also important in invadopodia function and formation and thus, ECM invasion. Src, a non-receptor kinase and its associated tyrosine kinases are known to promote cell invasion and invadopodia formation through adhesion regulation and signaling activity downstream of growth factors and integrin binding [18]. Specifically, Src is thought to promote actin assembly at adhesion sites[13]. Similarly, a number of small GTPases serve to direct cytoskeletal reorganization and thus, formation of invadopodia [10, 19, 20]. As previously mentioned, invadopodia require the use of MMPs to degrade the surrounding matrix, yet broad spectrum inhibition of MMPs does not abrogate cancer cell invasion [21], suggesting an alternative, non-mesemchymal invasion mechanism.

Tumor cells have been shown to utilize amoeboid movement to invade surrounding tissues, independent of protease degradation, by means of Rho/ROCK signaling [22, 23]. This type of movement has been shown to be especially important in conditions where proteolysis is inhibited [24, 25]. Thus, this mesenchymal to amoeboid transition (MAT) and its associated Rho-mediated signaling are of particular importance in mineralized tissues, where proteases cannot degrade the surrounding matrix.

Taken together, these findings all indicate that cell contractility, locomotion and adhesion play a critical role in the progression of cancer.

Bone Biology: Tumor invasion of mineralized tissues

Once breast cancer transitions to IDC and extravasates from the primary site, it enters either the circulatory or lymphatic system to metastasize to distant sites. While breast cancer is known to metastasize to both the lung and liver, it has a particular predilection for metastasizing to bone; over 70% of patients suffering from advanced breast cancer present with osteolytic bone metastases [26]. Patients with osteolytic metastases have a number of cancer-associated bone pathologies, including chronic pain, pathologic fracture and hypercalcemia [26]. Most importantly, the presence of bone metastases in breast cancer patients is associated with poor prognosis, reducing survival rate to approximately 27% as compared to 96% for patients with only primary tumors [1]. Nevertheless, the current standard of care focuses mainly on the treatment of cancer associated bone pathologies once tumor has already been established, rather than the prevention of metastases

formation. Bisphosphonates are commonly prescribed to slow cancer-induced osteolysis, but do little to eradicate the cancer itself. As such, bisphosphonate treatment is usually accompanied by either chemotherapy or radiation, which carry with it vast off-target cytotoxic effects and questionable efficacy in bone [27]. Thus, it is vital to understand the mechanisms by which cancer homes to and invades the bone for the development of effective metastasis therapies.

Bone comprises the majority of the body's connective tissue and is unique in the sense that it is mineralized (and thus, very rigid) and continuously regenerated throughout life as a result of bone turnover [28]. Mineral content accounts for approximately 50-70% of adult bone, providing mechanical strength and rigidity (E $O(10^9$ Pa))[28]. Bone is a complex tissue, serving many more functions beyond its apparent structural support for the body and protection of vital organs. The bone marrow serves to produce both red and white blood cells and store fat cells, while the bone matrix is the body's mineral reserve. The bone matrix is also a vast reserve of growth factors, serves to balance blood pH and is the body's largest endocrine organ, regulating phosphate and glucose metabolism [29]. Furthermore, bone contains a variety of different matrix proteins. In addition to type I collagen, and a number of other various protein types, the bone matrix has a significant concentration of glycoproteins with cell attachment activity [13, 28]. These proteins are required for cells to interact with the matrix and perform specific cell functions such as migration, proliferation and differentiation through specific cell surface receptors (integrins) resulting in transduced intracellular signals [28]. Many of these attachment proteins contain the RGD (Arg-Gly-Asn) binding sequence, such as

fibronectin, and the expression patterns for both the RGD proteins and associated integrins are variable, suggesting cell-matrix interactions may play a role in cell fate and maturation [28].

Bone is generated by mononucleoid cells (osteoblasts) responsible for formation of non-mineralized osteoid [30]. Bone formation by osteoblasts can be divided into four main stages (1) proliferation of the pre-osteoblasts, (2) osteoblast maturation and matrix secretion (3) post-translational modifications and (4) mineralization of the matrix. Stages (1) and (2) are driven by the release of growth factors facilitated by the resorption of the bone matrix by osteoclasts [31].

Osteoclasts are a member of the monocyte/macrophage family, and the sole cell type that can resorb the mineralized bone matrix. They require two main cytokines to differentiate, one being RANKL and the other being macrophage colony-stimulating factor (M-CSF) [32, 33]. Osteoclast efficacy depends largely on the cell's ability to form an acidified microenvironment between the cell's ruffled border and the bone matrix [34], thus bone resorption clearly depends on a physical intimacy between the osteoclast and the bone matrix. As previously mentioned, integrins play a vital role in anchoring cells to the extracellular matrix, and integrin signaling has been shown to be important in osteoclast function. Integrin $\alpha_v\beta_3$ expression is absent in osteoclast precursors, but markedly upregulated upon differentiation by RANK-L [35]. Furthermore, mice that lack expression of the β_3 integrin subunit develop a progressive increase in bone mass due to osteoclast dysfunction [36], suggesting that integrin activity, in particular that of $\alpha_v\beta_3$, is vital to normal bone metabolism. Since osteoclasts are stimulated by the release of

RANKL by osteoblasts, and osteoblasts are stimulated by growth factors released from the bone matrix [31], mechanisms of bone formation and resorption are highly coupled. Numerous pathologies, including cancer, disturb this delicate balance.

Once cancer cells have entered the blood stream, they must first home to the bone and subsequently establish themselves and proliferate in bone. Numerous factors contribute to both these processes, involving both the nature of the bone matrix and behavior of the cancer cell.

While several tumor-derived molecules such as E-cadherin and osteopontin have been identified in the development of bone metastases, it is those of chemokine origin that have consistently been identified as major players in cancer cell homing to bone. The chemokine receptor CXCR4 is upregulated in bone metastatic cancers [37], and its ligand, CXCL12/SDF-1 is readily found in the bone marrow. Both neutralizing antibodies to and genetic silencing of CXCR4 have been shown to reduce both breast and prostate tumor metastasis [38, 39]. Likewise, $\alpha_v\beta_3$ integrin, which binds the RGD sequence in various bone matrix proteins such as osteopontin, fibronectin and vitronectin, is likely implicated in the homing and invasion of the endosteum [40]. In fact, inhibition of $\alpha_v\beta_3$ reduced the presence of bone lesions in several animal models of breast cancer metastasis [41, 42]. In addition to matrix degradation in the primary site, MMPs have also been shown to be of importance in bone metastases. MMP secretion and expression is increased in bone metastatic breast cancer [37, 43], and high levels of MMPs correlate with poor patient outcome [44]. In bone, MMPs have been shown to cleave various tethered signaling molecules such as insulin-like growth factor 1 (IGF1), E-cadherin,

fibroblast growth factor (FGF), pro-TGF-β, and RANK-L [45-47]. Taken together, these data suggest that cancer metastasis to bone is a complex process involving numerous proteins, such as chemokines, integrins, proteinases and growth factors.

Once cancer cells become established in the bone microenvironment, they begin local invasion of the bone matrix. To do so, breast cancer cells disrupt balance of bone formation and resorption by secreting parathyroid hormone related protein (PTHrP) to recruit osteoclasts. In addition to its role in osteoclast recruitment, PTHrP is expressed in most tissues in the body during either development or adult life, where its function can be classified into of three categories. It is thought to regulate transepithelial calcium transport in the distal nephron, mammary epithelium and placenta. PTHrP also plays a role in growth, differentiation and development in the skin, hair follicles, mammary gland and growth plate [48]. Furthermore, PTHrP acts as a smooth muscle relaxant in the uterus, urinary bladder, stomach, ileum and mammary gland [48-50], where its expression is stimulated by mechanical stimulation suggesting a mechanoresponsive element in the regulation of PTHrP. In breast cancer, PTHrP is a major regulator in the development and establishment of osteolytic metastases. It is differentially expressed by tumor cells at sites of bone metastases and elevated in patients suffering from bone metastatic disease [51, 52]. PTHrP secreted by tumor cells stimulates expression of RANKL and inhibits expression of osteoprotegerin (OPG) by osteoblasts and stromal cells, respectively. This in turn stimulates osteoclastogenesis via the receptor RANK on osteoclast precursors [53], allowing tumor cells to invade the mineralized matrix. In fact, use of PTHrP neutralizing

antibody reduced the number and size of osteolytic lesions, as well as number of osteoclasts at the tumor-bone interface in a murine model of breast cancer metastasis [26]. Conversely, overexpression of PTHrP led to an increase in osteolytic metastases [54]. Similarly, metastatic breast cancer cell lines that do not express PTHrP do not form osteolytic lesions, but can be induced to do so by genetic alteration to express PTHrP [55]. It follows then that understanding the mechanism behind the initiation of PTHrP expression is vital to the development of effective therapies to prevent osteolytic metastases.

In addition to tumor cells changing and exploiting mechanisms of bone formation and resorption, bone itself is host to a plethora of cytokines and growth factors released from the bone matrix during remodeling that stimulate cancer growth. The most prominent of these growth factors is host-derived TGF-β, which furthers growth of the tumor through the production of osteolytic factors. Specifically, TGF-β is known to stimulate production of PTHrP by the tumor and blocking TGF-β signaling prevents both secretion of PTHrP by breast cancer cells and osteolytic metastases in a murine model of breast cancer [56]. The mechanism by which TGF-β promotes osteoclastogenesis is cell- and context-specific, acting through both Smad and p38 mitogen activated protein kinase (MAPK) [57] to stimulate not only PTHrP but also other osteolytic and prometastatic factors such as interleukin 11 (IL11) and connective tissue growth factor (CTGF) [37]. Thus, it is important to consider the effects of TGF-β when examining mechanisms of tumor establishment in bone and developing associated effective therapies.

Breast cancer cells interact with three vital components of the bone microenvironment: bone-forming osteoblasts, bone-resorbing osteoclasts and the growth factor-rich bone matrix. Tumor cells secrete factors that inhibit osteoblasts and stimulate osteoclasts, either directly or indirectly, and are in turn stimulated by growth factors released from the bone matrix to continue secreting osteoclastogenic factors. As such, the presence of osteolytic breast metastases presents a unique and complex problem requiring complete understanding of the interactions between cancer cells and their environment to develop effective therapies.

Mechanotransduction and Biophysics

Cells can interact with their environment both biochemically and physically, with the latter being heavily influenced by the mechanical properties of the cell's surroundings. The elastic modulus of the extracellular matrix has been shown to influence numerous cellular outcomes, including cancer cell invasiveness, development of malignant phenotypes and stem cell differentiation [58-61]. Within the body, there exist several orders of magnitude differences in tissue elasticity, ranging from elastic moduli of $O(10^3$ Pa) (e.g. brain matter, adipose tissue, healthy breast tissue) to $O(10^9$ Pa) (e.g. mineralized bone)[61-63] (Table 1.1).

Table 1.1. Elastic Moduli of various Tissues

Tissue Type	**Elastic Modulus (Pa)**
Brain	$10^2 - 10^4$
Lung	4×10^2
Breast	8×10^2

Muscle	$0.12 – 1.0 \times 10^5$
Fat	2×10^4
Artery	$0.1 – 3.8 \times 10^6$
Areolar connective tissue	$0.6 – 1.0 \times 10^5$
Smooth muscle	5×10^6
Bone	$17.1 – 28.9 \times 10^9$

Cells sense the rigidity of their surroundings through integrin clusters known as focal adhesions, which also serve as the cell's anchorage to the surrounding matrix [64]. Integrins also function to transmit forces generated by cells through interaction between the actin cytoskeleton and myosin II to the ECM [65]. Formation of focal adhesions requires the presence of a solid substratum, and is regulated by the GTP-binding protein Rho and its associated kinase, ROCK [66]. Rho then induces cell contractility, which in turn stimulates actin fiber assembly and aggregation of integrin clusters to activate focal adhesion kinase and initiate signaling [66]. The primary regulator of cell contractility is the phosphorylation of the light chain of myosin II (MLC) at Ser-19 and Thr-18 by myosin light chain kinase (MLCK), with the serine residue being the main phosphorylation site and the threonine residue phosphorylating at a slower rate under conditions of maximum stimulation [67, 68]. Rho serves to further enhance contractility via Rho-kinase (ROCK) by inhibiting dephosphorylation of MLC by myosin phosphatase (mPP) [69].

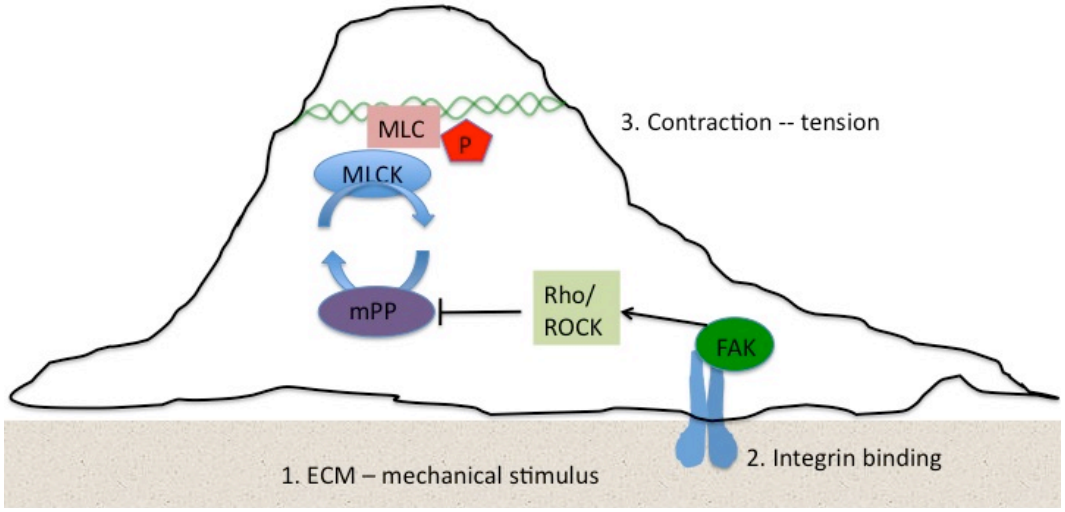

Figure 1.1. Generation of cytoskeletal tension in response to mechanical stimuli. The cell binds to the solid substrate and begins actin assembly and formation of integrin clusters (focal adhesions). This activates focal adhesion kinase (FAK) to initiate intracellular signaling to induce phosphorylation of myosin light chain (MLC) via myosin light chain kinase (MLCK) and Rho-kinase (ROCK). MLC is anchored to the actin cytoskeleton and contracts, resulting in contraction of the cell and generation of forces on the ECM via focal adhesions.

In addition to sensing the mechanical properties of their surroundings, integrins control a number of intracellular signaling pathways, suggesting that the physical forces they transmit are translated into downstream biochemical signals. In other words, since integrins serve to both transduce forces and sense the nature of the surrounding ECM, the rigidity of this ECM likely has an impact on integrin activity and signaling. Numerous cell types have been shown to exhibit increased cytoskeletal tension in response to increased substrate rigidity, including stem cells, neurons, epithelial cells and cancer cells [58-61, 70]. In general, increased substrate rigidity results in increased focal adhesion number and cell locomotion; and inhibition of myosin, which prevents the generation of contractile forces within the cell, abrogates these effects [60]. Specifically, naïve mesenchymal stem cells (MSCs) have been shown to differentiate into neuronal, myogenic and osteogenic lineages in the absence of exogenous growth factors when cultured on substrates that

approximated the mechanical properties of brain, muscle and non-mineralized osteum [61]. This differentiation was shown to be dependent on the cell's ability to generate tension, as treatment with Blebbistatin, a small molecule inhibitor that prevents the binding of myosin to the actin cytoskeleton, prevented the differentiation of MSCs on rigid substrates, demonstrating that the cell's ability to generate tension is required for rigidity effects on cell fate.

The mechanosensitivity of cancer cells in soft tissue has also been well established. With respect to breast cancer, it is well known that lysyl oxidase crosslinking of the breast ECM leads to stiffening of the matrix, and thus elevated Rho-dependent cytoskeletal tension and adhesion (a process known as mechanoreciprocity) [58, 59]. Furthermore, matrix stiffening has been shown to disrupt normal epithelial morphogenesis and promote a malignant phenotype through Rho-contractility and focal adhesion clustering [59]. Similarly, it has been demonstrated that matrix rigidity directly increases number and activity of invadopodia in Ca1d cells[71], further supporting the notion that matrix rigidity enhances breast cancer invasion and aggression. These studies demonstrate that the ECM stiffening in the breast associated with cancer plays a significant role in influencing the invasiveness of tumor cells.

However, the mechanoreciprocity that tumor cells experience in the primary site is different from conditions at the bone metastatic site. Not only is bone rigidity much higher than that of cancer-influenced breast tissue, but due to its mineral content, bone is at least six orders of magnitude more rigid than soft tissue independent of any ECM crosslinking induced by cancer. This would suggest that

there may be a constituently activated contractility state in cancer cells resident in the bone, and that therapies targeting mechanotransduction pathways could potentially be effective in preventing the establishment of bone metastases. Indeed, various antagonists to mechanostransduction effectors have shown promise as clinical therapies for the prevention of bone metastases. Rosenblatt, Liu and colleagues have recently demonstrated that the use of Y27632, a small molecule antagonist of ROCK, reduced tumor burden and incidence in a mouse model of breast cancer metastasis by 77% and 33%, respectively [72]. Similarly, inhibition of $\alpha_v\beta_3$ integrin or SFKs, which are both implicated in mechanotransduction and the generation of cytoskeletal tension, have been shown to reduce bone loss and skeletal metastases *in vivo* [42, 73], suggesting that mechanotransduction pathways are an important clinical target for the prevention of bone metastases.

Lastly, PTHrP, which plays a major role in driving tumor associated bone destruction, has been shown to be mechanoresponsive in smooth muscle cells, where it is implicated in cell contraction [49, 50]. Mechanical distention of the rat urinary bladder and abdominal aorta both *in vivo* and *in vitro* induced up to 4-fold increases in PTHrP mRNA expression [49, 50], further supporting the notion that matrix rigidity, which induces cytoskeletal tension, could influence PTHrP mRNA expression. Considering the vast increase in elastic modulus of bone as compared to soft tissue (10^6 increase or greater) and the established mechanosensitivity of cancer cells, it is likely that a mechanotransduction response to the rigidity of the bone microenvironment plays a role in PTHrP induced bone destruction.

Biomaterials for the Study of Mechanically Transduced Signaling

It is important to note at this point that the aforementioned studies on matrix rigidity and cell interaction all utilized hydrogel substrates with elastic moduli in the kPa range, while many tissues in the body far exceed those values, with the basement membrane being in the MPa range [74] and mineralized bone, the preferential target for breast cancer, being in the GPa range [75]. In fact, some studies have assumed that cells cultured on substrates exceeding 100 kPa are in a state of isometric contraction, and can thus do not generate differential responses to substrates in the MPa to GPa range[76]. In this work we present evidence that cells, in particular cancer cells, can sense and respond to rigidities spanning the entire spectrum of human tissue, from E $O(10^3$ Pa) to E $O(10^9$ Pa).

The challenge in studying cell response to the entire range of human tissue rigidity is twofold: (1) Traditional *in vitro* studies are normally performed in 2D monolayer culture, whereas most cells *in vivo* grow in a 3D network within the ECM, and (2) it requires, as of now, the use of a variety of mechanically tunable biocompatible substrates with equivalent surface chemistries as to minimize artifact effects. Soft tissues (E<100kPa) are best simulated by the use of hydrogel substrates, which can be biological or synthetic in nature, including type I collagen, gelatin and polyacrylamide hydrogels. Most cells adhere to the surface and proliferate readily when embedded in collagen or gelatin, but tuning the rigidity of these materials requires varying the concentration of gelatin or collagen, which would alter the ligand concentration for cell binding and could produce off-target effects. Polyacrylamide (PAA) gels can be tuned independently of ligand

concentration but require functionalization with a matrix protein via an acrylate linker to facilitate cell adhesion [60]. Additionally, PAA gels require the use of catalysts that are toxic when not bound in a polymer network, thereby rendering unsuitable for embedding cells within the 3D matrix (PAA gels are more suitable for 2-dimensional culture). Mimicking more rigid tissues requires the use of non-hydrogel materials. Biocompatible polyester polyurethanes (PUR), formed by reacting an isocyanate component with a polyalcohol, can be produced with moduli ranging from MPa to GPa by melt- or solvent-casting directly into the wells of a tissue culture plate [77] to form a 2D film for *in vitro* cell culture. The ability of PUR materials to support cell attachment and growth *in vivo* and *in vitro* is well documented [78-83], although some cell types require matrix proteins for attachment, which adsorb readily to PUR materials [77]. In such cases, it is vital that the surface concentration of these proteins is controlled and equal on all materials used to study matrix rigidity effects, since the presence of matrix proteins such as fibronectin can influence cell behavior.

While 2D *in vitro* culture is a valuable tool in beginning to understand cell behavior, cells grow within a 3D matrix in most physiological conditions. Thus, in addition to materials with suitable rigidity properties, the study of matrix rigidity effects on mechanotransduction requires materials that also mimic the structure and architecture of the ECM *in vitro*. Traditionally, *in vitro* studies are performed using a monolayer of cells grown on tissue culture polystyrene (TCPS, E~2GPa). However, the 3D ECM cells encounter *in vivo* can range in modulus from kPa to GPa [84]. Not surprisingly, cells have been shown to exhibit different behaviors when

cultured in 2D or 3D matrices. Polarity, morphology, and migration of both fibroblast and epithelial cells differ when grown in 2D and 3D culture [85-87]. This is especially important in cancer, as loss of epithelial cell polarity is associated with carcinogenesis and a disorganized cellular architecture is a hallmark of solid tumors [88, 89]. Normal epithelial cells grown in traditional monolayer culture are highly plastic and exhibit many characteristics displayed by tumor cells in vivo [90, 91], but differentiate normally when cultured within a 3D matrix [92, 93]. Taken together, these data illustrate the need for physiologically accurate and relevant synthetic biomaterials for *in vitro* study of cell behavior.

While previous studies involving 3D *in vitro* culture utilized cells embedded in hydrogels [86, 87, 94], these matrices are not physiologically relevant for mineralized tissues like bone, which is six orders of magnitude more rigid. PUR materials, in addition to being cast into 2D films by two-component liquid reactive molding, can also be synthesized as 3D scaffolds with interconnected pores to support cell growth *in vitro* and *in vivo* [79, 83, 95, 96]. Addition of water, a castor oil stabilizer and calcium stearate pore opener to the isocyanate/polyol mixture results in gas foaming of the polyurethane scaffold, yielding high porosity, pore interconnectivity and an environment favorable for cell ingrowth [95, 97]. As an alternative to gas foaming, incorporation of a leachable porogen, such as a salt or paraffin microbead, can also produce a 3D interconnected pore structure suitable for both *in vitro* study and *in vivo* implantation [98]. Using these methods, biocompatible polyurethane 3D materials can be tuned with elastic moduli ranging

from 10^6 – 10^9 Pa, and present a viable model for more rigid tissues, such as the basement membrane or trabecular bone.

At this point, it becomes important to define what mechanical properties cells actually "sense" in order to appropriately measure the mechanical properties of synthetic materials used *in vitro*. Tensile testing is a simple, yet powerful technique for assessing the bulk modulus of non-porous materials. Since most synthetic materials are isotropic and homogeneous, the physical orientation of the material during mechanical testing does not affect the reading. Biological tissues, such as bone or the basement membrane, are highly anisotropic and as such need to be oriented during testing in a way that is consistent with use and analysis. It is important to note that biological tissues also exhibit a toe region prior to the linear portion of the stress-strain curve, where deformation of the tissue is high and force is low. Nevertheless, the slope of the linear portion of the stress-strain curve (Young's Modulus, E), is a good measure of rigidity for a solid (non-porous) material. While most tissues as well as the synthetic materials used in cell culture exhibit viscoelastic behavior[99], the deformations that result from cell spreading and locomotion are small (<100 nm)[63], and can thus be assumed to be purely elastic. Furthermore, since most synthetic materials used for cell culture are isotropic, the Young's Modulus (E), or tensile modulus obtained from static force displacement testing is an appropriate parameter in defining the mechanical properties of these materials. Young's modulus is given by

$$E = \frac{\sigma}{\varepsilon}, \qquad (1.1)$$

where σ is defined as the tensile stress and ε is defined as the tensile strain. In order for Young's modulus to be an applicable measure of material stiffness, the polymer network must undergo affine deformation; that is, any macroscopic deformation resulting from an externally applied force must be translated uniformly to the microscopic level. Theories of rubber elasticity are derived under this assumption [100], as such theoretically calculated values for an affine polymeric material should agree with measured values. A theoretical elastic modulus value can then be calculated from a swelling experiment using rubber elasticity concepts and the Flory-Rehner equation [100]:

$$-[\ln(1-\nu_2)+\nu_2+\chi_1\nu_2^2] = V_1 n\left[\nu_2^{\frac{1}{3}} - \frac{\nu_2}{2}\right], \qquad (1.2)$$

where ν_2 is defined as the volume fraction of polymer in the swollen mass, V_1 is the molar volume of the solvent, χ_1 is the Flory Chi parameter for interaction between the polymer and solvent, and n is a function of the molecular weight between crosslinks. The elastic modulus, E, is then defined as

$$E = 3nRT \qquad (1.3)$$

[100], where R is the universal gas constant and T is the temperature.

It is also important to consider network mesh size when defining the physical properties of a cell culture material to ensure that the macromechanical properties measured during tensile testing are an appropriate estimate of the cell environment. In other words, if mesh size is significantly smaller than cell size, it is reasonable to assume that the cell is deforming the network and not its individual fibers. The mesh size of a polymer network, x_i, can be calculated if the molecular weight

between cross-links, M_c is known. M_c can be calculated from swelling data and the Flory Rehner equation using [100]

$$M_c = \frac{\rho}{n}. \tag{1.4}$$

Mesh size is then given by [100]

$$x_i = 2.24\left(\nu_2^{-\frac{1}{3}}\sqrt{\frac{2M_c}{M_r}}\right), \tag{1.5}$$

where all other variables are defined as above and M_r is the molecular weight of the polymer repeat unit.

While tensile testing is a valuable tool in determining the modulus of cell culture materials, the length scale of the cell has led some researchers to argue that nanoindentation may be a more appropriate technique for measuring the micromechanical properties of materials that the cell interacts with [101]. Indentation techniques are primarily a test of hardness, with hardness (H) being defined as the ratio of load (P) to the indentation area (A). Since indenter geometry is known, nanoindentation yields a load-displacement curve, where the slope of the unloading phase is defined as the stiffness, S, of the material from which Young's modulus can be calculated. Indentation techniques thus provide an alternative way of measuring the mechanical properties of the cell microenvironment, especially in cases where the cell resides within a 3D matrix, and the properties of the whole scaffold or tissue may differ from that of the bulk material. While a modulus value is sufficient for characterizing the linear elastic behavior of a non-porous material, characterizing porous scaffolds is somewhat more complex, as the mechanical properties of the scaffold differ from those of the bulk polymer it is made of. Since

scaffold pores *in vitro* are not collapsed, contributions of pore extension and compression are negligible [102]. Additionally, cell culture media is aqueous and, as such, has a low viscosity, making shear contributions of fluid flow negligible. Lastly, if the material is isotropic, it can be assumed that all pores deform and fail by the same mechanism, omitting any contributions to mechanical properties from specific pore geometry. Thus, porous *in vitro* scaffolds can be modeled as an array or cubic pores with length l [103]. Young's modulus of the scaffold can then be calculated from the linear-elastic deflection of the pore wall of length l under a force F at its midpoint. This results in a deflection, δ, proportional to the Young's modulus for the (nonporous) material of the pore wall, E_s. Using standard beam theory [104], E_s can then be related to the modulus of the whole foam, E^*, by the following equation [103]:

$$\frac{E^*}{E_s} = \left(\frac{\rho^*}{\rho_s}\right)^2 \qquad (1.2),$$

where ρ^* and ρ_s are defined as the densities of the scaffold and nonporous polymer, respectively. Thus, equation 1.2 provides a relationship between the elastic modulus for the material (measured with tensile testing) and the elastic modulus for the porous scaffold (measured in compression mode) and an alternative to indentation techniques.

In addition to accurately mimicking the mechanical environment experienced by cells *in vivo*, it is important to consider the role of matrix proteins in cell behavior. Fibronectin (Fn) in particular has been implicated in the pathogenesis of breast cancer. High serium Fn levels have long been known to correlate with

poor patient prognosis [105] and the Fn in bone marrow is thought to interact with cancer cells in bone metastatic lesions [106]. More recently, Fn has been implicated in survival protection of breast cancer cells within the human bone marrow [107]. Furthermore, inhibition of integrin $\alpha_v\beta_3$, a receptor to Fn, has been shown to ameliorate progression of various cancers, including the prevention of bone metastases in preclinical animal models [40-42, 108-110]. Thus, Fn is a viable and appropriate ECM protein for use with *in vitro* substrates in the study of bone metastases. However, adsorption of a matrix protein to a substrate introduces the question of whether the protein layer alters the rigidity of the underlying matrix sensed by the cells. Atomic force microscopy (AFM) studies of integrin-Fn bonds have demonstrated that cells can sense mechanical changes at distances of up to 150nm [63]. Considering that adsorbed Fn layers have a thickness of less than 1nm [111, 112], cells are likely to maintain their ability to differentiate between rigid and compliant matrices even in the presence of adsorbed protein. Furthermore, cells also preferentially bind to rigid Fn coated substrates as opposed to compliant Fn coated substrates, demonstrating the cells ability to differentiate between substrate rigidity, even in the presence of a layer of matrix protein [63].

Thus, considering the complexity of biological tissue and the importance of microenvironment architecture and rigidity on cell fate, it is important to both accurately design scaffold architecture and choose the appropriate mechanical testing technique when designing a synthetic substrate or scaffold to mimic native tissue.

Research Objective

The presence of bone metastases is associated with poor patient prognosis; breast cancer survival rates drop from 93 to 27% after the tumor has metastasized to bone[1], and current therapies only aim at slowing the rate of bone damage (bisphosphonates) or have vast off-target cytotoxic effects (chemotherapy and radiation). Thus there is a distinct clinical need for developing targeted bone metastasis therapies, which requires understanding of the mechanisms involved in the establishment and progression of bone metastatic disease.

There is a growing body of evidence to suggest that tissue rigidity influences the behavior of cancer cells in soft tissue [13, 58, 59, 62, 70, 113-115], but the differential rigidity of bone has to date been largely ignored within the context of cancer. This work aims to elucidate the mechanisms by which bone rigidity influences the metastatic potential and invasiveness of cancer through the use of 2D and 3D *in vitro* culture techniques.

Chapter II focuses on invadopodia-mediated mechanisms of invasion in primary breast tissue. This work was completed in collaboration with Drs. Alissa Weaver and Aron Parekh and published in the *Biophysical Journal* in 2011. Chapters III and IV discuss the role of mechanotransduction and bone matrix mechanical properties in the formation of osteolytic breast metastases. The data discussed in Chapter III can also be found in the November 2010 issue of *PLoS One,* while the content of Chapters IV and V are the subject of upcoming publications that are in preparation.

References

1. American Cancer Society. *Cancer Facts and Figures*. 2010.
2. EA McSherry, S.D., AM Hopkins, S McDonnell, *Molecular Basis of Invasion in Breast Cancer.* Cellular and Molecular Life Sciences, 2007. **64**: p. 3201-3218.
3. MW Beckmann, D.N., HG Schnurch, BA Gusterson, HG Bender, *Multistep carcinogenesis of breast cancer and tumor heterogeneity.* Journal of Molecular Medicine, 1997. **75**: p. 429-439.
4. MC Abba, J.D., KA Hawkins, Y Hu, H Sun, C Notcovich, C Gaddis, A Sahin, K Baggerly, CM Aldaz, *Transcriptomic changes in human breast cancer progression as determined by serial analysis of gene expresion.* Breast Cancer Research, 2004. **6**: p. R499-513.
5. Ma, S., Tuggle, Gaudet, Enright, McQuary, Payette, Pistone, Stecker, Zhang, *Gene expression profiles of human breast cancer progression.* PNAS, 2003. **100**: p. 5974-5979.
6. Nishidate, K., Lin, Mano, Miki, Kasumi, Yoshimoto, Tsunoda, Hirata, Nakamura, *Genome-wide gene-expression profiles of breast cancer cells purified with laser microbeam microdissection: identification of genes associated with progression and metastasis.* International Journal of Oncology, 2004. **25**: p. 797-819.
7. Porter, K., Nasser, Sgroi, Kaelin, Marks, Riggins, Polyak, *A SAGE view of breast tumor progression.* Cancer Research, 2001. **61**: p. 5697-702.
8. Schuetz, B., Clare, Nieselt, Sotlar, Walter, Fehm, Solomayer, Riess, Wallwiener, *Progression-specific genes identified by expression profiling of matched ductal carcinomas in situ and invasive breast tumors, combining laser capture microdissection and oligonucleotide microarray analysis.* Cancer Research, 2006. **66**(5278-5286).
9. Wang, G., Lapidus, Wells, Wyckoff, Sahai, Singer, Segall, Condeelis, *Identification and testing of a gene expression signature of invasive carcinoma cells within primary mammary tumors.* Cancer Research, 2004. **64**: p. 8585-8594.
10. Ridley, P., Johnston, Diekmann, Hall, *The small GTP-binding protein rac regulats growth factor induced membrane ruffling.* Cell, 1992. **70**: p. 401-410.
11. Nobes, H., *Rho, rac, and cdc42 GTPases regulate the assembly of multimolecular focal complexes associated witha ctin stress fibers, lamellipodia and filopodia.* Cell, 1995. **81**: p. 53-62.
12. Kozma, A., Best, Lim, *The Ras related protein Cdc42Hs and bradykinin promote formation of peripheral actin microspikes and filopodia in Swiss 3T3 fibroblasts.* Molecular Cell Biology, 1995. **15**: p. 1942-1952.
13. Weaver, A.M., *Invadopodia: specialized cell structures for cancer invasion.* Clin Exp Met, 2006. **23**: p. 97-105.
14. Mueller, G., Akiyama, *A novel protease docking function of integrin at invadopodia.* Journal of Biological Chemistry, 1999. **274**(35): p. 24947-24952.

15. Deryugina, R., Monosov, *MT1-MMP initiates activation of pro-mMP2 and integrin alphavbeta3 promotes maturation of MMP2 in breast carcinoma cells.* Experimental Cell Research, 2001. **263**(2): p. 209-223.
16. Monsky, L., Aoyama, et al., *A potential marker protease of invasiveness, seprase, is localized on invadopodia of human malignant melanoma cells.* Cancer Research, 1994. **54**(21): p. 5702-5710.
17. Nakahara, H., Thompson, et al., *Transmembrane/cytoplasmic domain-mediated membrane type 1 matrix metalloprotease docking to invadopodia is required for cell invasion.* PNAS, 1997. **94**(15): p. 7959-7964.
18. Frame, F., Carragher, *v-Src's hold over actin and cell adhesions.* Nat Rev Mol Cell Biol, 2002. **3**(4): p. 233-245.
19. Nobes, H., *Rho GTPases control polarity, protrusion and adhesion during cell movement.* J Cell Biol, 1999. **144**(6): p. 1235-44.
20. Ridley, H., *The small GTP-binding protein rho regulates the assembly of focal adhesions and actin stress fibers in response to growth factors.* Cell, 1992. **70**(3): p. 389-399.
21. Coussens, L.M., B. Fingleton, and L.M. Matrisian, *Matrix metalloproteinase inhibitors and cancer: trials and tribulations.* Science, 2002. **295**(2387-2392).
22. Wyckoff, P., Gschmeissner, Condeelis, Sahai, *ROCK and myosin dependent matrix deformation enables protease-independent tumor cell invasion in vivo.* Curr Biol, 2006. **16**: p. 1515-23.
23. Friedl, W., *Tumour-cell invasion and migration: diversity and escape mechanisms.* Nat Rev Cancer, 2003. **3**: p. 362-74.
24. Wolf, M., Leung, Engelke, von Andrian, Deryugina, Strongin, Brock, Friedl, *Compensation mechanism in tumor cell migration: mesenchymal amoeboid transition after blocking of pericellular proteolysis.* J Cell Biol, 2003. **160**: p. 267-77.
25. Sahai, M., *Differing modes of tumour cell invasion have distinct requirements of Rho/ROCK signalling and extracellular proteolysis.* Nat Cell Biol, 2003. **5**: p. 711-719.
26. Guise, T., et al., *Evidence for a causal role of parathyroid hormone-related protein in the pathogenesis of human breast cancer-mediated osteolysis.* J Clin Invest, 1996. **98**(7): p. 1544-1549.
27. Lipton, A., *Implications of bone metastases and the benefits of bone-targeted therapy.* Semin Oncol, 2010. **37**(2): p. S15-29.
28. PG Robey, A.B., *Extracellular Matrix and Biomineralization of Bone.* Primer on the Metabolic Bone Diseases and Disorders of Mineral Metabolism, 2006. **6**: p. 12-19.
29. NK Lee, e.a., *Endocrine Regulation of Energy Metabolism by the Skeleton.* Cell, 2007. **130**(3): p. 456-469.
30. JE Aubin, J.L., GS Stein *Bone Formation: Maturation and Functional Activities of Osteoblast Lineage Cells.* Primer on the Metabolic Bone Diseases and Disorders of Mineral Metabolism, 2006. **6**: p. 20-27.
31. Ross, F., *Osteoclast Biology and Bone Resorption.* Primer on the Metabolic Bone Diseases and Disorders of Mineral Metabolism, 2006. **6**: p. 30-35.

32. T Suda, e.a., *Modulation of osteoclast differentiation and function by the new members of the tumor necrosis factor receptor and ligand families.* Endocr. Rev, 1999. **20**: p. 345-57.
33. WJ Boyle, e.a., *Osteoclast differentiation and activation.* Nature, 2003. **423**: p. 337-342.
34. Ross, S.T.a.F., *Genetic REgulation of osteoclast development and function.* Nat Rev Genet, 2003 **4**: p. 638-649.
35. WC Horne, e.a., *The roles of Src kinase and Cbl proteins in the regulation of osteoclast differentiation and function* Immunol Rev, 2005. **208**: p. 106-125.
36. Teitelbaum, F.R.a.S., *avb3 and macrophage colony stimulating factor: Partners in osteoclast biology.* Immunol Rev, 2005. **208**: p. 88-105.
37. Kang, Y., et al., *A multigenic program mediating breast cancer metastasis to bone.* Cancer Cell, 2003. **3**: p. 537-49.
38. Muller, H., Soto, Ge, Catron, Buchanan, McClanahan, Murphy, Yan, Wagner, Barrera, Mohar, Verastegui, Zlotnik, *Involvement of chemokine receptors in breast cancer metastasis.* Nature, 2001. **410**: p. 50-56.
39. Sun, *Skeletal localization and neutralization of the sdf-1/cxcr4 axis blocks prostate cancer metastasis and growth in osseous sites in vivo.* J Bone Min R, 2005. **20**: p. 318-29.
40. Felding-Habermann, *Integrin activation controls metastasis in human breast cancer.* PNAS, 2001. **98**: p. 1853-58.
41. Harms, e.a., *A small molecule antagonist of the alphavbeta3 integrin suppresses MDA-MB-435 skeletal metastasis.* Clin Exp Met, 2004. **21**: p. 119-128.
42. Zhao Y, B.R., Treilleux I, Pujuguet P, Peyruchaud O, Baron R *Tumor alphavbeta3 integrin is a therapeutic target for breast cancer bone metastases.* Cancer Research, 2007. **67**(12): p. 5821-5830.
43. Bachmeier, e.a., *MMPs in breast cancer cell lines of different tumorigenicity.* Anticancer Res, 2001. **21**: p. 3821-28.
44. Nakopoulou, e.a., *MMP2 protein in invasive breast cancer and the impact of MMP2/TIMP2 phenotype in overall survival.* Breast Cancer Research, 2003. **77**: p. 145-55.
45. Lynch, C.C., et al., *MMP-7 promotes prostate cancer-induced osteolysis via the solubilization of RANKL.* Cancer Cell, 2005. **7**: p. 485-96.
46. Lynch, C.C. and L.M. Matrisian, *Matrix metalloproteinases in tumor-host cell communication.* Differentiation, 2002. **70**: p. 561-73.
47. Dallas, e.a., *Proteolysis of latent transforming growth factor beta binding protein 1 by osteoclasts.* J Biol Chem, 2002. **277**: p. 21352-60.
48. WM Philbrick, e.a., *Defining the Roles of Parathyorid Hormone Related Protein in Normal Physiology.* Physiological Reviews, 1996. **76**(1): p. 127-143.
49. CJ Pirola, e.a., *Mechanical stimuli induce vascular PTHrP gene expression in vivo and in vitro.* Endocrinology, 1994. **134**: p. 2230-6.
50. M Yamamoto, e.a., *PTHrP in the rat urinary bladder: a smooth muslce relaxant produces locally in response to mechanical stress.* PNAS, 1992. **89**: p. 5326-30.

51. Powell, G.J., et al., *Localization of parathyroid hormone-related protein in breast cancer metastases: increased incidence in bone compared with other sites.* Cancer Res, 1991. **51**(11): p. 3059061.
52. Southby, J., et al., *Immunohistochemical localization of parathyroid hormone-related protein in human breast cancer.* Cancer Res, 1990. **50**(23): p. 7710-6.
53. Roodman, *Mechanisms of Bone Metastasis.* N Engl J Med, 2004. **350**: p. 1655-64.
54. TA Guise, e.a., *PTHrP expression by breast cancer cells enhance osteolytic bone metastases in vivo.* J Bone Min R, 1994. **9**: p. S128.
55. RJ Thomas, e.a., *Breast cancer cells interact with osteoblasts to support osteoclast formation.* Endocrinology, 1999. **140**: p. 4451-4458.
56. JJ Yin, e.a., *TGF beta signaling blockade inhibits PTHrP secretion by breast cancer cells and bone metastases development.* J Clin Invest, 1999. **103**: p. 197-206.
57. SM Kakonen, e.a., *Transforming growth factor beta stimulates parathyroid hormone related protein an dosteolytic metastases via Smad and MAPK signaling pathways.* J Biol Chem, 2005. **227**(24571-78).
58. Paszek, M.J. and V.M. Weaver, *The tension mounts: mechanics meets morphogenesis and malignancy.* J Mammary Gland Biol Neoplasia, 2004. **9**: p. 325-342.
59. Paszek, M.J., et al., *Tensional homeostasis and the malignant phenotype.* Cancer Cell, 2005. **8**: p. 241-254.
60. Pelham, R.J., Jr. and Y. Wang, *Cell locomotion and focal adhesions are regulated by substrate flexibility.* Proc Natl Acad Sci USA, 1997. **94**: p. 13661-13665.
61. Engler, A.J., et al., *Matrix Elasticity Directs Stem Cell Lineage Specification.* Cell, 2006. **126**: p. 677-689.
62. Butcher, D.T., T. Alliston, and V.M. Weaver, *A tense situation: forcing tumour progression.* Nat Rev Cancer, 2009. **9**(2): p. 108-22.
63. SW Moore, e.a., *Stretchy proteins on stretchy substrates: the important elements of integrin-mediated rigidity sensing.* Dev Cell, 2010. **19**: p. 194-206.
64. A Katsumi, e.a., *Integrins in Mechanotransduction* J Biol Chem, 2004. **279**: p. 12001-12004.
65. Huang, I., *The structural and mechanical complexity of cell growth* Nat Cell Biol, 1999. **1**: p. E131-136.
66. Burridge, C.-W., *Focal adhesions, contractility and signalig.* Ann. Rev. Cell Dev. Biol, 1996. **12**: p. 463-519.
67. Sellers, J., *Regulation of cytoplasmic and smooth muscle myosin.* Curr Opin Cell Biol, 1991. **3**: p. 98-104.
68. JL Tan, e.a., *Control of nonmuscle myosins by phosphorylation.* Ann Rev Biochem, 1992. **61**: p. 721-59.
69. K Kimura, e.a., *Regulation of myosin phosphatase by Rho and Rho-associated kinase.* Science, 1996. **273**: p. 245-48.
70. Yeung, T., et al., *Effects of Substrate Stiffness on Cell Morphology, Cytoskeletal Structure, and Adhesion.* Cell Motil. Cytoskeleton, 2005. **60**: p. 24-34.
71. Alexander, N.R., et al., *Extracellular matrix rigidity promotes invadopodia activity.* Curr Biol, 2008. **18**(17): p. 1295-1299.

72. Liu, S., et al., *Inhibition of rho-associated kinase signaling prevents breast cancer metastasis to human bone.* Cancer Res, 2009. **69**(22): p. 8742-51.
73. Myoui A, N.R., Williams PJ, Hiraga T, Tamura D, Michigami T et. al., *c-Src tyrosine kinase activity is associated with tumor colonization in bone and lung in an animal model of human breast cancer metastasis.* Cancer Research, 2003. **63**(16): p. 5028-5033.
74. LW Welling, e.a., *Mechanical Properties of Basement Membrane.* NIPS, 1995. **10**: p. 30-35.
75. Evans, F., *Mechanical Properties of Bone*. American Lecture Series. Vol. 881. 1973, Springfield, IL: C. C. Thomas.
76. DE Discher, e.a., *Tissue cells feel and respond to the stiffness of their substrate.* Science, 2005. **310**(5751): p. 1139-43.
77. Ruppender NS, M.A., Martin TJ, Mundy GR, Sterling JA and Guelcher SA, *Matrix Rigidity Induces Osteolytic Gene Expression of Metastatic Breast Cancer Cells.* PLoS One, 2010. **5**(11): p. e15451.
78. Li, B., et al., *The effects of rhBMP-2 released from biodegradable polyurethane/microsphere composite scaffolds on new bone formation in rat femora.* Biomaterials, 2009. **30**(35): p. 6768-79.
79. Srinivasan, A., et al. *In vitro biocompatibility and biodegradation of poly(esterurethane urea) scaffolds*. in *Trans 31st Annual Meeting Society for Biomaterials*. 2006. Pittsburgh, PA.
80. Guelcher, S., *Biodegradable polyurethanes: synthesis and applications in regenerative medicine. .* Tissue Eng In Press, 2008.
81. Guelcher, S.A., et al., *Synthesis, mechanical properties, biocompatibility, and biodegradation of polyurethane networks from lysine polyisocyanates.* Biomaterials, 2008. **29**(12): p. 1762-1775.
82. Guelcher, S.A., et al., *Synthesis of biocompatible polyurethanes from aliphatic diisocyanates and novel diurea diol chain extenders.* Acta Biomateriala, 2005. **1**: p. 471 - 484.
83. Guelcher, S.A., et al., *Synthesis and biocompatibility of polyurethane foam scaffolds from lysine diisocyanate and polyester polyols.* Tissue Eng, 2006. **12**(5): p. 1247-1259.
84. E Cukierman, e.a., *Taking Cell-Matrix Adhesions to the Third Dimension.* Science, 2001. **294**(5547): p. 1708-12.
85. Bissell, C.R.a.M., *Dynamic reciprocity revisited: a continuous, bidirectional flow of information between cells and the ECM regulates mammary epithelial cell function.* Biochem Cell Biol, 1995. **78**(7-8): p. 391-7.
86. Bard, T.E.a.J., *Collagen substrata for studies on cell behavior.* J Cell Biol, 1972. **54**(3): p. 626-37.
87. Broecker, P.F.a.E., *The biology of cell locomotion within three-dimensional extracellular matrix.* Cellular and Molecular Life Sciences, 2000. **57**(1): p. 41-64.
88. Weitzman, B.a., *Culture of normal and malignant primary epithelial cells in a physiological manner simulates in vivo patterns and allows discrimination of cell type.* Cancer Research, 1993. **53**: p. 2644-54.

89. Taylor-Papadimitrou, D.A.a.J., *Cell adhesion molecules in the normal and cancerous mammary glad.* J Mam Gland Biol Neoplasia, 1996. **1**: p. 207-18.
90. Bissell, M., *The differentiated state of normal and malignant cells or how to define a normal cell culture.* Int Rev Cytol, 1982. **70**: p. 27-100.
91. OW Petersen, e.a., *Interaction with basement membrane serves to rapidly distinguish growth and differentiation pattern of normal and malignant human breast epithelial cells.* PNAS, 1992. **89**: p. 9064-8.
92. AW Stoker, e.a., *Designer environments for the analysis of cell and tissue function.* Curr Opin Cell Biol, 1990. **2**: p. 864-74.
93. HK Kleinman, e.a., *Use of extracellular matrix components for cell culture.* Anal Biochem, 1987. **66**: p. 1-13.
94. Zaman, M.H., et al., *Migration of tumor cells in 3D matrices is governed by matrix stiffness along with cell-matrix adhesion and proteolysis.* PNAS, 2006. **103**(29): p. 10889-10894.
95. Hafeman, A.E., et al., *Local delivery of tobramycin from injectable biodegradable polyurethane scaffolds.* J Biomater Sci, Polym Ed, 2008. **In Press**.
96. Kavlock, K.D., et al., *Synthesis and characterization of segmented poly(esterurethane urea) elastomers for bone tissue engineering.* Acta Biomater, 2007. **3**(4): p. 475-484.
97. Hafeman, A., et al., *Injectable biodegradable polyurethane scaffolds with release of platelet-derived growth factor for tissue repair and regeneration.* Pharm Res, 2008. **25**(10): p. 2387-99.
98. Bruin, P., et al., *Design and synthesis of biodegradable poly(ester-urethane) elastomer networks composed of non-toxic building blocks.* Makromol Chem, Rapid Commun, 1988. **9**: p. 589-594.
99. Zhang, G., *Evaluating the Viscoelastic Properties of Biological Tissues in a New Way.* J Muscoskelet Neonatal Interactions, 2005. **5**(1): p. 45-50.
100. Sperling, L.H., *Introduction to Physical Polymer Science*. 3rd ed2001, New York: Wiley-Interscience.
101. DD Wright-Charlesworth, e.a., *Nanoindentation of injection molded PLA and self reinforced composite PLA after in vitro conditioning for three months.* J. Biomed. Mat. Res, 2005. **74A**(3): p. 388-396.
102. Kraynik, W.a., *The linear elastic properties of open cell foams.* J. Appl. Mech, 1988. **55**: p. 341-346.
103. Ashby, L.G.a.M., *Cellular Solids: Structure and Properties*. 2nd ed1997, Cambridge, UK: Cambridge University Press.
104. Goodier, S.T.a.J., *Theory of Elasticity*. 2nd ed1970, New York: McGraw-Hill.
105. A Ruelland, e.a., *Level of plasma fibronectin in patients with Breast Cancer.* Clinica Chimica Acta, 1988. **178**(3): p. 283-287.
106. Van der Velde-Zimmermann, D., et al., *Fibronectin distribution in human bone marrow stroma: matrix assembly and tumor cell adhesion via alpha5 beta1 integrin.* Exp Cell Res, 1997. **230**(1): p. 111-20.
107. R Wieder, e.a., *A model for metastatic breast cancer dormancy through fibronectin mediated survival signaling.* PNAS Clin Oncol, 2003. **22**.

108. Schneider JG, A.S., Weilbaecher KN, *Integrins and Bone Metastasis: Integrating tumor cell and stromal cell interactions.* Bone.
109. BP Eliceiri, e.a., *Src-mediated coupling of focal adhesion kinase to integrin alphavbeta5 in vascular endothelial growth factor signaling.* J Biol Chem, 2002. **157**(1): p. 149-60.
110. Bakewell, S.J., et al., *Platelet and osteoclast β3 integrins are critical for bone metastasis.* Proc Natl Acad Sci U S A, 2003. **100**(24): p. 14205–14210.
111. A Dekker, e.a., *Adhesion of endothelial cells and adsorption of serum proteins on gas plasma-treated PTFE.* Biomaterials, 1991. **12**(2): p. 130-8.
112. M Al-Jawad, e.a., *Fibronectin adsorption studied using neutron reflectometry and complementary techniques.* The European Physical Journal E: Soft matter and biological physics, 2009. **30**(2): p. 175-9.
113. Enderling, H., et al., *Dependence of invadopodia function on collagen fiber spacing and crosslinking: computational modeling and experimental evidence.* Biophys J, 2008. **95**(5): p. 2203-2218.
114. Wang, F., et al., *Reciprocal interactions between β1-integrin and epidermal growht factor receptor in three-dimensional basement membrane breast cultures: a different perspective in epithelial biology.* Proc Natl Acad Sci USA, 1998. **95**: p. 14281-14286.
115. Weaver, A., *Invadopodia Review.* 2006.

CHAPTER II

SENSING AND MODULATION OF INVADOPODIA ACROSS A WIDE RANGE OF RIGIDITIES

Introduction

Invasion by epithelial cancer cells across the basement membrane (BM) is considered to be a critical rate-limiting step in cancer metastasis [1]. The BM is a thin, dense extracellular matrix (ECM) composed of a highly ordered and crosslinked type IV collagen network, along with laminin, nidogen/entactin, and various proteoglycans and glycoproteins [2]. Once malignant cells penetrate this barrier, they must navigate the adjacent stroma and enter the vasculature in order for metastasis to occur.

ECM tensile properties (i.e., stiffness or rigidity) have been implicated in the malignant transformation of the breast through activation of cellular mechanotransduction signaling pathways [3]. This relationship is consistent with findings from both mouse tumor [4, 5] and clinical [6, 7] studies that show a strong correlation between tissue density and cancer development and invasiveness. On the cellular level, our group has linked mechanosensing of rigid substrates *in vitro* to the formation and activity of invadopodia, punctate, actin-rich structures with associated cell-surface proteinases that degrade ECM and have been implicated in cancer invasion and metastasis [8, 9]. While it is evident that the mechanical nature of tumor-associated ECM can drive an invasive phenotype, the relevant rigidity

range with respect to the BM and stroma is unclear.

A significant challenge that exists in the field is to recapitulate *in vitro* physiologically relevant *in vivo* characteristics [10]. For example, although biological hydrogels such as collagen and Matrigel are extremely useful to mimic the stromal and BM environments, they lack many of the physical characteristics of *in vivo* tissues [1, 11] that contribute to their mechanical properties. Specifically, both pepsinized collagen gels and Matrigel are uncrosslinked, have very low elastic moduli, and provide little barrier to cellular migration and invasion [11, 12]. Several recent studies have utilized processed [13, 14] and native [11, 12] biological tissues as *ex vivo* organotypic models to recapitulate the *in vivo* ECM environment experienced by invasive cells. Similarly, tissue "scaffolds" that are prepared from naturally occurring ECMs for tissue engineering and clinical applications have resulted in biological materials that have been thoroughly tested to ensure that they maintain their *in vivo* physical and mechanical properties [15]. For example, urinary bladder matrix (UBM), which has an intact BM with an adjacent fibrous stroma [16], is well-characterized and readily handled for mechanical testing [17] and ex vivo culturing [16].

Despite these tissue surrogates, regulation of behavior by tissue rigidity is usually explored *in vitro* with artificial substrates that are easily synthesized and manipulated to yield specific mechanical properties. One of the most common approaches is to graft ECM molecules onto polyacrylamide (PAA) gels of different rigidities. These hydrogels have been utilized to explore a host of biological processes such as migration [18] and stem cell differentiation [19] since their

mechanical properties are elastic and tunable and their optical properties allow for favorable microscopic imaging. Using these substrates, we found that the number and degradative ability of invadopodia increased when the rigidity was increased by one order of magnitude, from E = 1 to 10 kPa [8]. Despite these findings, the PAA gels are limited since they can be synthesized with elastic moduli that span just a few orders of magnitude (typically ~0.1-30 kPa) [19, 20] in contrast to biological tissues that have elastic moduli spanning up to nine orders of magnitude (0.1 kPa-10 GPa) [21, 22]. Alternatively, rubber-like polymers such as polyurethane (PUR) elastomers can be synthesized to reach much larger moduli values in the high MPa-GPa region [23, 24].

In this study, we focused on defining how breast cancer cells respond to a wide range of substrate rigidities and how that response corresponds to physiological ECM microenvironments that might be encountered in a developing or metastatic tumor. To determine the mechanical influence of relevant in vivo environments, we utilized either intact UBM as our model of stroma, or a thin delaminated version that has the majority of the stroma removed from the BM (UBM-BM). We first characterized the physical and mechanical properties of UBM-BM and compared them to UBM. Since both UBM-BM and UBM had much higher elastic moduli than previously tested in our *in vitro* invadopodia study [8], we developed synthetic invadopodia substrates (PAA and PUR) that span the kPa-GPa rigidity range and determined the corresponding degradative capabilities of breast cancer cells. Surprisingly, breast cancer cells can sense a wide range of rigidities, as measured by ECM degradation and invadopodia formation, and further validated

with the expression of several genes that were found to peak at either relatively low or high moduli. Furthermore, there is an optimal peak of ECM degradation on the 30 kPa substrate, which is closer to the rigidity of the stroma than to the BM. Consistent with rigidity playing a role *in vivo*, breast cancer cells formed significantly more invadopodia when cultured on the stromal side of UBM-BM when compared to those cultured on the BM side. Experiments repeated with 804G rat bladder carcinoma cells on synthetic substrates and UBM-BM yielded similar results, indicating a common response between cell types of different tissue origin.

Materials and Methods

UBM preparations

UBM and UBM-BM were kindly provided by Dr. Stephen Badylak (University of Pittsburgh). UBM-BM is prepared from porcine bladders similarly to UBM [25], except that the tissue is further mechanically delaminated close to the BM such that the remaining tissue is extremely thin and appears translucent.

Immunohistochemistry (IHC)

Formalin-fixed, agar-coated samples were sectioned for either hematoxylin and eosin staining (Richard Allan Scientific, Kalamazoo, MI) or immunostaining with rabbit type IV collagen (Abcam, Cambridge, MA) or anti-laminin (Sigma, St. Louis, MO) antibodies, and visualized with the Envision+ HRP/DAB system (Dako, Carpinteria, CA) and Mayer's hematoxylin.

Electron microscopy (EM)

Samples were fixed in 2.5% glutaraldehyde, serially dehydrated, critical point dried, and sputter coated with 60% gold and 40% palladium for visualization with a Hitachi S4200 field emission scanning EM. Samples were either mounted with double-sided tape onto stages or anchored onto CellCrown inserts (Scaffdex, Finland). To visualize the type IV collagen network using a Philips CM-12 transmission EM, samples were salt extracted to remove non-collagenous molecules from the BM [26], fixed in 2.5% glutaraldehyde, serially dehydrated, resin embedded, sectioned and stained with 1% uranyl acetate and 1% lead citrate.

Dynamic mechanical analysis (DMA) and rheology

15×6.5 mm UBM or UBM-BM samples were mounted in a tension submersion clamp of a TA Instruments Q800 DMA, allowed to equilibrate at room temperature for 30 min, and stretched at a strain rate of 1%/min. Stress, defined as force divided by the initial cross-sectional area (measured with calipers and given in Fig. 2.2B), was plotted versus strain. T3000 and T900 PURs were tested at a rate of 3 N/min, whereas T300 PURs were loaded at a rate of 5 mm/min using a 3-point bending apparatus. Elastic moduli were determined by linear regression of the stress-strain curves. Soft and hard PAAs were previously tested using rheometry [8], and the rigid PAA was tested similarly. We previously showed that the ECM layers on the synthetic substrates do not substantially alter their mechanical properties [8].

Swelling

The swelling ratio was calculated as follows:

$$Q = \frac{1}{\nu_2} = \rho_p \left[\left(\frac{Q_m}{\rho_s} \right) + \left(\frac{1}{\rho_p} \right) \right] \qquad (2.1)$$

where ν_2^{-1} is the volume fraction, r_p is the protein density assumed to be 1.27 g/cm^3 for collagen, r_s is the water density assumed to be 1 g/cm^3, and Q_m is the mass ratio of water to protein. Protein fractions were calculated as the inverse of the swelling ratio (i.e., volume fraction of protein).

AFM of UBM-BM stromal and BM surfaces

The modulus, E, is calculated with the following equation [1]:

$$F_{tip} = \frac{4}{3} E \sqrt{R d^3} + F_{adh} \qquad (2.2)$$

F_{tip} is the force on the tip, E is the Young's modulus, R is the tip radius, d is the distance between the sample and the tip, and F_{adh} is the adhesive force between the tip and the sample. Raw moduli values were plotted versus percentage of total area within a sample. Scan parameters were: scan size 5 mm x 5 mm, peak force set point 1 nN, and maximum modulus 25 MPa. The AFM probe tips were silicon-nitride cantilever (SNL) from Veeco, with spring constants between 0.07 – 0.1 N/m and radii between 25 – 40 nm. Each tip was calibrated for spring constant and radius

prior to sample measurements. Tissue samples were hydrated in PBS and held taut during AFM scans in Cell Crown inserts, with the system inverted so that the tissue was not resting on the bottom of the Petri dish during the scans. For modulus determination, three independent samples of tissue were scanned and the weighted average of the modulus for each area scanned was calculated as follows:

$$\mathrm{E} = \frac{\sum w_i E_i}{\sum w_i} \qquad (2.3)$$

where w_i is the percent of times a modulus of value E_i was observed. Adjacent sections of each sample were taken, so that measurements could be made of both stroma and BM sides of each sample. A total of three measurements per sample per side were taken.

Invadopodia assay on synthetic substrates and tissue-derived scaffolds

Mechanically tunable substrates approximately 75 mm thick were made from PAA hydrogels and PUR elastomers based on previously established methods [18, 27]. Briefly, they were cast on activated glass coverslips of 35 mm MatTek dishes and conjugated with 1% gelatin (crosslinked with 0.5% glutaraldehyde) and FITC-labeled fibronectin [8, 28]. The rigid PAA was formed from 12% acrylamide and 0.6% bis-acrylamide. PURs were prepared from lysine diisocyanate and different equivalent weights of polyester polyalcohols synthesized from a glycerol starter and a 70%/30% mixture of caprolactone/glycolide for the T3000 (3000 Da)

and T900 (900 Da) PURs and 100% caprolactone for the T300 (300 Da) PUR [29]. PURs were soaked with 100 mg/ml poly-D-lysine at 37°C for 1 hour then coated as described above. UBM-BM samples were secured in Cell Crown inserts until taut but without significant strain (i.e., low strain). A low density (~3,000 cells/cm^2) of MCF10A CA1d cells were incubated on all substrates for 18 hours.

Immunofluorescence (IF)

To identify invadopodia, cells were fixed and stained with Alexa Fluor 546 phalloidin (Invitrogen) and 4F11 antibody (Upstate Biotechnology, Lake Placid, NY) to respectively identify F-actin and cortactin. Fluorescent images were either captured on a Nikon Eclipse TE2000-E microscope with a 40X Plan Fluor oil immersion lens or on a Zeiss LSM 510 confocal microscope with a Plan Apo 63X oil immersion lens, 0.2 μm Z-sections. For the synthetic substrates, areas of FITC-Fibronectin degradation were thresholded and quantified with Metamorph software based on loss of FITC-signal, and active and total invadopodia were manually counted and cell size quantified as previously described [8].

Quantitative real-time PCR

To measure changes in gene expression, mRNA reverse transcription was carried out using the SuperScript III kit (Invitrogen) per manufacturer's instructions. Briefly, total RNA was extracted using the RNeasy Mini Kit (Qiagen). The SuperScript III First Strand Synthesis System for quantitative RT-PCR primed with random hexamers was used to synthesize cDNA using between 1 and 5μg total

RNA. In order to obtain enough RNA, invadopodia assays on the different synthetic substrates were scaled up and performed in either 60 mm Petri dish lids or 12-well plates for the PAAs and PURs, respectively, and seeded with ~15,000-50,000 cells/cm^2. The expression of ADAMTS1, MMP1, LAMB1, and MMP14 was measured by quantitative RT-PCR using validated TaqMan primers with the 7300 Real-Time PCR System (Applied Biosystems). Assays were performed in triplicate on the RealPlex Machine (Eppendorf) under the following cycling conditions following a 10-minute incubation period at 95°C: 95°C for 15 seconds, 60°C for 60 seconds. The expression of OPN was determined using SYBR green primers as described previously [2]. Quantification was performed using the DDct method using 18S as an internal control.

S*tatistics*

Data were evaluated for normality with the Shapiro-Wilk or Kolmogorov-Smirnov test. Data passing the normality test were analyzed by either a Student's t-test or one-way ANOVA. Otherwise, they were analyzed by a Mann-Whitney or Kruskal-Wallis test. If significance was determined within a group, a Tukey or Tamhane post-hoc test was used for pairwise comparisons. $p<0.05$ was considered statistically significant. All statistical analyses were performed with PASW Statistics 18 (SPSS, Chicago, IL).

Results

The goal of this study was to test how mechanical properties that correspond to those found in tissues affect the formation and activity of cancer cell invadopodia. To isolate rigidity effects but also relate them to relevant *in vivo* physical properties, we used a combination of synthetic invadopodia substrates of tunable rigidity and tissue-derived ECM scaffolds that model the BM and stromal environments.

Characterization of model BM and stromal matrices

To obtain the relevant rigidities of stroma and BM, we began by characterizing the properties of the model ECM scaffold UBM and UBM-BM, respectively. Our rationale for using bladder-derived scaffolds is based on the presence of a large BM surface in bladder that can be isolated and used for both mechanical testing and experimental studies. By contrast, it is not easily possible to isolate the BM from ductal tissues such as breast for *in vitro* studies. UBM is a well-characterized decellularized ECM scaffold that is predominately composed of stromal connective tissue of the tunica propria underlying a thin BM layer [16]; thus we used it as a model of stroma. As a model of BM, we obtained UBM-BM, which is created from the same precursor tissue as UBM but is further mechanically delaminated to remove the majority of the connective tissue layer and leave a thin layer of BM. To verify the presence and structural integrity of the BM in UBM-BM due to this additional processing, we performed IHC staining and EM.

As opposed to the thick stromal layer in UBM (Fig. 2.1A, double-headed arrow), UBM-BM contained a thin, supporting layer of connective tissue (Fig. 2.1B,

double-headed arrow). On the top side, UBM-BM maintained a smooth and contoured surface (Fig. 2.1B, asterisk) consistent with the BM ultrastructure as observed in UBM [16]. Upon salt extraction, UBM-BM retained a filamentous meshwork composed of 100-200 nm pores (Fig. 2.1C) as previously described for BMs from a variety of tissues (26, 30). Dense positive IHC staining for both type IV collagen (Fig. 2.1D) and laminin (Fig. 2.1E) was observed in a continuous pattern localized to the luminal side that was also consistent with the presence of an intact BM in UBM-BM.

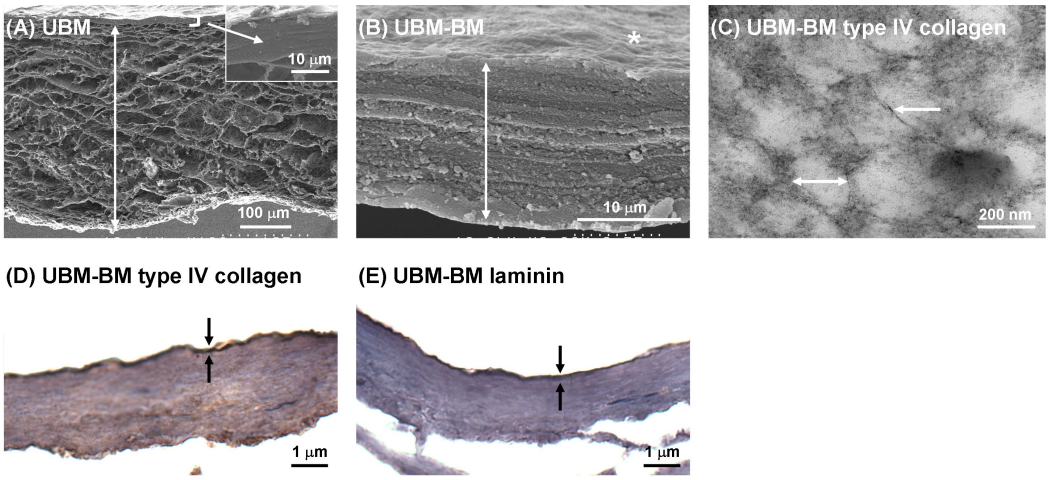

Figure 2.1. Characterization of UBM-BM and UBM. As model BM and stromal matrices, we characterized two *ex vivo* tissue scaffolds: UBM-BM and UBM. **(A)** SEM image (×180) of a UBM cross-section revealed a thick stromal layer of connective tissue (double-headed arrow) underlying a thin layer that includes the BM (bracket and inset image). **(B)** UBM-BM was created by mechanically delaminating porcine bladders to a further extent than UBM to yield a very thin layer of connective tissue (double-headed arrow) underlying the BM (asterisk) that was equivalent to the top portion of UBM (bracket and inset image of (A)) as shown in a cross-sectional SEM image (×8,000). **(C)** Upon salt extraction of noncollagenous components, TEM imaging (×110,000) revealed that UBM-BM contained filaments (single-headed arrow) and 100-200 nm diameter pores (double-headed arrow) consistent with the polygonal type IV collagen network of a BM. The integrity of the BM of UBM-BM was confirmed histologically with continuous positive staining for **(D)** type IV collagen and **(E)** laminin (between the arrows).

UBM-BM is mechanically rigid

The mechanical properties of UBM-BM and UBM as BM and stroma models, respectively, were first determined using dynamic mechanical analysis (DMA). Since collagen is a well-known tensile load-bearing protein [5, 31] and UBM is a fairly isotropic material [17], stress-strain data was generated by uniaxial tensile mechanical loading. Although collagen-rich biological tissues exhibit complex nonlinear viscoelastic behavior, their biomechanical response can be approximated as pseudoelastic to yield repeatable stress-strain curves once preconditioned to obtain a "steady state" mechanical response [31]. Previous work has shown that ECM scaffolds do not necessarily require preconditioning to reach repeatable stress-strain responses [32, 33]. In our preliminary experiments, successive loading cycles did not yield significant shifts in the stress-strain curves; therefore, preconditioning was assumed.

During mechanical loading, both UBM-BM and UBM exhibited strain stiffening (Fig. 2.2A), a typical phenomenon observed for collagenous tissues that is characterized by a transition from a compliant response at low strain (the "toe" region of the curve representing low physiologic loading) to a stiffer response at high strain (the "linear elastic" region of the curve representing high physiologic loading). UBM-BM exhibited steeper toe and linear elastic regions of the stress-strain curves indicating stiffer mechanical behavior than UBM that were verified with linear regressions to determine the elastic moduli at both low and high strain (Fig. 2.2B). For both scaffolds, the moduli were in the MPa range. The elastic moduli for UBM-BM in the low and high strain regions were respectively 4.5- and

6.4-fold larger than for UBM. UBM-BM experienced a higher degree of strain stiffening with an increase in modulus from the toe to the linear elastic region by 8.6- versus 6.1-fold for UBM.

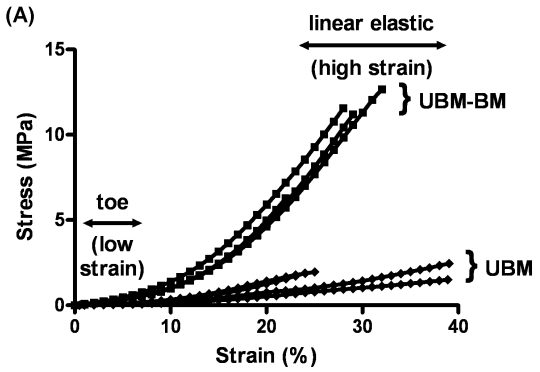

(B)

	UBM	UBM-BM
Thickness (μm)	121.8 ± 15.8	27.8 ± 3.3*
E_{low} (MPa)	1.8 ± 0.2	8.1 ± 0.7*
E_{high} (MPa)	10.9 ± 2.1	70.0 ± 3.3*
Swelling Ratio	10.3 ± 1.6	2.8 ± 0.2*
Protein Fraction	0.097	0.353

Figure 2.2. Stress-strain curves and elastic moduli for UBM-BM and UBM. (A) To determine the elastic moduli of our BM and stromal models, we performed uniaxial tensile DMA of UBM-BM and UBM. Both materials exhibited classic strain stiffening; however, UBM-BM exhibited steeper slopes in both the low strain toe region and high strain linear elastic region indicating stiffer mechanical behavior. One data point per % strain was reported for graphical representation. **(B)** Low and high strain elastic moduli were calculated from the slopes of the toe and linear elastic regions, respectively. Consistent with the UBM-BM being stiffer, this BM model had a smaller swelling ratio and larger protein fraction. Data are presented as mean ± SE, and * indicates $p<0.05$ for UBM-BM versus UBM comparisons. n=4 for the thickness, E_{low}, and E_{high} values, and n~20 for the swelling ratios, respectively.

As a second method to quantitate the rigidity of the stroma and BM, we performed AFM on the stromal and BM sides of UBM-BM (Fig 2.3). Of note, AFM measurements are at the nm-μm scale, which is similar to the subcellular-cellular scale [21, 34]. Interestingly, although there was a range of BM moduli (Fig 2.3B), the weighted average BM side modulus measured by AFM was ~3 MPa (Fig 2.3C), which is similar to moduli measured for retinal BM by AFM [35, 36] and >2-fold lower than the modulus measured by DMA tensile testing. The stromal side weighted average

modulus measured by AFM was ~0.4 MPa (Fig 2.3C), which was also lower than that measured by tensile testing (Fig. 2.2B). Similar to the DMA test results, however, the stromal side average elastic modulus was 7.5-fold lower than that of the BM side average modulus.

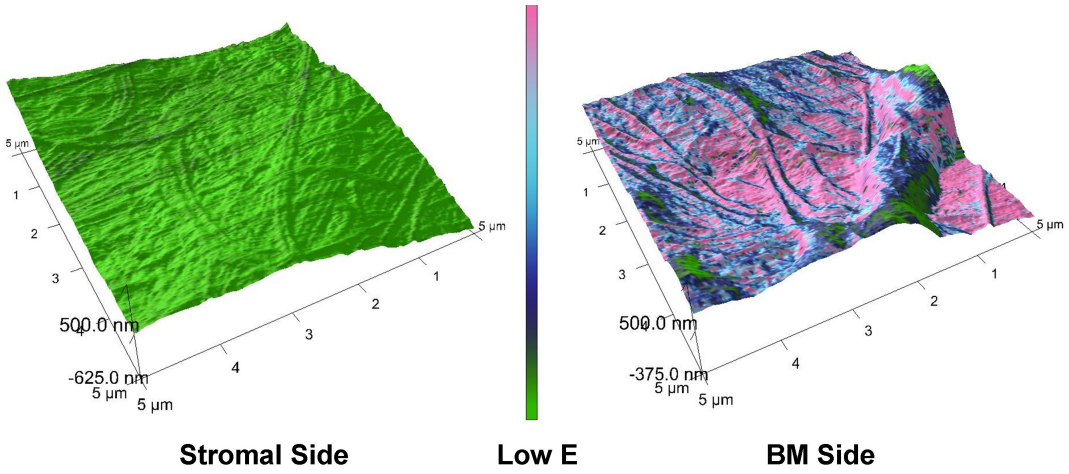

Figure 2.3. Atomic Force Microscopy measurements of the stromal and BM sides of UBM-BM. To determine whether rigidity differences between the stroma and BM were conserved at the nano-microscale on each side of UBM-BM, (A) the stromal and BM sides of UBM-BM were scanned to determine (B) the distribution of elastic moduli in a 5×5 µm sample area (representative examples shown). (C) Weighted averages were calculated for each sample and showed significantly larger elastic moduli for the BM side. Data are presented as mean ± SE, and * indicates $p<0.05$ for stromal versus BM side comparisons. n=9 total for each side from 3 independent UBM-BM specimens.

UBM-BM is highly crosslinked and dense

BM is thought to be a highly dense and crosslinked material. To indirectly measure the degree of crosslinking in each material, we determined the swelling ratio, Q, of UBM-BM and UBM. Q represents the ratio of wet to dry volume (or mass) of a polymer network such as type I pepsinized collagen gels [37]. As expected, UBM-BM had a significantly smaller Q than UBM (almost 4-fold smaller), indicating a much more highly crosslinked network (Fig. 2.2B). This finding is consistent with

the dynamic mechanical properties of these materials and with BM being the predominant component of UBM-BM unlike the stromal-dominated UBM (Fig 2.1). The inverse of Q yields the the protein fraction, n_2, which is likewise 4-fold larger for UBM-BM compared to UBM (Fig. 2.2B).

Development of invadopodia substrates that span eight orders of magnitude in rigidity

Since the elastic moduli of our model BM and stromal matrices, measured either by DMA or AFM, were considerably larger than those of the PAA gels that were previously tested for rigidity regulation of invadopodia [8], we developed synthetic substrates for invadopodia testing that span a wider range of rigidity. These substrates included 3 PAA and 3 PUR substrates of defined rigidity that were polymerized in a thin layer on top of MatTek glass dishes and overlaid with 1% gelatin/FITC-fibronectin . Since PAA is fairly elastic with a loss tangent much less than 1 (estimated as ~0.2 from our previous rheometric measurements), the soft (storage modulus G'~360 Pa) and hard (G'~3,300 Pa) PAA gels [8] were assumed incompressible and elastic such that the elastic modulus E=3G' [3]. An additional "rigid" PAA gel was synthesized using published protocols [38] and had a measured storage modulus of G'=9,248 ± 598 Pa. Therefore, the elastic moduli of the soft, hard, and rigid PAA gels were calculated to be E = 1,071, 9,929, and 28,283 Pa, respectively. In contrast, elastomeric PURs have larger moduli and were therefore tested by uniaxial tensile loading (T3000 and T900 PURs) or three-point bending (T300 PUR) using DMA yielding moduli values of 3.07, 5.58, and 1,853 MPa, respectively. Glass was used as the ceiling of the rigidity spectrum with a known

modulus of 69 GPa [39]. The elastic moduli of these materials span eight orders of magnitude (Fig. 2.4), include MPa rigidities, and were used as substrates for invadopodia assays.

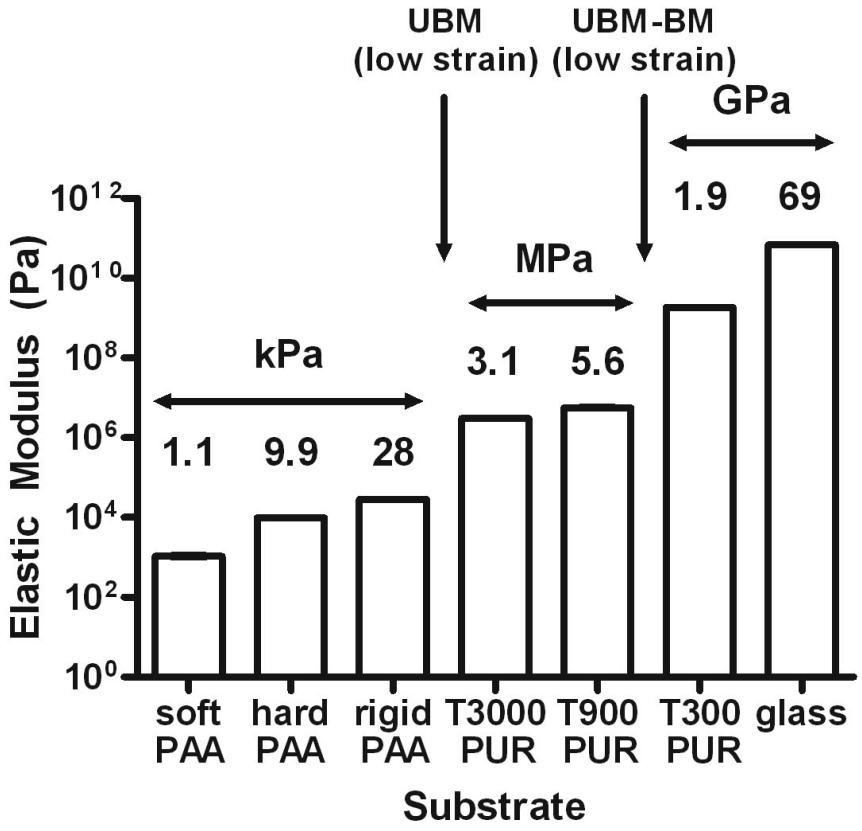

Figure 2.4. PAA, PUR, and glass substrates span eight orders of magnitude in rigidity. To isolate the effects of rigidity on invadopodia activity and span the MPA range of our stromal and BM model substrates, we synthesized PAA and PUR substrates with tunable rigidities. PAA elastic moduli were based on measurements of the storage modulus using rheometry for soft, hard [8] or rigid PAA. PUR elastic moduli were calculated by DMA mechanical testing. The glass elastic modulus was reported from the literature [39]. Data are presented as mean ± SE. Arrows indicate the rigidity regions relevant to the UBM and UBM-BM scaffolds. All elastic moduli were statistically significant from each other except between the T900 and T300 PUR substrates ($p=0.28$) (significances not shown on graph). $n=5$ and 4 for rigid PAA and all PUR substrates, respectively.

ECM degradation as a function of rigidity exhibits a positively skewed distribution with a maximum at 30 kPa

To assess regulation of invadopodia activity by substrate rigidity, CA1d breast carcinoma cells were cultured overnight on the FITC-Fn/gelatin/synthetic substrates, followed by fixation and immunostaining for the invadopodia markers actin and cortactin (Fig 2.5) and quantitation of invadopodia-associated ECM degradation and activity (Fig 2.6). As before [8], CA1d cells degraded more ECM on hard PAA (10 kPa) surfaces as compared to soft PAA (1 kPa) surfaces. Interestingly, however, there was a peak of ECM degradation activity with the highest ECM degradation/cell occurring on the rigid PAA (E=30 kPa) substrates, followed by the hard PAA (E=10 kPa) substrates (Fig 2.6A). Contrary to expectation, there was significantly less ECM degradation/cell on the more rigid PURs and glass substrates (Fig 2.6A).

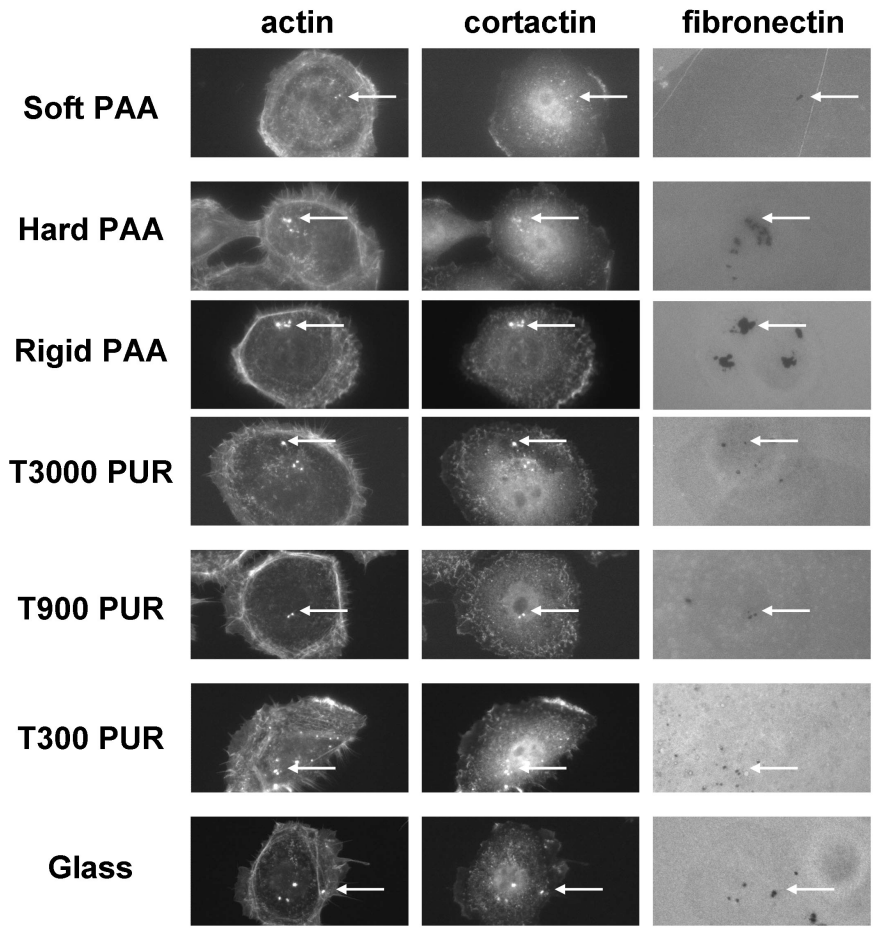

Figure 2.5. Optimal peak of invadopodia-associated ECM degradation on 10 and 30 kPa substrates. Culture of breast cancer cells on synthetic substrates gave a surprising peak of ECM degradation activity on the hard and rigid PAA substrates, with reduced degradation at higher rigidities. Representative wide-field immunofluorescence images of CA1d breast carcinoma cells after overnight culture on each of the rigidity substrates. Active degrading invadopodia are identified by colocalization of actin and cortactin-positive puncta with black degraded areas of the 1% gelatin/FITC fibronectin matrix (arrows).

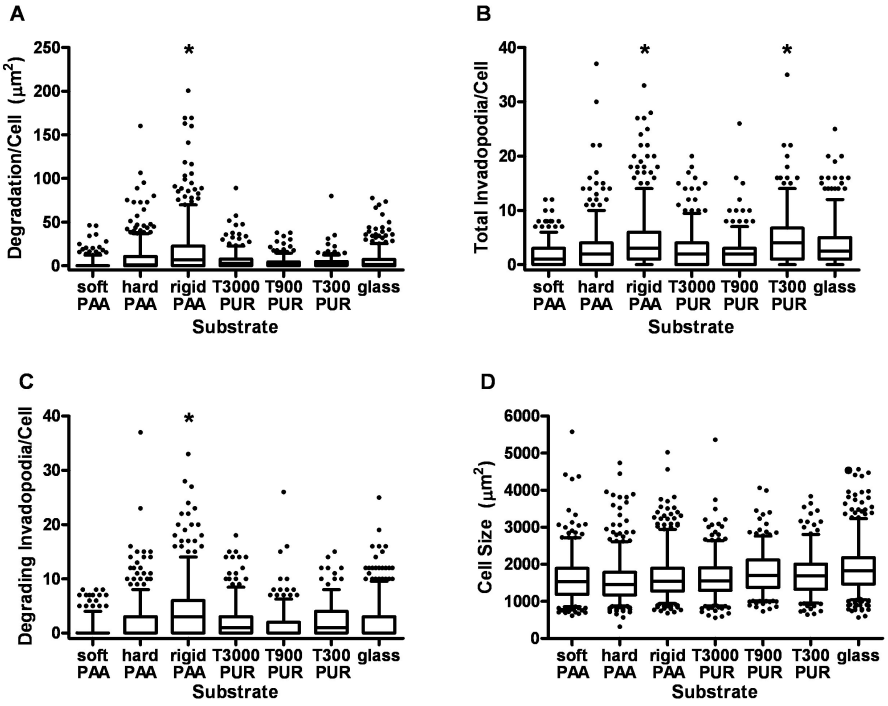

Figure 2.6. Quantification of invadopodia numbers and activity on synthetic substrates. **(A)** Degradation area/cell peaked statistically on the rigid PAA substrates (i.e., significantly different from all other substrates) with a median value of 6.68 μm². **(B)** Number of total invadopodia/cell (actively degrading and non-degrading) peaked statistically on both the rigid PAA (30 kPa) and T300 PUR (2 GPa) substrates with respective median values of 3 and 4. **(C)** Number of invadopodia actively degrading ECM/cell (as identified by colocalization of actin and cortactin over black areas only) peaked statistically only on the rigid PAA substrates with a median value of 3. **(D)** Cell size were significant between some substrates but not between the majority of comparisons (except glass which was significantly different than all other substrates but the T900 PUR; significances not shown on graph). Data are presented as box and whisker plots with solid lines indicating medians, whiskers representing 95% confidence intervals, and dots representing outliers. For comparisons depicted on the graphs, * indicates $p<0.05$ as described above for specific comparisons. For all statistical comparisons between groups, refer to Supp Table 1. n~300-500 cells for each substrate, from 4-6 independent experiments.

We observed a similar trend with bladder carcinoma cells in which degradation/cell peaks in the kPa range but decreases in the GPa range (Fig 2.7). In addition, quantification of the total invadopodia/cell gave two separate peaks, centered around the rigid PAA (E=30 kPa) and the most rigid PUR (T300, E = 1.8 GPa) (Fig 2.6B). These data suggest that cells not only sense a much wider rigidity range than previously thought [40, 41], but that rigidity affects two different contributing processes to invadopodia activity: invadopodia formation and ECM degrading capability. We also saw differences in gene expression across a wide range of rigidities (Fig 2.8), consistent with cellular sensing of rigidity in both the kPa and the MPa-GPa range. The number of degrading invadopodia/cell (Fig 2.6C) paralleled the ECM degradation/cell curve (Fig 2.6A), with a major peak of degradation activity on the rigid PAA (E=30 kPa) substrates. Cell size was not significantly altered and could not account for the observed differences in invadopodia activity (Fig 2.6D).

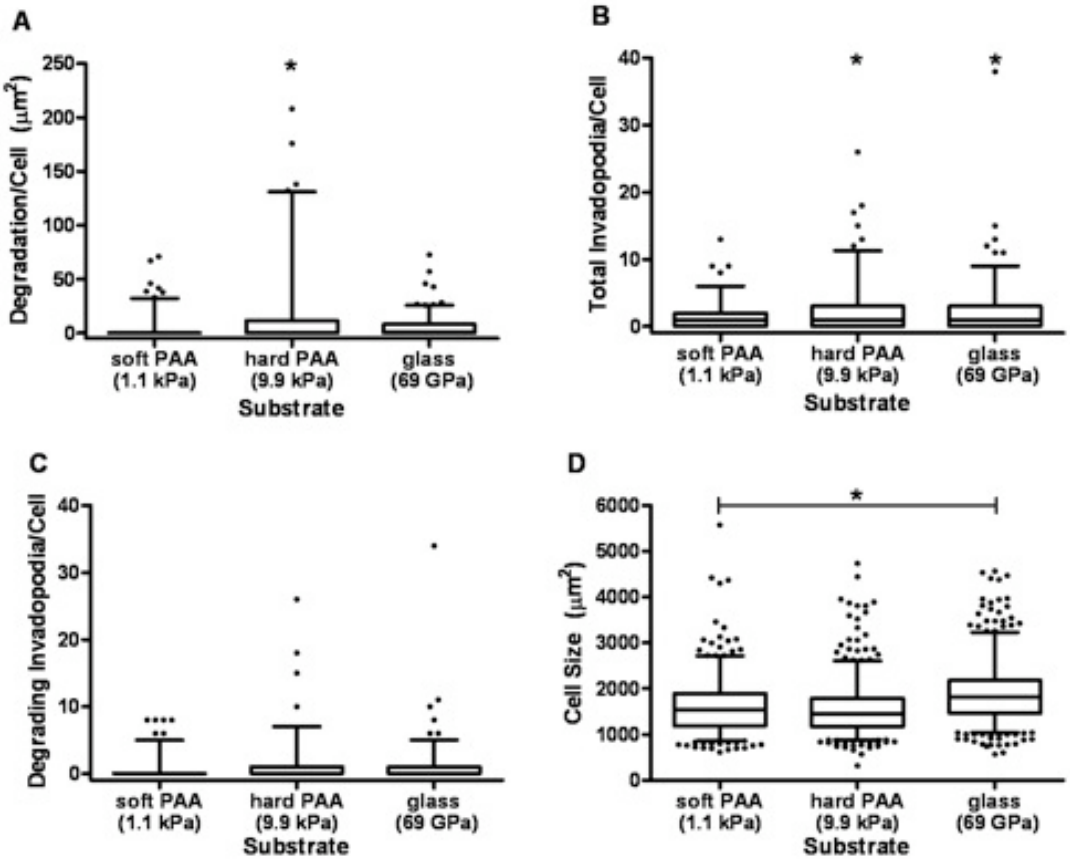

Figure 2.7. Quantification of invadopodia activity in 804G cells cultured on synthetic invadopodia substrates. (A) Similar to the results with CA1d cells, degradation area per cell peaked statistically on the hard PAA substrates (i.e., significantly different from the soft PAA and glass). (B) Number of total invadopodia (actively degrading and non-degrading) per cell peaked statistically on both the hard PAA (10 kPa) and the glass (69 GPa) (i.e., significantly different from the soft PAA but not each other). (C) Number of actively degrading invadopodia per cell (as identified by colocalization of actin and cortactin over black degraded areas only) were not statistically different although values were small since 804G cells do not make as many invadopodia/cell as CA1d cells. (D) Cell sizes on the soft PAA and glass were statistically significant from each other but neither were significantly different from the hard PAA value. Data were highly nonparametric and therefore presented as box and whisker plots with the solid lines indicating the medians, whiskers representing the 95% confidence intervals, and dots representing outliers. For comparisons depicted on the graphs, * indicates $p<0.05$ as described above for specific comparisons. n=143, 126, and 170 cells for the soft PAA, hard PAA, and glass substrates, respectively combined from 3 independent experiments.

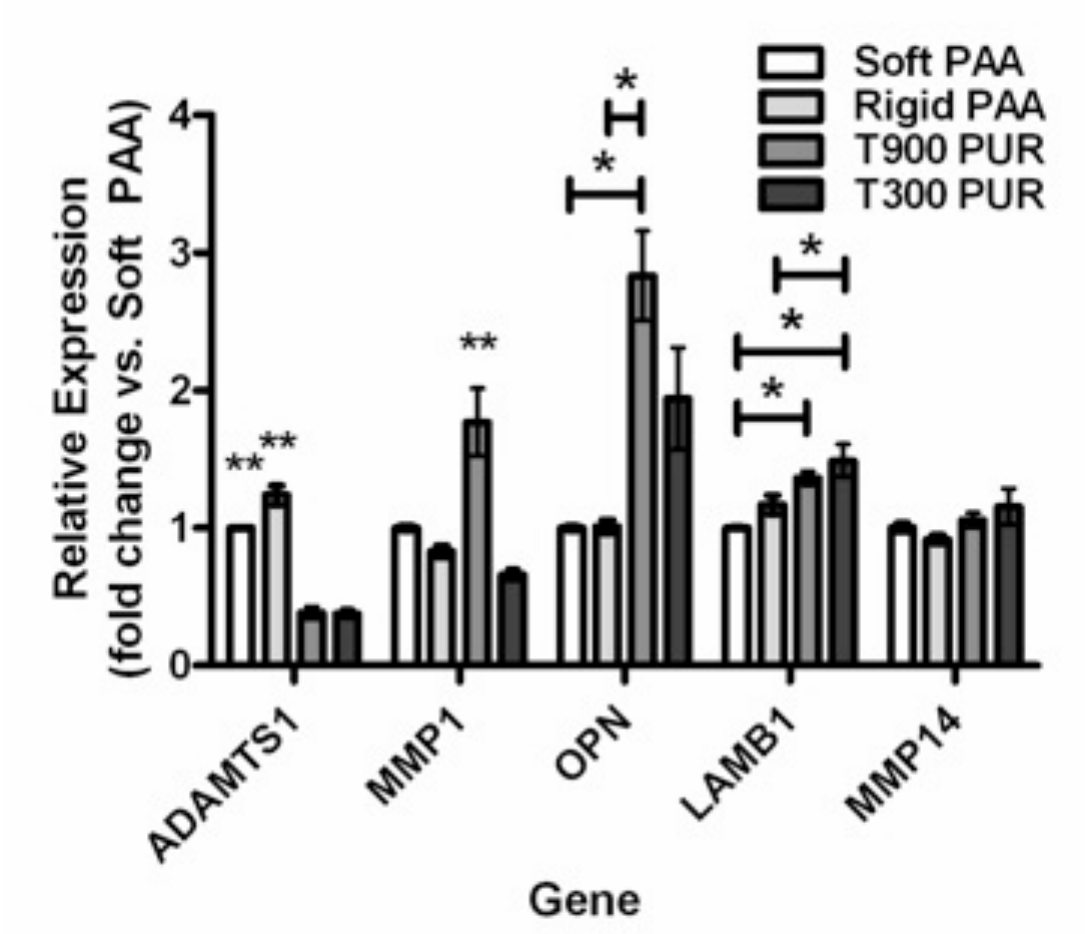

Figure 2.8. Gene expression in MCF10A CA1d breast carcinoma cells is regulated across a wide rigidity range. Relative fold changes in mRNA levels of ADAMTS1 (ADAM metallopeptidase with thrombospondin type 1 motif, 1) peaked on the more compliant PAAs (E=1-30 kPa) while MMP1 (matrix metallopeptidase 1) levels peaked on the more rigid T900 PUR (E=6 MPa). Significant differences were also found in expression levels between some of the PURs (E=6 MPa-2GPa) and PAAs (E=1-30 kPa) for OPN (osteopontin) and LAMB1 (laminin, beta1) as well indicating the ability of these cells to respond to different orders of magnitude in rigidity. No differences were found in the expression of MMP14 (matrix metallopeptidase 14) on any of the substrates. Data were normalized to 18S expression and shown as fold changes compared to the Soft PAA. Data are presented as mean ± standard error, and * and ** indicates $p<0.05$ for pairwise and group comparisons, respectively. Gene expression was measured in triplicate for each experiment and overall for 3 independent experiments on the 4 substrates.

Invadopodia formation is enhanced on the stromal side of UBM-BM versus the BM side.

Our data up to this point indicate that optimal invadopodia activity occurs in cells somewhere between 10 kPa - 3 MPa (Figs 2.5, 2.6A). For comparison, the mechanical analyses of stromal tissue give E=0.4 MPa (AFM) or 2 MPa (low strain DMA) and of BM tissue gave E=3 MPa (AFM) or 8 MPa (low strain DMA), suggesting that from the rigidity standpoint cells might have more invadopodia activity in stromal tissue than on BM. To test this hypothesis, CA1d breast carcinoma cells were seeded on either the BM or stromal side of UBM-BM overnight and fixed and stained for actin and cortactin as markers of invadopodia (Fig 2.9A-D). Widefield imaging was used for invadopodia quantification in CA1d cells (Fig 2.9A-B), while confocal imaging confirmed colocalization of the markers within the invadopodia structures and their formation on both surfaces (Fig. 2.9C-D). The vast majority of cells exhibited at least one invadopodium, 88% and 93% on the BM and stromal sides, respectively. Interestingly, cells seeded on the stromal side exhibited significantly more invadopodia/cell than on the BM side (Fig 2.9E) and were also larger in size (Fig 2.9F), suggesting that the softer substrate is indeed conducive to formation of invadopodia. In addition, we tested 804G bladder carcinoma cells and also found that more invadopodia/cell were formed on the stromal side than on the BM side (Fig 2.10) and that the majority of cells formed at least one invadopodium on the stromal and BM surfaces, 87% and 77%, respectively. The enhanced formation of invadopodia on the softer stromal side of the UBM-BM is consistent with an "optimal rigidity" regime in the 10 kPa-3MPa range identified in our

synthetic substrate studies (Fig 2.6), although we cannot rule out other contributing factors such as differences in ECM composition or topology.

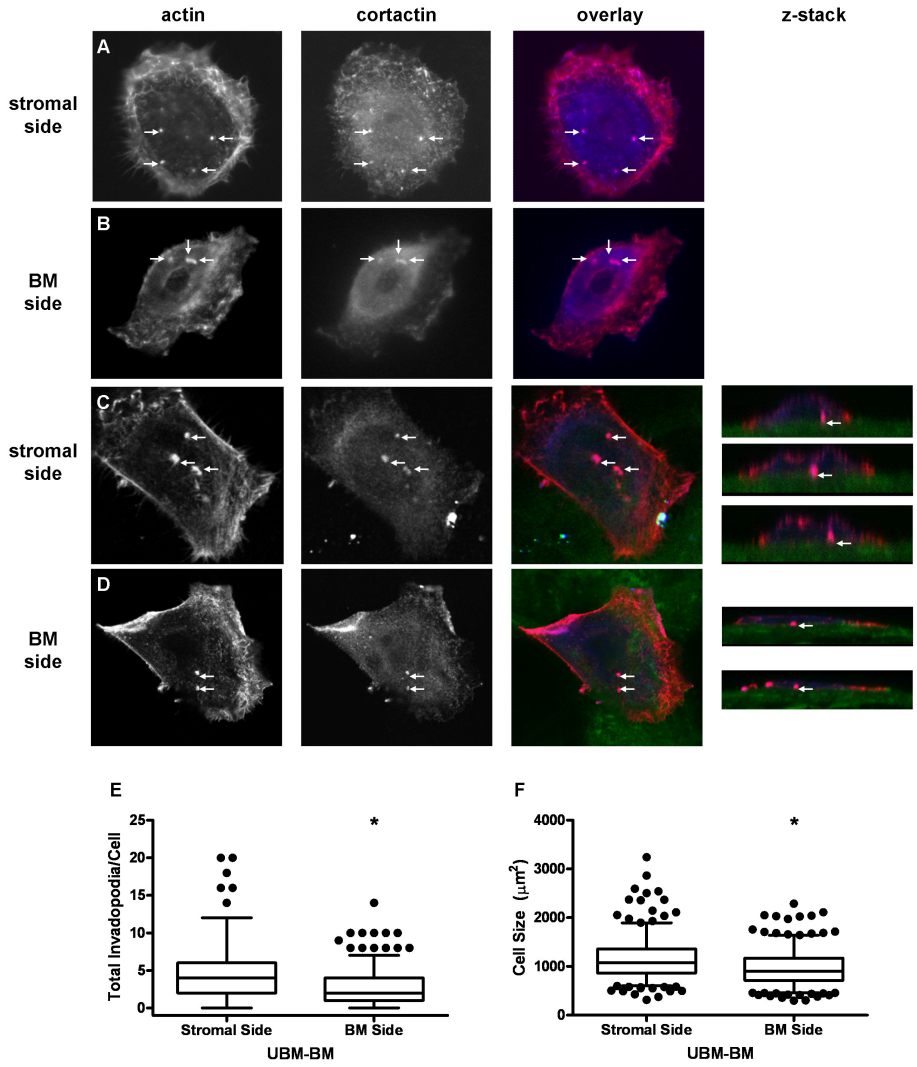

Figure 2.9. Invadopodia formation is enhanced on the stromal side of UBM-BM. To determine whether the stroma or BM are more permissive for formation of invadopodia, CA1d breast cancer cells were cultured overnight on the stromal or BM side of UBM-BM. Invadopodia (arrows) were identified by colocalization of actin (red) and cortactin (blue) for quantification on the **(A)** stroma or **(B)** BM using widefield fluorescence imaging and confirmed with confocal imaging **(C**, **D,** z-stacks**)**. The matrix surfaces were identified using collagen autofluorescence (green). **(E)** Quantification of invadopodia formation on the stromal and BM sides of UBM-BM reveals a statistically significant increase in the total invadopodia/cell in cells cultured on the stroma. **(F)** Cell size was statistically greater on the stroma as well. Data are presented as box and whisker plots with solid lines indicating medians, whiskers representing 95% confidence intervals, and dots representing outliers. * indicates $p<0.05$ for BM and stromal side comparisons. n~300 cells from 2 independent experiments.

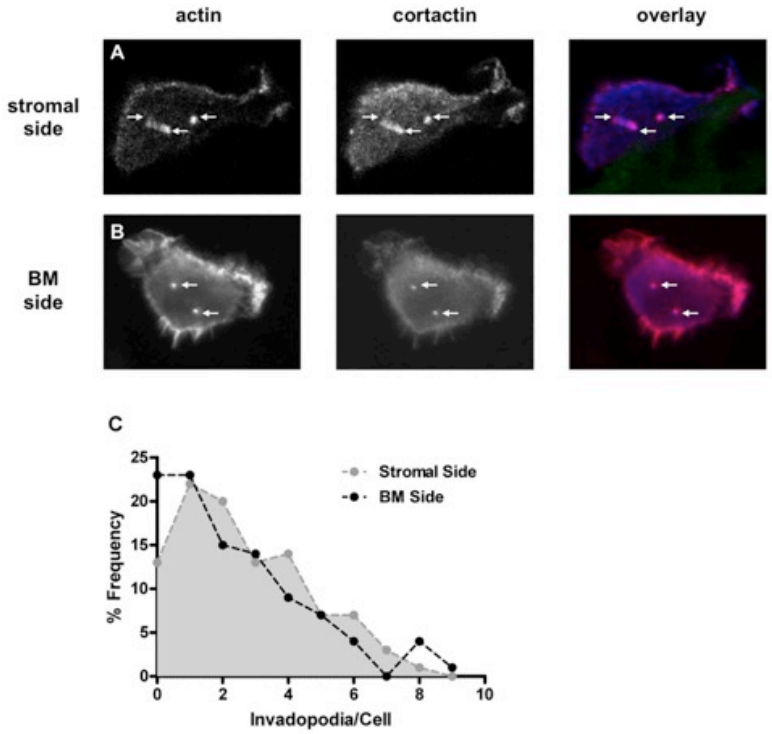

Figure 2.10. Quantification of invadopodia numbers in 804G cells plated on stromal and BM sides of UBM-BM. Invadopodia (arrows) were identified by colocalization of actin (red) and cortactin (blue) for quantification on the (A) stroma and (B) BM using confocal and widefield fluorescence imaging, respectively. (C) Quantitation of invadopodia formation by 804G bladder carcinoma cells reveals a statistically significant increase ($p<0.05$) in the total invadopodia per cell (based number of actin- and cortactin-double positive puncta) in cells cultured on the stromal side of UBM-BM, as compared to the BM side. Data were highly nonparametric and are presented as an area fill, and n=171 and 163 cells for the stromal and BM sides, respectively, from 2 independent experiments.

Discussion

Mechanical signals are known to regulate a myriad of biological phenomena including stem cell differentiation [19], cellular motility [18], tissue morphogenesis [3, 42], and invadopodia activity [8]. However, we and others have used a limited range of substrate rigidity to test cellular responses, generally 0.1-30 kPa [3, 18, 19]; thus it is unclear what the rigidity "ceiling" is for mechanosensing. It is also unclear how *in vivo* tissue rigidities correspond to *in vitro* cellular responses. In this study, we sought to determine the optimal rigidity range that promotes ECM degradation by invasive cancer cells and to connect our findings to tissue mechanics. Using both bulk tensile testing and nanoindentation methods we characterized the mechanical properties of both the stromal and BM components of urinary bladder-derived tissue scaffolds and found that BM had a rigidity of 3-8 MPa at low strains and stromal tissue was ~6-fold less rigid. Using synthetic substrates that span a wide range of rigidities, we found that breast cancer cells optimally degrade ECM on the ~30 kPa substrates with lower activity on substrates of higher rigidity (3 MPa-69 GPa). Interestingly, there were two peaks of invadopodia formation, located around ~30 kPa and 1.8 GPa, suggesting separate regulation of invadopodia formation and acquisition of proteolytic activity and indicating a very wide rigidity range that elicits cellular responses. Gene expression data also support a wide range of rigidity sensing by cells. Consistent with our synthetic substrate data, the stromal side of the tissue scaffold UBM-BM supported better formation of invadopodia by breast cancer cells than the BM side of UBM-BM. A similar trend was observed with bladder carcinoma cells. Overall, our data suggest that the high rigidity of BM can

serve as a restraining factor for invadopodia-associated ECM degradation and that cells can sense differences in rigidity even in the MPa-GPa range.

Tissue rigidity has recently been implicated as a microenvironmental factor that promotes the development and progression of breast cancers. In humans, mammographically dense breast tissue is associated with the development of invasive breast carcinomas [6, 7]. In mouse tumor studies, the accumulation and crosslinking of stromal collagen fibers was shown to directly promote formation and invasion of mammary tumors [4, 43]. Mechanotransduction signaling is thought to be critical for all of these effects [3, 5, 42, 43]. With regard to the rigidity of breast tissue, which represents a mixture of adipose, collagenous stromal, and ductal epithelial components, various elastic moduli have been reported. Similar to our tensile DMA data in which the elastic moduli were in the low MPa range for the stromal-dominated UBM, tensile loading of breast tissue has yielded an apparent peak elastic modulus of 2.2 MPa [44]. However, indentation testing by several groups using 4-5 mm diameter tips has yielded much softer moduli, with a range of 167 Pa-30 kPa for normal tissue and 10-90 kPa for carcinomatous tissue [3, 45-47]. Using AFM (25-40 nm tips), we obtained an intermediate average elastic modulus of 400 kPa for the stromal component of UBM-BM. These differences may be due to the different modes of deformation, the percent strain that was tested, and mechanical differences in bladder versus breast stroma. Our data do not resolve these differences, nor can our tests indicate what cells feel in the heterogenous local breast microenvironment; however, our data do indicate that the stroma is less rigid than the BM. Furthermore, stromal tissue is much closer in rigidity to the optimal

rigidity range for invadopodia activity as defined using uniform synthetic substrates of tunable rigidity. While the length scale at which matrix rigidity is probed has a significant effect on the measured mechanical properties of stromal tissue, testing results for BM have been more consistent between nanoindentation versus macroscopic testing methods. Both techniques yield elastic moduli in the 1-20 MPa range [35, 36, 48], likely because the tissue properties do not change greatly across the nano-, micro-, and macroscale due to the high degree of crosslinking, small pore size and uniformity of the matrix composition [1, 2].

This study used two different experimental systems to compare the effect of rigidity on invadopodia formation: native tissue scaffolds and synthetic substrates. The synthetic substrate data is much more controlled, because of the ability to tune rigidity without changing other parameters. However, both the mechanical testing and invadopodia experiments with the tissue scaffolds gives context to our findings with the synthetic substrates. Based on elastic moduli measurements, the total invadopodia numbers for breast and bladder cancer cells cultured on the BM and stromal sides of UBM-BM fits the trend seen for the polymer substrates. Thus, more invadopodia were formed on the stromal component, which is closer in elastic modulus to the peak seen on the 30 kPa rigid PAA than is the BM substrate. Correlating the invadopodia numbers to degradation, these results would suggest that the stroma may be more conducive to degradation than the BM when considering rigidity as the predominant factor. If we theoretically extrapolate on this finding and consider the early events in invasion as the BM is broken down by proteolysis at the primary tumor site, the BM will begin to weaken causing a

decrease in elastic modulus and, according to our data, a shift to the left of the degradation curve suggesting an increase in degradation. However, we must emphasize that the topology and chemical components of the ECM will also have an impact on cellular phenotype [49]. In addition, ECM degradation is not the only factor that will affect invasion in a 3-dimensional matrix [50]. Nonetheless, substrate stiffness has been shown to be more important in determining cell shape than adhesive ligand density [51], implying that rigidity has an extremely strong influence on cellular behavior. In addition, chemical components could synergize with rigidity to limit invasiveness on BM substrates, e.g. the BM component Laminin-332 was recently shown to limit invadopodia formation [52].

One of the most interesting findings of this study is that cells can apparently sense a wide range of rigidity, from kPa to GPa. This conclusion is supported by three major pieces of data. First, we find a peak of invadopodia-associated ECM degradation activity at ~30 kPa, with reduction in activity at higher rigidities. More convincingly, there are two significant peaks of total invadopodia formation associated with substrate rigidity, one at ~30 kPa and the other at 1.8 GPa. Finally, we find regulation of gene expression across this same range (kPa-GPa). Thus, although above a certain rigidity (e.g. 100 kPa) cells are thought to be performing isometric exercise [40, 41] and might not feel differences from contraction, our data indicate that cells can sense rigidity differences even on highly rigid substrates. Since some physiologic substrates, such as BM and bone, are in the MPa-GPa range [35, 53, 54], it seems likely that mechanosensing across the full range could appropriately regulate behavior. Consistent with that idea, a recent study using

substrates with kPa-GPa moduli has shown that preosteoblastic cells differentially sense and respond to moduli above 100 kPa by changing gene and protein expression [55, 56]. Likewise, breast and other cancer cell types that metastasize to bone may also experience low GPa rigidities, since calcified bone has an elastic modulus reported to be 10-30 GPa by both nanoindentation and tensile testing methods [21, 57]. We speculate that differential sensing between MPa and GPa rigidities, combined with other contextual cues, might allow cells to distinguish between BM and bone. Nonetheless, future studies should investigate whether other cellular responses are altered in high rigidity regimes and how cell type of origin affects rigidity sensing at different matrix elasticities.

References

1. Rowe, R. G., and S. J. Weiss. 2008. Breaching the basement membrane: who, when and how? *Trends in cell biology* 18:560-574.
2. Kalluri, R. 2003. Basement membranes: structure, assembly and role in tumour angiogenesis. *Nat Rev Cancer* 3:422-433.
3. Paszek, M. J., N. Zahir, K. R. Johnson, J. N. Lakins, G. I. Rozenberg, A. Gefen, C. A. Reinhart-King, S. S. Margulies, M. Dembo, D. Boettiger, D. A. Hammer, and V. M. Weaver. 2005. Tensional homeostasis and the malignant phenotype. *Cancer Cell* 8:241-254.
4. Provenzano, P. P., D. R. Inman, K. W. Eliceiri, J. G. Knittel, L. Yan, C. T. Rueden, J. G. White, and P. J. Keely. 2008. Collagen density promotes mammary tumor initiation and progression. *BMC medicine* 6:11.
5. Provenzano, P. P., D. R. Inman, K. W. Eliceiri, and P. J. Keely. 2009. Matrix density-induced mechanoregulation of breast cell phenotype, signaling and gene expression through a FAK-ERK linkage. *Oncogene* 28:4326-4343.
6. Vacek, P. M., and B. M. Geller. 2004. A prospective study of breast cancer risk using routine mammographic breast density measurements. *Cancer Epidemiol Biomarkers Prev* 13:715-722.
7. Boyd, N. F., J. M. Rommens, K. Vogt, V. Lee, J. L. Hopper, M. J. Yaffe, and A. D. Paterson. 2005. Mammographic breast density as an intermediate phenotype for breast cancer. *Lancet Oncol* 6:798-808.
8. Alexander, N. R., K. M. Branch, A. Parekh, E. S. Clark, I. C. Iwueke, S. A. Guelcher, and A. M. Weaver. 2008. Extracellular Matrix Rigidity Promotes Invadopodia Activity. *Curr Biol* 18:1295-1299.
9. Weaver, A. M. 2008. Invadopodia. *Curr Biol* 18:R362-364.
10. Parekh, A., and A. M. Weaver. 2009. Regulation of cancer invasiveness by the physical extracellular matrix environment. *Cell adhesion & migration* 3:288-292.
11. Sabeh, F., R. Shimizu-Hirota, and S. J. Weiss. 2009. Protease-dependent versus -independent cancer cell invasion programs: three-dimensional amoeboid movement revisited. *J Cell Biol* 185:11-19.
12. Hotary, K., X. Y. Li, E. Allen, S. L. Stevens, and S. J. Weiss. 2006. A cancer cell metalloprotease triad regulates the basement membrane transmigration program. *Genes Dev* 20:2673-2686.
13. Akgul, B., R. Garcia-Escudero, L. Ghali, H. J. Pfister, P. G. Fuchs, H. Navsaria, and A. Storey. 2005. The E7 protein of cutaneous human papillomavirus type 8 causes invasion of human keratinocytes into the dermis in organotypic cultures of skin. *Cancer Res* 65:2216-2223.
14. McDaniel, S. M., K. K. Rumer, S. L. Biroc, R. P. Metz, M. Singh, W. Porter, and P. Schedin. 2006. Remodeling of the mammary microenvironment after lactation promotes breast tumor cell metastasis. *Am J Pathol* 168:608-620.
15. Badylak, S. F. 2004. Xenogeneic extracellular matrix as a scaffold for tissue reconstruction. *Transpl Immunol* 12:367-377.

16. Brown, B., K. Lindberg, J. Reing, D. B. Stolz, and S. F. Badylak. 2006. The basement membrane component of biologic scaffolds derived from extracellular matrix. *Tissue engineering* 12:519-526.
17. Gilbert, T. W., S. Wognum, E. M. Joyce, D. O. Freytes, M. S. Sacks, and S. F. Badylak. 2008. Collagen fiber alignment and biaxial mechanical behavior of porcine urinary bladder derived extracellular matrix. *Biomaterials* 29:4775-4782.
18. Pelham, R. J., Jr., and Y. Wang. 1997. Cell locomotion and focal adhesions are regulated by substrate flexibility. *Proc Natl Acad Sci U S A* 94:13661-13665.
19. Engler, A. J., S. Sen, H. L. Sweeney, and D. E. Discher. 2006. Matrix elasticity directs stem cell lineage specification. *Cell* 126:677-689.
20. Engler, A. J., F. Rehfeldt, S. Sen, and D. E. Discher. 2007. Microtissue elasticity: measurements by atomic force microscopy and its influence on cell differentiation. *Methods in cell biology* 83:521-545.
21. Moore, S. W., P. Roca-Cusachs, and M. P. Sheetz. 2010. Stretchy proteins on stretchy substrates: the important elements of integrin-mediated rigidity sensing. *Dev Cell* 19:194-206.
22. Nemir, S., and J. L. West. 2010. Synthetic materials in the study of cell response to substrate rigidity. *Ann Biomed Eng* 38:2-20.
23. Guelcher, S. A. 2008. Biodegradable polyurethanes: synthesis and applications in regenerative medicine. *Tissue engineering* 14:3-17.
24. Oertel, G. 1994. Polyurethane Handbook. Hanser Publications, Munich.
25. Freytes, D. O., S. F. Badylak, T. J. Webster, L. A. Geddes, and A. E. Rundell. 2004. Biaxial strength of multilaminated extracellular matrix scaffolds. *Biomaterials* 25:2353-2361.
26. Yurchenco, P. D., and G. C. Ruben. 1987. Basement membrane structure in situ: evidence for lateral associations in the type IV collagen network. *The Journal of cell biology* 105:2559-2568.
27. Storey, R. F., J. S. Wiggins, and A. D. Puckett. 1994. Hydrolyzable poly(ester-urethane) networks from L-lysine diisocyanate and D,L-lactide/e-caprolactone homo- and copolyester triols. *Journal of Polymer Science Part A: Polymer Chemistry* 32:2345-2363.
28. Kandow, C. E., P. C. Georges, P. A. Janmey, and K. A. Beningo. 2007. Polyacrylamide hydrogels for cell mechanics: steps toward optimization and alternative uses. *Methods in cell biology* 83:29-46.
29. Guelcher, S., A. Srinivasan, A. Hafeman, K. Gallagher, J. Doctor, S. Khetan, S. McBride, and J. Hollinger. 2007. Synthesis, in vitro degradation, and mechanical properties of two-component poly(ester urethane)urea scaffolds: effects of water and polyol composition. *Tissue engineering* 13:2321-2333.
30. Inoue, S. 1994. Basic structure of basement membranes is a fine network of "cords," irregular anastomosing strands. *Microscopy research and technique* 28:29-47.
31. Fung, Y. 1997. Biomechanics: Mechanical Properties of Living Tissues. Springer-Verlag, New York.
32. Gilbert, T. W., M. S. Sacks, J. S. Grashow, S. L. Woo, S. F. Badylak, and M. B. Chancellor. 2006. Fiber kinematics of small intestinal submucosa under

biaxial and uniaxial stretch. *Journal of biomechanical engineering* 128:890-898.
33. Freytes, D. O., R. M. Stoner, and S. F. Badylak. 2008. Uniaxial and biaxial properties of terminally sterilized porcine urinary bladder matrix scaffolds. *J Biomed Mater Res B Appl Biomater* 84:408-414.
34. Machalek, A. 2005. An Owner's Guide to the Cell. In Inside the Cell. NIGMS, editor. NIGMS.
35. Candiello, J., M. Balasubramani, E. M. Schreiber, G. J. Cole, U. Mayer, W. Halfter, and H. Lin. 2007. Biomechanical properties of native basement membranes. *The FEBS journal* 274:2897-2908.
36. Candiello, J., G. J. Cole, and W. Halfter. Age-dependent changes in the structure, composition and biophysical properties of a human basement membrane. *Matrix Biol* 29:402-410.
37. Chan, B. P., and K. F. So. 2005. Photochemical crosslinking improves the physicochemical properties of collagen scaffolds. *Journal of biomedical materials research* 75:689-701.
38. Yeung, T., P. C. Georges, L. A. Flanagan, B. Marg, M. Ortiz, M. Funaki, N. Zahir, W. Ming, V. Weaver, and P. A. Janmey. 2005. Effects of substrate stiffness on cell morphology, cytoskeletal structure, and adhesion. *Cell motility and the cytoskeleton* 60:24-34.
39. Callister, W. 2000. Fundamentals of Material Science and Engineering: An Interactive E-Text. John Wiley & Sons, Inc., Somerset, NJ.
40. Discher, D. E., P. Janmey, and Y. L. Wang. 2005. Tissue cells feel and respond to the stiffness of their substrate. *Science (New York, N.Y* 310:1139-1143.
41. Wells, R. G., and D. E. Discher. 2008. Matrix elasticity, cytoskeletal tension, and TGF-beta: the insoluble and soluble meet. *Science signaling* 1:pe13.
42. Wozniak, M. A., R. Desai, P. A. Solski, C. J. Der, and P. J. Keely. 2003. ROCK-generated contractility regulates breast epithelial cell differentiation in response to the physical properties of a three-dimensional collagen matrix. *J Cell Biol* 163:583-595.
43. Levental, K. R., H. Yu, L. Kass, J. N. Lakins, M. Egeblad, J. T. Erler, S. F. Fong, K. Csiszar, A. Giaccia, W. Weninger, M. Yamauchi, D. L. Gasser, and V. M. Weaver. 2009. Matrix crosslinking forces tumor progression by enhancing integrin signaling. *Cell* 139:891-906.
44. Edsberg, L. E., R. Cutway, S. Anain, and J. R. Natiella. 2000. Microstructural and mechanical characterization of human tissue at and adjacent to pressure ulcers. *Journal of rehabilitation research and development* 37:463-471.
45. Krouskop, T. A., T. M. Wheeler, F. Kallel, B. S. Garra, and T. Hall. 1998. Elastic moduli of breast and prostate tissues under compression. *Ultrason Imaging* 20:260-274.
46. Samani, A., J. Zubovits, and D. Plewes. 2007. Elastic moduli of normal and pathological human breast tissues: an inversion-technique-based investigation of 169 samples. *Phys Med Biol* 52:1565-1576.
47. Van Houten, E. E. W., M. M. Doyley, F. E. Kennedy, J. B. Weaver, and K. D. Paulsen. 2003. Initial in vivo experience with steady-state subzone-based MR

elastography of the human breast. *Journal of Magnetic Resonance Imaging* 17:72-85.
48. Welling, L. W., M. T. Zupka, and D. J. Welling. 1995. Mechanical-Properties of Basement-Membrane. *News in Physiological Sciences* 10:30-35.
49. Geiger, B., J. P. Spatz, and A. D. Bershadsky. 2009. Environmental sensing through focal adhesions. *Nature reviews* 10:21-33.
50. Brabek, J., C. T. Mierke, D. Rosel, P. Vesely, and B. Fabry. The role of the tissue microenvironment in the regulation of cancer cell motility and invasion. *Cell Commun Signal* 8:22.
51. Engler, A. J., M. A. Griffin, S. Sen, C. G. Bonnemann, H. L. Sweeney, and D. E. Discher. 2004. Myotubes differentiate optimally on substrates with tissue-like stiffness: pathological implications for soft or stiff microenvironments. *The Journal of cell biology* 166:877-887.
52. Liu, S., H. Yamashita, B. Weidow, A. M. Weaver, and V. Quaranta. Laminin-332-beta1 integrin interactions negatively regulate invadopodia. *Journal of cellular physiology* 223:134-142.
53. Welling, L. W., M. T. Zupka, and D. J. Welling. 1995. Mechanical properties of basement membrane. *News Physiol Sci* 10:30-35.
54. Nyman, J. S., H. Leng, X. Neil Dong, and X. Wang. 2009. Differences in the mechanical behavior of cortical bone between compression and tension when subjected to progressive loading. *Journal of the mechanical behavior of biomedical materials* 2:613-619.
55. Khatiwala, C. B., S. R. Peyton, M. Metzke, and A. J. Putnam. 2007. The regulation of osteogenesis by ECM rigidity in MC3T3-E1 cells requires MAPK activation. *Journal of cellular physiology* 211:661-672.
56. Smith, K. E., S. L. Hyzy, M. Sunwoo, K. A. Gall, Z. Schwartz, and B. D. Boyan. The dependence of MG63 osteoblast responses to (meth)acrylate-based networks on chemical structure and stiffness. *Biomaterials* 31:6131-6141.
57. Chevalier, Y., D. Pahr, H. Allmer, M. Charlebois, and P. Zysset. 2007. Validation of a voxel-based FE method for prediction of the uniaxial apparent modulus of human trabecular bone using macroscopic mechanical tests and nanoindentation. *J Biomech* 40:3333-3340.

CHAPTER III

MATRIX RIGIDITY INDUCES OSTEOLYTIC GENE EXPRESSION OF METASTATIC BREAST CANCER CELLS

Introduction

Nearly 70% of breast cancer patients with advanced disease will develop bone metastases that are commonly associated with pain, hypercalcemia, and pathologic fracture [1]. Once established in bone, tumor cells begin to produce factors that cause changes in normal bone remodeling. The best-described example is the expression of parathyroid hormone-related protein (PTHrP), which is expressed at higher levels in bone metastases from breast cancers than it is in isolated primary tumors or soft tissue metastases [2,3]. In the bone microenvironment, enhanced expression of PTHrP stimulates osteoclasts to resorb bone [4]. As the bone is resorbed, the release of transforming growth factor beta (TGF-β) from the bone matrix contributes to further increase PTHrP expression [5]. Thus, while TGF-β released from the bone matrix sustains the "vicious cycle" of bone resorption in the later stages of bone disease, the environmental factors driving tumor cells to express PTHrP in the early stages of development of metastatic bone disease prior to bone resorption are unknown.

In addition to its osteolyic function in metastatic bone disease, PTHrP also performs a number of normal physiological functions, including the regulation of smooth muscle tone. Mechanically transduced signals have been shown to regulate

PTHrP expression and secretion in a variety of smooth muscle beds [6]. Mechanical distension of the abdominal aorta [7], the uterus, and the bladder [8] in rats increased PTHrP expression by a factor of two or more. Because of the dramatically ($\sim 10^6$) higher rigidity of mineralized bone tissue compared to breast tissue, tumor cells are likely to generate higher cytoskeleton-dependent forces in the bone microenvironment. Therefore, we hypothesized that the differential rigidity of the bone microenvironment might influence PTHrP expression by tumor cells through mechanically transduced signals.

Previous studies have shown that matrix rigidity regulates invasiveness at the primary site [9,10]. When cells encounter a mechanically rigid matrix, integrins become activated, which stimulates RhoGTPase-dependent actomyosin contractility. However, while normal cells tune their contractility in response to matrix rigidity, tumor cells exhibit altered tensional homeostasis, as evidenced by their higher contractility and spreading relative to non-malignant mammary epithelial cells on compliant matrices [11]. Inhibition of RhoGTPase signaling in tumor cells by treating with Rho-associated kinase (ROCK) inhibitors reduces tumor cell contractility and spreading [11]. Additionally, ROCK expression is higher in metastatic human mammary tumors relative to non-metastatic tumors, and inhibition of ROCK signaling decreases cell proliferation *in vitro* and metastasis to bone *in vivo* [12].

To test our hypothesis that cytoskeleton-dependent forces regulate PTHrP expression in tumor cells, we designed a 2D tumor cell mono-culture system. Previous studies investigating the effects of matrix rigidity on cell migration,

differentiation, and invasion have utilized *in vitro* cell culture on 2D model substrates, such as Matrigel™ [13,14], crosslinked gelatin [15], and synthetic hydrogels [16,17]. However, the applicability of these substrates to the bone microenvironment is limited, due to the inability to achieve a sufficiently high elastic modulus that is relevant to mineralized bone tissue. In this study, we prepared polyacrylamide (PAA) hydrogels as a model for breast tissue and poly(ester urethane) films [18,19] as a model for tissues ranging from the basement membrane to bone. We measured changes in gene expression by metastatic tumor cells in response to the rigidity of the substrate. In addition, we investigated the effects of ROCK and TGF-β inhibition and stimulation using pharmacological agents and genetically modified cells to identify the signaling pathways through which rigidity regulates gene expression.

Materials and Methods

Materials

Materials synthesis. Methyl 2,6-diisocyanatohexane (lysine methyl ester diisocyanate, LDI) was purchased from Kyowa Hakko USA (New York, NY). The structures of these polyisocyanates are shown in Figure 3.1. Coscat 83, an organobismuth urethane catalyst, was supplied by ChasChem, Inc. (Rutherford, NJ). Stannous octoate, glycerol, poly(e-caprolactone) triol (300 Da), and e-caprolactone were purchased from Aldrich (St. Louis, MO), and glycolide was purchased from Polysciences (Warrington, PA). Glycerol was dried at 10 mm Hg for 3 hours at 80°C and e-caprolactone was dried over anhydrous magnesium sulfate prior to use. All

other materials were used as received. Two-component cast poly(ester urethane)s were mixed using a Hauschild SpeedMixer™ DAC 150 FVZ-K (FlackTek Inc., Landrum, SC).

Cell culture. Dulbecco's modification of Eagle's medium (DMEM) and McCoy's 5A were purchased from Invitrogen (Carlsbad, CA). Fetal bovine serum (FBS) was purchased from Hyclone Laboratories (Logan, UT). Penicillin, streptomycin, L-glutamine, trypsin, sodium pyruvate, essential and non-essential amino acids were all acquired from Mediatech (Manassas, VA). MDA-MB-231, RWGT2 and MCF-7 cells were purchased from ATCC (Manassas, VA). MDA-MB-231 and RWGT2 cells were then selected for ability to metastasize to bone [20].

Antibodies, Primers and Reagents. The RNeasy™ mini kit was purchased from Qiagen (Valencia, CA). Superscript III cDNA synthesis kits were purchased from Invitrogen (Carlsbad, CA). qPCR primers for PTHrP, Gli2, TGF-β and 18S (TaqMan) were obtained from Applied Biosciences (Carlsbad, CA), while primers for OPN, IL11, CXCR4, MMP9 and 18S (SYBR) were purchased from Operon (Huntsville, AL) [21]. The PTHrP immunoradiometric assay was purchased from Diagnostic Systems Labs (Brea, CA). Antibodies for phopho-myosin light chain 2 (Ser19, Ser19/Thr18) and anti-Rabbit IgG were procured from Cell Signaling Technologies (Danvers, MA), while β-actin and Fibronectin antibodies came from Sigma (St. Louis, MO) and Millipore (Billerica, MA), respectively. The ECL chemiluminescence kit was purchased from Amersham (Piscataway, NJ) while the ABTS substrate kit was produced by Vector Laboratories (Burlingame, CA). The mechanotransduction inhibitors Blebbistatin and Y27632 were both procured from Sigma (St. Louis, MO).

Methods

Synthesis of substrates for in vitro studies. Polyurethane (PUR) films and polyacrylamide (PAA) hydrogels were synthesized to provide 2D substrates with elastic moduli ranging from ~1kPa to > 1 GPa for *in vitro* studies of mechanosensitivity. PUR substrates were synthesized by reactive liquid molding of a lysine methyl ester diisocyanate (LDI) quasi-prepolymer, a poly(e-caprolactone-*co*-glycolide) triol, and COSCAT 83 bismuth catalyst using published techniques.[18] Briefly, the quasi-prepolymer was synthesized by charging poly(e-caprolactone) (PCL, 300 g mol^{-1}) to a flask fitted with a reflux condenser and heated to 60°C in an oil bath. Lysine diisocyanate methyl ester (LDI, Kyowa Hakko) was then charged, the reactor immersed in an oil bath maintained at 90°C, and Coscat 83 was added while stirring under dry argon. The reaction was allowed to proceed for three hours under vacuum at 90°C, at which time the reactor was purged with dry argon and the quasi-prepolymer was poured into a vessel stored at 4°C. Structure was verified by nuclear magnetic resonance spectroscopy (NMR, Bruker, 300 MHz), molecular weight was measured by GPC, and % free NCO was measured by titration.

Polyester triols ranging from 300 to 3000 g mol^{-1} (100 – 1000 g eq^{-1}) were synthesized from a glycerol starter, 70% e-caprolactone and 30% glycolide monomers, and stannous octoate catalyst as described previously.[22] Briefly, the appropriate amounts of dried glycerol, dried e-caprolactone, glycolide, and stannous octoate (0.1 wt-%) were mixed in a 100-ml flask and heated under an argon atmosphere with mechanical stirring to 135°C. The mixture was allowed to react for ~30 h and subsequently removed from the oil bath. NMR was used to verify the

structure of the polyester triols, with deuterated dichloromethane (DCM) as a solvent. The hydroxyl (OH) number was measured by titration (Metrohm 798 MPT Titrino) according to ASTM D-4662-93 as described.[18] Substrates were synthesized by mixing an appropriate amount of poly(e-caprolactone-*co*-glycolide) triol with LDI quasi-prepolymer, and COSCAT 83 catalyst (Vertellus) for 20s in a Hauschild SpeedMixer™ DAC 150 FVZ-K vortex mixer (FlackTek, Inc, Landrum, SC). The targeted index (ratio of NCO to OH equivalents times 100) was 105. The resultant mixture was poured into the wells of a tissue culture plate and allowed to cure for 24h at 60°C. To facilitate cell adhesion and ensure that the surface chemistry was constant for all substrates tested, fibronectin (Fn) was adsorbed to the surface of the substrates by incubating them in a 4μg/mL solution of Fn in PBS at 4°C overnight.

Polyacrylamide (PAA) hydrogels were synthesized by copolymerizing a 10% solution of acrylamide and bis-acrylamide in water via free-radical polymerization using a redox pair of initiators (tetramethyl ethylene diamine (TEMED) and 10% ammonium persulphate (APS) in water). Additionally, acrylic acid N-hydrosuccinimide (NHS) ester was copolymerized to the surface of the gels. The NHS-acrylate layer was then allowed to react with a solution of Fn in HEPES. To measure the surface concentration of Fn, coated substrates were incubated in a solution of Fn antibody (1:1000) followed by incubation with a secondary HRP-conjugated antibody. The relative amount of adsorbed antibody was then quantified by reaction with 2'-azino-bis(3-ethylbenzthiazoline-6-sulphonic acid) (ABTS) and subsequent optical density reading at 405nm. All PUR and PAA substrates were

prepared at the same surface concentration of Fn that yielded an optical density of 0.12 absorbance units cm^{-2}.

Dynamic mechanical properties of substrates. Tensile modulus and strength of the PUR films were measured at 37°C for 3×15×1mm films using a TA Instruments Q800 DMA (controlled force displacement ramp, 1 N min^{-1} to 18 N min^{-1}) [22]. Storage and loss moduli for the polyacrylamide gels under shear conditions were measured using a TA Instruments AR-G2 Rheometer (TA Instruments, New Castle, DE) at 37°C, using a 20-mm circular head as described previously.[15,23] Gels were compressed between a heated Peltier plate and a 20-mm upper plate and subjected to an oscillating (0.1 – 10 Hz) shear strain that was validated to be in the linear range by strain sweep tests.

Swelling experiments and calculation of network mesh size. To determine the mesh size of the polymer network, PUR substrates were swollen in dichloromethane for 24h at room temperature, while PAA gels were swollen in water and subsequently lyophilized to determine swelling ratios. The molecular weight between crosslinks, M_c , was then determined with the Flory-Rehner equation[24],

$$-\left[\ln(1-v_2)+v_2+\chi_1 v_2^2\right]=V_1 n\left[v_2^{\frac{1}{3}}-\frac{v_2}{2}\right] \tag{3.1}$$

where v_2 is the volume fraction of the polymer in the swollen mass, χ_1 is the Flory-Huggins interaction parameter, V_1 is the molar volume of the solvent, and *n* represents the number of active network chain segments per unit volume. The molecular weight between crosslinks is then given by

$$M_c = \frac{\rho}{n} \tag{3.2}$$

where ρ is the density of the polymer network and *n* is the crosslink density (mol cm^{-3}). Mesh size, x_i, was then estimated by [25]

$$x_i = 2.24 l \left(\nu_2^{-\frac{1}{3}} \sqrt{\frac{2M_c}{M_r}} \right) \tag{3.3}$$

where M_r is the molecular weight of the repeat unit and l is the carbon-carbon bond length. Assuming the materials were perfectly elastic (Poisson's ratio n = 0.5), the elastic and shear moduli (*E, G)* are related to the crosslink density:

$$E = 3nRT \tag{3.4}$$

$$E = 3G \tag{3.5}$$

Cell culture. MDA-MB-231 and RWGT2 cells were maintained and cultured at 37°C under 5% CO_2 in 1x DMEM plus 10% heat inactivated FBS and 1% penicillin/streptomycin. MCF7 cells were maintained and cultured at 37°C under 5% CO_2 in 1x McCoy's 5A plus 10% heat inactivated FBS, and 1% penicillin/streptomycinm L-glutamine, amino acids, non-essential amino acids and sodium pyruvate each. Cells were harvested with trypsin from substrates after 24h in culture for mRNA extraction (Qiagen RNeasy kit). Conditioned media was collected after 48h in the presence of protease inhibitor for secreted protein analysis. To image cell morphology as a function of substrate rigidity, cells stably expressing GFP were cultured on 0.45kPa (D), 3.3MPa (E) and 1.7GPa (F) substrates and visualized at 24 hours using phase contrast, GFP and DAPI.

Quantitative real-time PCR. To measure changes in gene expression, mRNA reverse transcription was carried out using the SuperScript III kit per manufacturer's instructions. Briefly, total RNA was extracted using the RNeasy Mini Kit. The SuperScript III First Strand Synthesis System for quantitative RT-PCR primed with random hexamers was used to synthesize cDNA using between 1 and 5μg total RNA. The expression of PTHrP, Gli2, and TGF-β was measured by quantitative RT-PCR using validated TaqMan primers with the 7300 Real-Time PCR System (Applied Biosciences). Assays were performed in triplicate on the RealPlex Machine (Eppendorf) under the following cycling conditions: 95°C for 15 seconds, 58°C for 30 seconds, and 68°C for 30 seconds. Quantification was performed using the absolute quantitative for human cells method using 18S as an internal control. The expression of osteopontin (OPN), interleukin 11 (IL-11), CXCR4, connective tissue growth factor (CTGF), and matrix metalloproteinase- 9 (MMP-9) were determined using SYBR green primers as described previously [21].

Immunoradiometric assays. PTHrP protein secretion was measured in conditioned medium using a two-site immunoradiometric assay (IRMA) per manufacturer's instructions. All secreted protein values were normalized for cell number.

TGF-β signaling assay. MDA-MB-231 cells were transiently transfected with 1μg 3TPLux, a TGF-β responsive reporter construct [26], using lipofectamine plus (Invitrogen). pRLTK *Renilla* was cotransfected as a control reporter vector. After 24h in serum-free culture on substrates ranging from 1.7GPa to 0.45kPa, cells were lysed in Passive Lysis Buffer (Promega) and the oxidation of luciferin was measured

using a luminometer (TD 20/20, Turner Designs) using a Dual Luciferase Assay Kit (Promega) per manufacturer's instructions.. Luciferase activity was then normalized by the *Renilla* control.

Western Blotting. Cells cultured as described above were harvested into a radio-immunoprecipitation assay lysis buffer containing a cocktail of protease inhibitors (Roche, Basel, Switzerland). Equal protein concentrations were prepared for loading with NuPAGE sample buffer (Invitrogen) and separated on a gradient (4%-20%) SDS-PAGE gel (Biorad). After transferring to a PVDF, membranes were blocked with 5% BSA in TBS containing 0.1% Tween-20 for 1h at room temperature, followed by incubation with either phospho-myosin light chain 2 (Ser19) or phospho-myosin light chain 2 (Thr18/Ser19) (1:1000) antibodies overnight at 4°C. After washing, membranes were blotted with anti-rabbit IgG (1:5000), and bands were detected by enhanced chemiluminescence. Membranes were then stripped and reprobed using an antibody for β-actin (1:5000) as a loading control.

Inhibition of mechanotransduction. Cells were plated as described above and allowed to adhere for 4h, at which point they were treated with either Y27632 (20μM) or Blebbistatin (50μM). Cells were harvested 24h or 48h post-treatment for mRNA and secreted protein and analyzed as described above. MDA-MB-231, RWGT2 and MCF-7 cells were transfected with either cDNA encoding a dominant active (Δ4) or dominant negative (KDΔ4) mutant of ROCK [27,28] (a generous gift of Dr. Kazuyuki Itoh, Osaka Medical Center for Cancer and Cardiovascular Diseases, Osaka, Japan) using lipofectamine plus (Invitrogen) per manufacturer's instructions.

Inhibition of ROCK in the presence of exogenous TGF-b. Cells were plated and treated with either Y27632 or Blebbistatin as described previously. Cells were then either co-treated with 5 ng/mL TGF-β or TGF-β vehicle (5% BSA-HCl) and harvested for mRNA after 24h for qPCR analysis.

Results

Characterization of PUR and PAA substrates

The characterization of the substrates is summarized in Figure 3.1. As shown in Figure 3.1A and B, the PUR films were crosslinked networks. The elastic modulus of the films increased with decreasing equivalent weight, defined as the molecular weight divided by the functionality (f = 3 for a triol). The mesh size of the PUR films ranged from 8.7 – 24 nm, which is at least 2 orders of magnitude smaller than the size of the cells. Therefore, the cells migrate on the surface since they cannot penetrate the films. The mesh size of the PAA gels was 3.3 μm, which is also smaller than the size of the cells. As shown in Figure 3.1C, we obtained reasonable agreement (within a factor of 2) between the measured modulus and that calculated from the swelling experiments using eq (4). PUR substrates were coated with Fn by adsorption, while Fn was grafted to PAA gels (Figure 3.1D). The concentration of Fn on all surfaces was maintained at 0.12 absorbance units cm^{-2} by controlling the concentration of Fn in the solution.

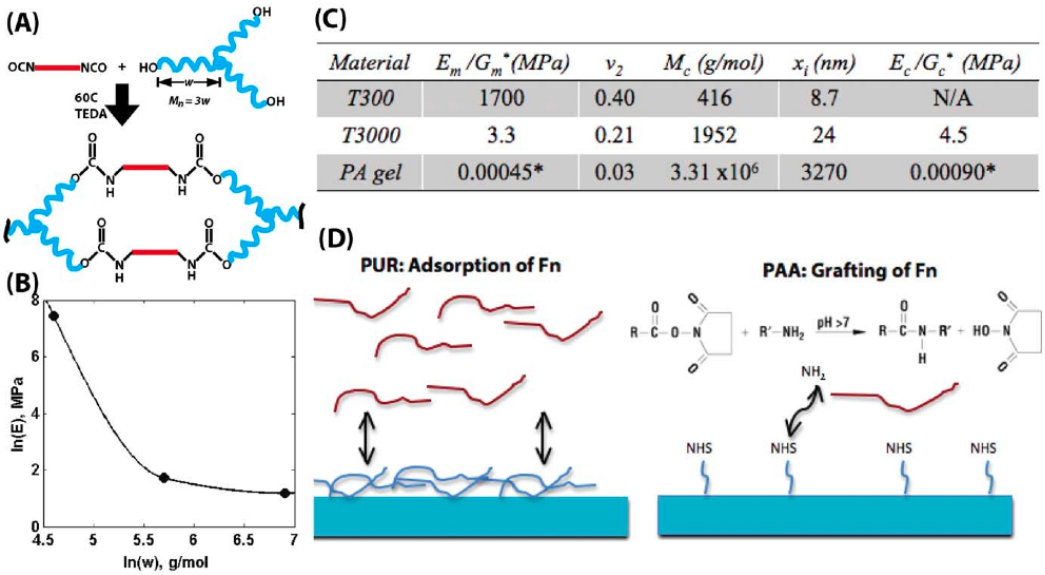

Material	E_m / G_m^* *(MPa)*	v_2	M_c *(g/mol)*	x_i *(nm)*	E_c / G_c^* *(MPa)*
T300	1700	0.40	416	8.7	N/A
T3000	3.3	0.21	1952	24	4.5
PA gel	0.00045*	0.03	3.31 x10^6	3270	0.00090*

Figure 3.1. Schematic of materials synthesis and characterization. (A) Synthesis of PUR networks from an LDI quasi-prepolymer (red) and a poly(ε-caprolactone-co-glycolide) triol with molecular weight $M_n = 3w$, where w is the equivalent weight (g eq^{-1}). (B) Experimental values of the elastic modulus E of PUR networks as a function of equivalent weight w. (C) Physical characteristics of polymer networks as calculated from rubber elasticity theory. E_m and G_m represents measured elastic and shear moduli, v_2 is the fraction of polymer in the swollen mass, M_c is the calculated molecular weight between cross-links and E_c and G_c are the calculated elastic and shear moduli. (D) Schemes for providing a uniform surface concentration of fibronectin (Fn) for polyurethane networks and polyacrylamide gels.

Bone-like mechanical properties stimulate expression of PTHrP

To investigate the effects of substrate modulus on gene expression of cancer cells *in vitro*, we synthesized 2D substrates with tunable elastic moduli ranging from 0.45 kPa to 67 GPa for culture with several cell lines, namely MDA-MB-231 (osteolytic metastatic mammary adenocarcinoma), RWGT2 (osteolytic metastatic lung squamous cell carcinoma), and MCF-7 (non-osteolytic ductal mammary carcinoma). MDA-MB-231 and RWGT2 cells showed 2.5-fold and 2-fold increases in PTHrP mRNA expression respectively in response to substrates with moduli exceeding 1 GPa compared to substrates with moduli < 100 kPa (Figure 3.2A and B). In contrast, MCF-7 cells, which are known not to cause osteolytic lesions showed no

difference in PTHrP expression in response to substrate stiffness (Figure 3.2C). The effects of substrate modulus on PTHrP gene expression followed a sigmoid curve that saturates between 1.7 and 67GPa, which overlaps with the elastic modulus of bone. PTHrP secretion data measured by IRMA and changed similarly for all cell lines (Figure 3.2A-C). Additionally, the morphology of MDA-MB-231 cells changed with substrate rigidity (Figure 3.2D-F), where GFP (green) is expressed throughout the cell and the DAPI (blue) stain binds to the DNA in the nucleus. Similar effects were observed with RWGT2 cells, and no effects were obtained with MCF7 cells.

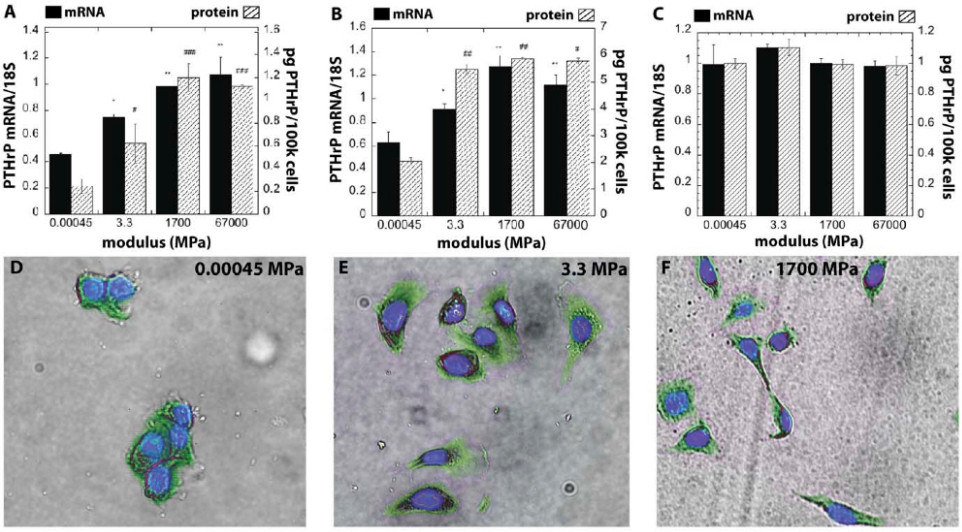

Figure 3.2. Expression and secretion of PTHrP by osteolytic, metastatic tumor cells increases with increasing substrate modulus. PTHrP mRNA normalized by 18S as measured by qPCR and secreted PTHrP as measured by IRMA for (A) MDA-MB-231 , (B) RWGT2, and (C) MCF-7 cells on substrates of increasing elastic modulus. *,# = p<.05; **,##= p<.01; ***,###=p<.005 compared to 0.00045MPa value. Changes in MCF-7 cells were not significant. (D) – (F) Morphology of MDA-MB-231 cells cultured on substrates of varying elastic modulus 4 hours post-attachment. Nuclei were stained using DAPI (blue) and cells were visualized with both visible light and GFP (green). Similar effects of the modulus on cell morphology were observed for RWGT2 cells, while no effects were observed for MCF-7 cells.

Expression of Gli2, a transcription factor known to regulate PTHrP [4], also showed a 5-fold increase on hard substrates in both MDA-MB-231 and RWGT2 (Figure 3.3) but not in MCF-7.

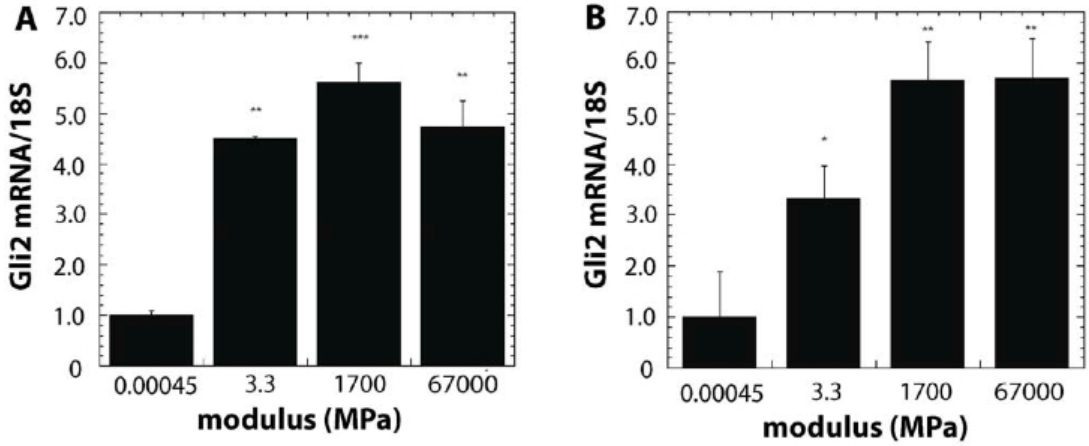

Figure 3.3. Expression of Gli2 and by MDA-MB-231 and RWGT2 cells increases with increasing substrate modulus. Expression of Gli2 mRNA normalized by 18S as measured by qPCR for (A) MDA-MB-231 and (B) RWGT2 cells on substrates of varying elastic modulus. Gli2 signaling increased 25-fold as the modulus increased from 3.3 to 1700 MPa (data not shown). *,# = p<.05; **,##= p<.01; ***,###=p<.005 compared to 0.00045MPa value.

To verify that these data were not the result of an overall down-regulation of gene expression on soft substrates, several other factors of known importance in bone metastases [29] were examined as summarized in Table 3.1. Expression of the osteolytic factor IL-11 was relatively insensitive to substrate rigidity for all three cell lines tested. Factors showing the most dramatic change in expression as a function of rigidity include osteopontin (OPN) and MMP-9. Expression of OPN, which is incidentally associated with primary site invasion, was 5 – 18 times higher when MDA-MB-231 or RWGT2 cells were seeded on soft substrates. Interestingly, expression of OPN by MCF-7 cells was relatively independent of rigidity. Expression of MMP-9 was 10 – 30 times higher on soft substrates for MDA-MB-231, but the

effects of rigidity on MMP-9 expression observed for RWGT2 and MCF-7 cells were substantially smaller.

Table 3.1. Expression of a selected panel of genes associated with osteolytic bone disease as a function of substrate rigidity

	MDA-MB-231		RWGT2		MCF-7	
Gene	**3.3 MPa**	**1700 MPa**	**3.3 MPa**	**1700 MPa**	**3.3 MPa**	**1700 MPa**
IL-11	1.5	1.4	1.1	1.1	1.1	−1.1
OPN	−18	−18	−5.0	−2.3	1.4	−1.1
MMP-9	−32	−11	−1.3	−1.4	3.7	1.3
CXCR4	−2.0	1.1	1.4	1.7	2.4	1.3
CTGF	1.8	2.0	1.1	1.0	2.4	1.3

Substrate-mediated gene expression changes in bone-metastatic cancers are regulated by ROCK-I

ROCK signaling regulates actomyosin contractility and cytoskeleton-dependent forces by phosphorylating motor proteins, such as the regulatory MLC, LIMK1/2 and MYPT1 (myosin-binding subunit of MLC) [12]. Thus, ROCK activation leads to increased actomyosin contractility, which led us to question whether the effects of substrate rigidity on PTHrP expression are mediated by ROCK. To determine whether the observed changes in mechanotransduction were linked to expression of osteoclastogenic factors, we first cultured MDA-MB-231 cells on soft (3.3 MPa) and hard (1700 MPa) PUR substrates and measured ROCK activity after 24h by Western blotting. As shown in Figure 3.4A, cells seeded on more rigid substrates expressed higher levels of phosphorylated MLC (pMLC), implying that ROCK activity increased on more rigid substrates. To further test the hypothesis

that modulus effects on PTHrP expression were mediated by ROCK, we pharmacologically inhibited mechanotransduction in MDA-MB-231 and RWGT2 cells on 2GPa tissue culture polystyrene substrates with blebbistatin or the ROCK inhibitor, Y27632.

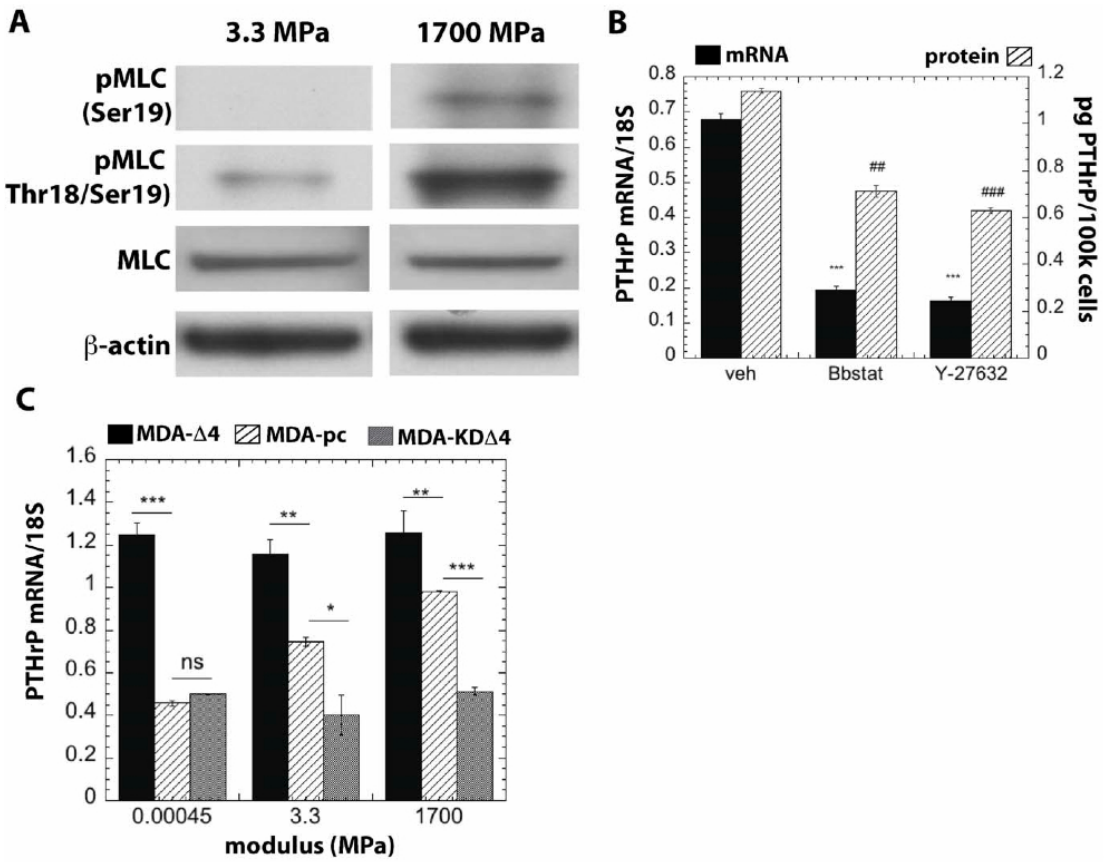

Figure 3.4. Mechanotransduction signals are regulated by values of the substrate modulus in the MPa range. (A) Western blot analysis of myosin light chain phosphorylation shows higher pMLC expression by MDA-MB-231 cells seeded on more rigid (1700 MPa) relative to softer (3.3 MPa) PUR substrates. (B) Pharmacological inhibition of actomyosin contractility (blebbistatin) and ROCK (Y-27632) decreases PTHrP gene expression and protein secretion in MDA-MB-231 cells. Similar patterns were observed for RWGT2 cells (data not shown). The optimal doses of blebbistatin and Y-27632 were identified to be 50 mM and 20 mM, respectively through dose-response experiments (data not shown). (C) PTHrP is over-expressed and does not increase with rigidity in MDA-MB-231 cells genetically modified to express a constitutively active form of ROCK (MDA-D4 cells). Similarly, PTHrP expression does not increase with rigidity in MDA-MB-231 cells genetically modified to express a dominant negative form of ROCK (MDA-KDΔ4 cells). MDA cells transfected with a plasmid control (MDA-pc) show significant increases in PTHrP expression with rigidity.

Inhibition of actomyosin contractility by blebbistatin and inhibition of ROCK-I by Y-27632 induced a significant decrease in PTHrP mRNA expression in both MDA-MB-231 and RWGT2 cells (Figure 3.4B), suggesting that the upregulation of PTHrP on rigid substrates is mediated by ROCK. Conversely, pharmacologically inhibiting mechanotransduction with either blebbistatin or Y27632 resulted in an increase of OPN mRNA expression in both MDA231 and RWGT2. Neither blebbistatin nor Y27632 had an effect on IL-11 mRNA expression in either cell type. MDA-MB-231 cells were also genetically modified to produce constitutively active (MDA-Δ4) and dominant negative (MDA-KDΔ4) forms of ROCK. As shown in Figure 3.4C, expression of PTHrP by MDA-Δ4 cells seeded on 2GPa substrates was upregulated relative to plasmid control (pc) cells and did not increase with increasing modulus. Expression of PTHrP by MDA-KDΔ4 cells seeded on the same substrates was down-regulated and did not increase with increasing substrate rigidity. Taken together, the data in Figure 3.4 indicate that the effects of substrate modulus on PTHrP gene expression are mediated by ROCK.

TGF-β mediates the effects of substrate rigidity on Gli2 and PTHrP through ROCK

While Figure 3.4 shows that ROCK regulates PTHrP expression, TGF-β is also known to stimulate PTHrP production [5]. Therefore, we investigated its role in regulating the response of the tumor cells to rigidity. As shown in Figure 3.5A, MDA-MB-231 cells transfected to express a dominant negative form of the TGF-β Type II receptor (MDA-TβRIIDcyt cells) showed only a ≤1.6-fold increase in PTHrP expression as substrate rigidity increased from 0.45 kPa to 1700 MPa. Similarly,

MCF-7 cells, which do not express the TGF-β Type II receptor, also showed ≤1.1-fold increase in PTHrP gene expression with substrate rigidity (Figure 3.5A). Thus, cells that are non-responsive to TGF-β did not respond to substrate modulus. Interestingly, intracellular TGF-β signaling, as measured by the 3TPLux assay, increased with substrate rigidity, as shown in Figure 3.5B. This is at least in part due to an increase in TGF-β1 expression by cells on more rigid substrates (Figure 3.5C).

A

Fold Increase in PTHrP mRNA relative to Soft PAA Gel		
Cell Type	3.3 MPa	1700 MPa
MDA-pcDNA	17	46
MDA-TβRIIΔcyt	1.1	1.6
MCF-7	1.1	1.0

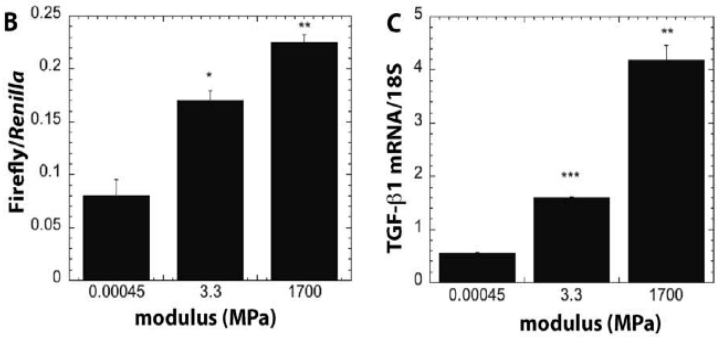

Figure 3.5. TGF-β mediates the response of MDA-MB-231 cells to substrate rigidity. (A) PTHrP gene expression increases significantly for MDA-MB-231 cells transfected with the plasmid control (MDA-pc), while MDA-MB-231 cells transfected to express a dominant negative form of the TGF-β Type II receptor (MDA-TβRIIDcyt) and MCF-7 cells that do not express the TGF-β Type II receptor show no increase in expression with rigidity. (B) TGF-β signaling was measured in MDA-MB-231 cells transfected with the 3TP-Lux TGF-β reporter construct. This showed an increase in TGF-β signaling when cells are grown on rigid substrates. (C) TGF-β1 mRNA expression by MDA-MB-231 cells increased on more rigid substrates.

We next investigated whether blocking ROCK inhibits the effects of exogenous TGF-β on the stimulation of Gli2 and PTHrP expression by treating cells with TGF-β and inhibiting mechanotransduction with blebbistatin (Figure 3.6A and B) or Y27632 (Figure 3.6C and D). We found that blebbistatin blocked the ability of TGF-β to stimulate Gli2 and PTHrP expression. Similar results were seen with Y27632 treatments. Using a molecular approach, we treated the KDΔ4 cells with TGF-β and found that TGF-β could no longer stimulate Gli2 (Figure 3.6E) or PTHrP

(Figure 3.6F), thus suggesting that ROCK is required for TGF-β to stimulate Gli2 and PTHrP.

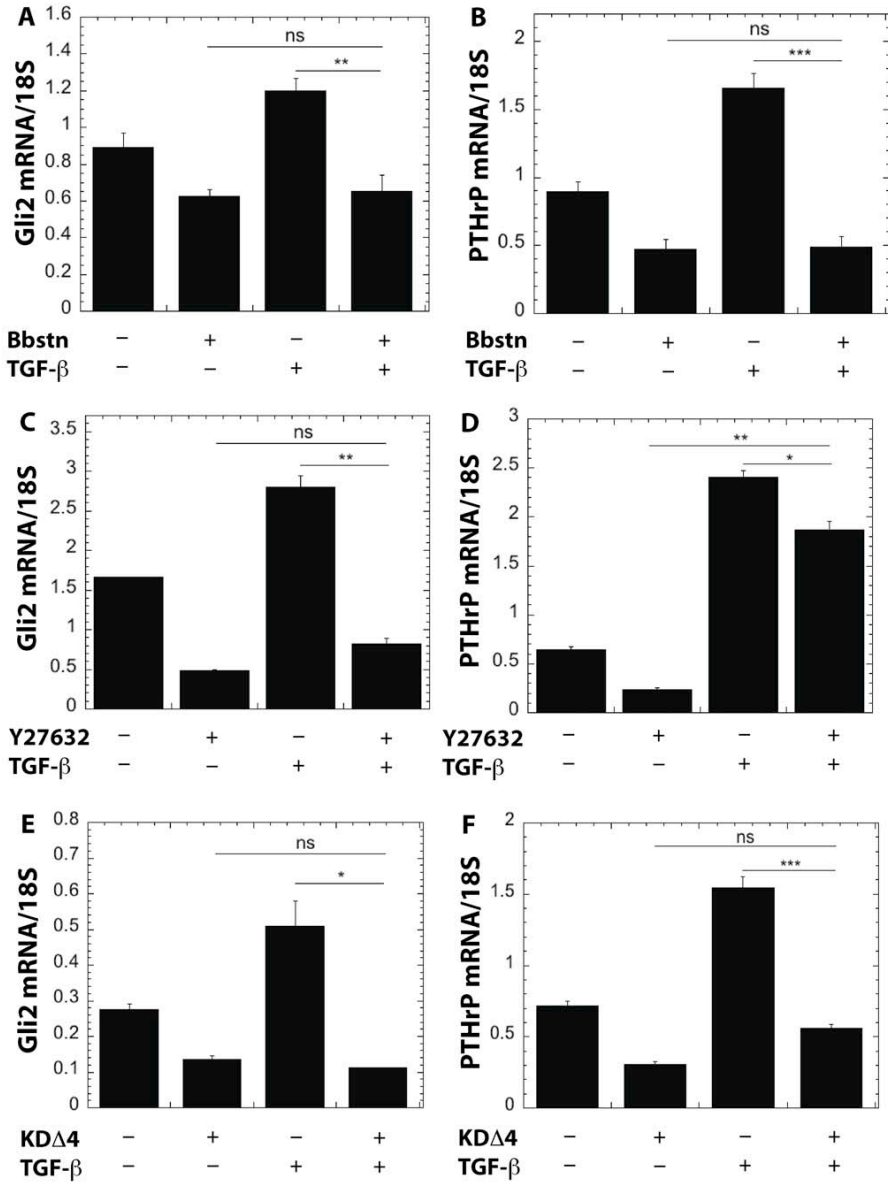

Figure 3.6. Inhibition of mechanotransduction and ROCK suppresses PTHrP expression induced by exogenous TGF-β. Treatment with blebbistatin inhibits expression of (A) Gli2 and (B) PTHrP by MDA-MB-231 cells cultured on TCPS. Treatment with 5 ng/ml exogenous TGF-β increases PTHrP and Gli2 expression, and treatment with both TGF-β and blebbistatin reduces expression to levels observed for blebbistatin alone. Similarly, treatment of MDA-MB-231 cells with the ROCK inhibitor Y-27632 inhibits (C) Gli2 and (D) PTHrP expression. In the presence of both exogenous TGF-β and Y-27632, both PTHrP and Gli2 expression are significantly reduced, but PTHrP expression is only partially inhibited relative to treatment with Y-27632 alone. Expression of (E) Gli2 and (F) PTHrP in MDA-MB-231 cells genetically modified to express a dominant negative form of ROCK (MDA-MB-231 KDΔ4) is significantly lower than that measured for plasmid control MDA-MB-231 cells. Treatment with exogenous TGF-β does not significantly increase Gli2 or PTHrP expression in KDΔ4 cells.

Discussion

How tumor cells respond to matrix rigidity is an area of increasing interest, with several groups investigating how the increasing rigidity of soft tissue can alter tumor cell behavior and gene expression. Mechanically transduced signals can induce phenotypic transformation of cells by altering Rho-dependent actomyosin contractility to regulate cellular outcomes, including motility and invasiveness [30], tissue morphogenesis [31], invadopodia activity [32], and stem cell differentiation [33]. While the invasiveness of cancer cells has been reported to increase with the rigidity of the matrix for soft hydrogels [9,10,15,23], the range of substrate rigidity used to investigate cellular responses was generally <100 kPa. A recent study has shown that single cell populations (SCPs) derived from MDA-MB-231 cells exhibited increased proliferation and migration when seeded on matrices with rigidities corresponding to the native rigidities of the organs where metastasis was observed [30]. Thus SCPs targeted specifically to bone proliferated faster and were more invasive on rigid tissue culture polystyrene compared to soft PAA gels. However, whether the differential rigidity of bone alters expression of osteolytic factors by tumor cells has not been investigated. In this study, we show that not only do cells respond with changed behavior when exposed to surfaces with rigidities comparable to bone, but also that specific genes involved in tumor-induced bone disease are upregulated. This is especially important in metastatic cancer, since many cancers (such as those of the breast and lung) preferentially metastasize to bone.

Expression of the osteolytic factor PTHrP is more prevalent in bone versus soft tissue metastases as observed in clinical populations [2,3]. We hypothesized that the differential rigidity of the bone microenvironment induces tumor cells to increase expression of osteolytic factors by altering Rho-dependent actomyosin contractility. To test our hypothesis, we cultured tumor cells on 2D substrates with rigidities ranging from that of breast tissue to mineralized bone. Considering that tumor cell interactions with Fn are important for the development of secondary tumors inside the bone marrow stroma [34], substrates were uniformly coated with Fn to better simulate the bone microenvironment and control the surface chemistry. When MDA-MB-231 or RWGT2 tumor cells were grown on rigid substrates (1.7 and 67 GPa) with moduli bracketing that of mineralized bone matrix (18.4 GPa) [35], both Gli2 and PTHrP expression were 2 – 4 times higher compared to soft PAA gels (0.45 kPa). Gli2 and PTHrP expression did not increase for moduli above 1 GPa. When cells were seeded on a soft PUR substrate with modulus (3.3 MPa) approaching that of the basement membrane [36], PTHrP expression was intermediate between the soft PAA and the rigid PUR substrates. Similar observations have been reported for MC3T3-E1 pre-osteoblastic cells, which showed higher expression of markers of osteoblast differentiation when cultured on rigid TCPS (2GPa) compared to 424 and 14 kPa hydrogels [16]. A recent review has reported that actomyosin appeared diffuse for cells cultured on soft gels, in contrast to the stress fibers and strong focal adhesions that predominate when cells were cultured on rigid (e.g., 30 – 100 kPa) gels or glass (67 GPa) [37]. Based on these observations, it has been suggested that cells cultured on substrates having a

modulus equal to or greater than that of stiff gels are in a state of isometric contraction. However, our data show that tumor cells respond to substrate rigidity in the MPa range. While other genes may also increase in addition to Gli2 and PTHrP, we found minimal changes in many of the genes identified previously to be associated with metastasis to bone [29]. Two genes that did change were OPN and MMP-9, which were expressed at a greater amount on softer substrates. This is consistent with clinical data correlating high expression of OPN in metastatic tumor cells [38].

In addition to its role as the factor responsible for humoral hypercalcemia of malignancy (HHM), PTHrP is also expressed by a variety of normal fetal and adult cells, including keratinocytes, mammary epithelial cells, renal tubular epithelial cells, chondrocytes, osteoblasts, and smooth muscle cells [6]. Mechanical stretch induces PTHrP gene expression and protein production in a variety of smooth muscle beds [6], including the abdominal aorta [7], uterus [39,40], and bladder [8]. In addition, mechanical distension of breast tissue caused by suckling induces a rapid and transient response in PTHrP mRNA expression and protein concentration in lactating mammary tissue in rats [41]. While mechanically induced PTHrP signaling has been shown for normal cells, these effects have not been previously reported for metastatic tumor cells.

When cells encounter a mechanically rigid matrix, integrins become activated, which stimulates RhoGTPas-dependent actomyosin contractility [11]. Thus cells exert actomyosin contractility and cytoskeleton-dependent forces in response to matrix rigidity cues. Inhibition of RhoGTPase signaling in tumor cells by

treating with ROCK or myosin 2 inhibitors reduces tumor cell contractility and spreading [11], as well as invadopodia-associated extracellular matrix degradation [15]. Similarly, in this study we observed that expression of phosphorylated myosin light chain (pMLC), which is regulated by ROCK, is increased on rigid substrates. Furthermore, inhibition of tumor cell actomyosin contractility in both pharmacological and genetic models decreased Gli2 and PTHrP expression. A recent study has suggested that increased ROCK signaling contributes to breast cancer metastasis [12]. ROCK expression is increased in metastatic human mammary tumors and breast cancer cell lines, and inhibition of ROCK signaling reduces tumor cell metastasis to bone *in vivo*. Taken together, these observations suggest that inhibiting ROCK or the pathway it stimulates may be an effective approach for treatment of breast cancer metastases in the clinic. Since ROCK is ubiquitously expressed in many tissues and is required for normal mechanotransduction responses in cells, global inhibition in patients may not be an ideal clinical approach. However, the ROCK inhibitors fasudil and Y-27632 have been used successfully in preclinical models of pulmonary and cardiac disease, and a few clinical studies have shown that fasudil is a safe and effective treatment for patients with severe pulmonary hypertension [42].

Mechanical signals induced by substrate rigidity regulate the expression of Gli2 and PTHrP though ROCK. Our observation that the expression of Gli2 by tumor cells is regulated by matrix rigidity is consistent with previous studies suggesting that Hh genes are regulated during development by mechanically transduced signals [43,44]. While ROCK is ubiquitously expressed in many tissues and cells in the body,

the postnatal expression of Gli2 is primarily restricted to the growth plate [45] and hair follicle [46,47]. Thus Gli2 may be a potentially more useful target than ROCK for treating bone metastases in the clinic. Preclinical studies have indicated that inhibiting Gli2 activity reduces PTHrP expression and osteolysis [48].

Interestingly, substrate rigidity activates ROCK through a TGF-β-dependent mechanism. As shown in Figure 3.6, blocking ROCK either pharmacologically or genetically inhibits most of the incremental PTHrP expression resulting from treatment with exogenous TGF-β. In addition, TGF-β signaling increases with substrate rigidity, which has also been reported for myofibroblasts cultured on relatively rigid (>10 kPa) hydrogels, where cell-generated forces deform the TGF-β latent complex resulting in release of soluble TGF-β [49,50]. However, in the present study, the expression of TGF-β1 (but not β2 or β3) also increased with rigidity, suggesting a pivotal role for autocrine TGF-β signaling in this response. This observation is in agreement with previous studies reporting that mechanical stretch or laminar shear stress increases TGF-β expression and production in endothelial [51,52] and activated hepatic stellate (HSCs) cells [53]. A mechanotransduction pathway requiring autocrine TGF-β signaling was found to regulate expression of perlecan in endothelial cells [51]. In another study, transfection of HSCs with a dominant negative form of Rho inhibited the increased production of TGF-β induced by mechanical stretch [53]. In the bone microenvironment, as osteoclasts resorb host bone, TGF-β released from the bone matrix stimulates the tumor cells to produce more PTHrP, leading to the vicious cycle of osteoclast-mediated bone resorption associated with metastatic bone disease [5]. Our data show that the

increased PTHrP expression induced by exogenous TGF-β *in vitro* is mediated by the rigidity of the substrate on which the tumor cells are cultured. These observations suggest a role for the differential rigidity of the mineralized bone microenvironment in both the initiation and maintenance of the vicious cycle when osteolytic tumor cells metastasize to bone.

While the interpretation of these experiments is somewhat limited by the use of 2D surfaces, which are known to regulate migration and invasion of tumor cells in ways that differ from 3D matrices [14], the 2D substrates enabled us to independently investigate how rigidity influences gene expression over the 0.45 kPa to 67 GPa range. A recent study has shown that MDA-MB-231 single cell clonal populations proliferated faster on 2D substrates having mechanical properties comparable to that of the organs where metastasis was observed [30]. Thus the response to rigidity in various SCPs in 2D cell culture correlated with the tissue tropism observed *in vivo*. In the present study, tumor cells changed their gene expression patterns when encountering substrates having rigidities in the MPa to GPa range, suggesting that the differential rigidity of the bone microenvironment may contribute to the initial establishment and function of tumor cells in bone. Although the modulus of the tissue that the cells are interacting with in the bone microenvironment is not precisely known, mineralized bone tissue is orders of magnitude more rigid than the primary site, and well within the range of the rigid substrates used in this study. We are currently developing a 3D co-culture system *in vivo* to capture more representative features of the bone microenvironment, such as cellular migration and invasion in a 3D matrix and tumor-stromal cell interactions.

Conclusions

In this study, we have shown that tumor cells respond to 2D substrates with rigidities comparable to that of bone by increasing expression and secretion of the osteolytic factor PTHrP. The cellular response is regulated by Rho-dependent actomyosin contractility mediated by TGF-β signaling. Inhibition of ROCK using both pharmacological and genetic models decreased PTHrP expression. Furthermore, cells expressing a dominant negative form of the TGF-β receptor did not respond to substrate rigidity, and inhibition of ROCK decreased PTHrP expression induced by exogenous TGF-β. These observations suggest a role for the differential rigidity of the mineralized bone microenvironment in early stages of tumor-induced osteolysis, which is especially important in metastatic cancer since many cancers (such as those of the breast and lung) preferentially metastasize to bone.

References

1. Guise T, Yin J, Taylor S, Kumagai Y, Dallas M, et al. (1996) Evidence for a causal role of parathyroid hormone-related protein in the pathogenesis of human breast cancer-mediated osteolysis. J Clin Invest 98: 1544-1549.
2. Southby J, Kissin MW, Danks JA, Hayman JA, Moseley JM, et al. (1990) Immunohistochemical localization of parathyroid hormone-related protein in human breast cancer. Cancer Res 50: 7710-7716.
3. Powell GJ, Southby J, Danks JA, Stillwell RG, Hayman JA, et al. (1991) Localization of parathyroid hormone-related protein in breast cancer metastases: increased incidence in bone compared with other sites. Cancer Res 51: 3059061.
4. Sterling JA, Oyajobi BA (2006) The hedgehog signaling molecule Gli2 induces parathyroid hormone-related peptide expression and osteolysis in metastatic human breast cancer cells. Cancer Res 66: 7548-7553.
5. Yin JJ, Selander K, Chirgwin JM, Dallas M, Grubbs BG, et al. (1999) TGF-beta signaling blockade inhibits PTHrP secretion by breast cancer cells and bone metastases development. J Clin Invest 103: 197-206.
6. Philbrick WM, Wysolmerski JJ, Galbraith S, Holt E, Orloff JJ, et al. (1996) Defining the roles of parathyroid hormone-related protein in normal physiology. Physiol Rev 76: 127-173.
7. Pirola CJ, Wang HM, Strgacich MI, Kamyar A, Cercek B, et al. (1994) Mechanical stimuli induce vascular parathyroid hormone-related protein gene expression in vivo and in vitro. Endocrinology 134: 2230-2236.
8. Yamamoto M, Harm SC, Grasser WA, Thiede MA (1992) Parathyroid hormone-related protein in the rat urinary bladder: a smooth muscle relaxant produced locally in response to mechanical stretch. Proc Natl Acad Sci U S A 89: 5326-5330.
9. Paszek MJ, Zahir N, Johnson KR, Lakins JN, Rozenberg GI, et al. (2005) Tensional homeostasis and the malignant phenotype. Cancer Cell 8: 241-254.
10. Paszek MJ, Weaver VM (2004) The tension mounts: mechanics meets morphogenesis and malignancy. J Mammary Gland Biol Neoplasia 9: 325-342.
11. Butcher DT, Alliston T, Weaver VM (2009) A tense situation: forcing tumour progression. Nat Rev Cancer 9: 108-122.
12. Liu S, Goldstein RH, Scepansky EM, Rosenblatt M (2009) Inhibition of rho-associated kinase signaling prevents breast cancer metastasis to human bone. Cancer Res 69: 8742-8751.
13. Zaman MH, Kamm RD, Matsudaira P, Lauffenburger DA (2005) Computational Model for Cell Migration in Three-Dimensional Matrices. Biophys J 89: 1389-1397.
14. Zaman MH, Trapani LM, Sieminski A, MacKellar D, Gong H, et al. (2006) Migration of tumor cells in 3D matrices is governed by matrix stiffness along with cell-matrix adhesion and proteolysis. PNAS 103: 10889-10894.

15. Alexander NR, Branch KM, Iwueke IC, Guelcher SA, Weaver AM (2008) Extracellular matrix rigidity promotes invadopodia activity. Curr Biol 18: 1295-1299.
16. Khatiwala CB, Peyton SR, Metzke M, Putnam AJ (2006) The Regulation of Osteogenesis by ECM Rigidity in MC3T3-E1 Cells Requires MAPK Activation. J Cellular Physiology 211: 661-672.
17. Engler AJ, Sen S, Sweeney HL, Discher DE (2006) Matrix Elasticity Directs Stem Cell Lineage Specification. Cell 126: 677-689.
18. Guelcher SA, Dumas J, Srinivasan A, Didier JE, Hollinger JO (2008) Synthesis, mechanical properties, biocompatibility, and biodegradation of polyurethane networks from lysine polyisocyanates. Biomaterials 29: 1762-1775.
19. Guelcher S (2008) Biodegradable polyurethanes: synthesis and applications in regenerative medicine. . Tissue Eng In Press.
20. Guise TA, Yoneda T, Yates AJ, Mundy GR (1993) The combined effect of tumor-produced parathyroid hormone-related protein and transforming growth factor-alpha enhance hypercalcemia in vivo and bone resorption in vitro. J Clin Endocrinol Metab 77: 40-45.
21. Javelaud D, Mohammad KS, McKenna CR, Fournier P, Luciani F, et al. (2007) Stable overexpression of Smad7 in human melanoma cells impairs bone metastasis. Cancer Res 67: 2317-2324.
22. Hafeman A, Li B, Yoshii T, Zienkiewicz K, Davidson J, et al. (2008) Injectable biodegradable polyurethane scaffolds with release of platelet-derived growth factor for tissue repair and regeneration. Pharm Res 25: 2387-2399.
23. Enderling H, Alexander NR, Clark E, Branch KM, Estrada L, et al. (2008) Dependence of invadopodia function on collagen fiber spacing and crosslinking: computational modeling and experimental evidence. Biophys J 95: 2203-2218.
24. Sperling LH (2001) Introduction to Physical Polymer Science. New York: Wiley-Interscience.
25. Raeber GP, Lutolf MP, Hubbell JA (2005) Molecularly engineered PEG hydrogels: a novel model system for proteolytically mediated cell migration. Biophys J 89: 1374-1388.
26. Kakonen SM, Selander KS, Chirgwin JM, Yin JJ, Burns S, et al. (2002) Transforming growth factor-beta stimulates parathyroid hormone-related protein and osteolytic metastases via Smad and mitogen-activated protein kinase signaling pathways. J Biol Chem 277: 24571-24578.
27. Narumiya S, Tanji M, Ishizaki T (2009) Rho signaling, ROCK and mDia1, in transformation, metastasis and invasion. Cancer Metastasis Rev 28: 65-76.
28. Itoh K, Yoshioka K, Akedo H, Uehata M, Ishizaki T, et al. (1999) An essential part for Rho-associated kinase in the transcellular invasion of tumor cells. Nat Med 5: 221-225.
29. Kang Y, Siegel PM, Shu W, Drobnjak M, Kakonen SM, et al. (2003) A multigenic program mediating breast cancer metastasis to bone. Cancer Cell 3: 537-549.
30. Kostic A, Lynch CD, Sheetz MP (2009) Differential matrix rigidity response in breast cancer cell lines correlates with the tissue tropism. PLoS One 4: e6361.

31. Paszek MJ, Weaver VM (2004) The tension mounts: mechanics meets morphogenesis and malignancy. J Mammary Gland Biol Neoplasia 9: 325-342.
32. Alexander NR, Branch KM, Parekh A, Clark ES, Iwueke IC, et al. (2008) Extracellular Matrix Rigidity Promotes Invadopodia Activity. Curr Biol 18: 1295-1299.
33. Engler AJ, Sen S, Sweeney HL, Discher DE (2006) Matrix elasticity directs stem cell lineage specification. Cell 126: 677-689.
34. Van der Velde-Zimmermann D, Verdaasdonk MA, Rademakers LH, De Weger RA, Van den Tweel JG, et al. (1997) Fibronectin distribution in human bone marrow stroma: matrix assembly and tumor cell adhesion via alpha5 beta1 integrin. Exp Cell Res 230: 111-120.
35. Cuppone M, Seedhom BB, Berry E, Ostell AE (2004) The longitudinal Young's modulus of cortical bone in the midshaft of human femur and its correlation with CT scanning data. Calcif Tissue Int 74: 302-309.
36. Candiello J, Balasubramani M, Schreiber EM, Cole GJ, Mayer U, et al. (2007) Biomechanical properties of native basement membranes. FEBS Journal 274: 2897-2908.
37. Discher DE, Janmey P, Wang YL (2005) Tissue cells feel and respond to the stiffness of their substrate. Science 310: 1139-1143.
38. Hotte SJ, Winquist EW, Stitt L, Wilson SM, Chambers AF (2002) Plasma osteopontin: associations with survival and metastasis to bone in men with hormone-refractory prostate carcinoma. Cancer 95: 506-512.
39. Daifotis AG, Weir EC, Dreyer BE, Broadus AE (1992) Stretch-induced parathyroid hormone-related peptide gene expression in the rat uterus. J Biol Chem 267: 23455-23458.
40. Thiede MA, Daifotis AG, Weir EC, Brines ML, Burtis WJ, et al. (1990) Intrauterine occupancy controls expression of the parathyroid hormone-related peptide gene in preterm rat myometrium. Proc Natl Acad Sci U S A 87: 6969-6973.
41. Thiede MA, Rodan GA (1988) Expression of a calcium-mobilizing parathyroid hormone-like peptide in lactating mammary tissue. Science 242: 278-280.
42. Barman SA, Zhu S, White RE (2009) RhoA/Rho-kinase signaling: a therapeutic target in pulmonary hypertension. Vasc Health Risk Manag 5: 663-671.
43. Nowlan NC, Prendergast PJ, Murphy P (2008) Identification of mechanosensitive genes during embryonic bone formation. Plos Computational Biology 4: e1000250.
44. Tang GH, Rabie AB, Hagg U (2004) Indian hedgehog: a mechanotransduction mediator in condylar cartilage. J Dent Res 83: 434-438.
45. Miao D, Liu H, Plut P, Niu M, Huo R, et al. (2004) Impaired endochondral bone development and osteopenia in Gli2-deficient mice. Exp Cell Res 294: 210-222.
46. Mill P, Mo R, Fu H, Grachtchouk M, Kim PC, et al. (2003) Sonic hedgehog-dependent activation of Gli2 is essential for embryonic hair follicle development. Genes Dev 17: 282-294.

47. Eichberger T, Kaser A, Pixner C, Schmid C, Klingler S, et al. (2008) GLI2-specific transcriptional activation of the bone morphogenetic protein/activin antagonist follistatin in human epidermal cells. J Biol Chem 283: 12426-12437.
48. Johnson RW, Nguyen MP, Padalecki SS, Grubbs BG, Merkel AR, et al. (Submitted) TGF-β promotion of Gli2 induced PTHrP expression is independent of canonical Hedgehog signaling. Cancer Res.
49. Wipff PJ, Rifkin DB, Meister JJ, Hinz B (2007) Myofibroblast contraction activates latent TGF-1 from the extracellular matrix. J Cell Biol 179.
50. Wells RG, Discher DE (2008) Matrix elasticity, cytoskeletal tension, and TGF-beta: the insoluble and soluble meet. Science Signaling 1.
51. Baker AB, Ettenson DS, Jonas M, Nugent MA, Iozzo RV, et al. (2008) Endothelial cells provide feedback control for vascular remodeling through a mechanosensitive autocrine TGF-beta signaling pathway. Circ Res 103: 289-297.
52. Ohno M, Cooke JP, Dzau VJ, Gibbons GH (1995) Fluid shear stress induces endothelial transforming growth factor beta-1 transcription and production. Modulation by potassium channel blockade. J Clin Invest 95: 1363-1369.
53. Sakata R, Ueno T, Nakamura T, Ueno H, Sata M (2004) Mechanical stretch induces TGF-beta synthesis in hepatic stellate cells. Eur J Clin Invest 34: 129-136.

CHAPTER IV

BONE MATRIX RIGIDITY STIMULATES SIGNALING THROUGH $\alpha_V\beta_3$, Src AND MAPK TO INDUCE EXPRESSION OF PTHrP BY MDA-MB-231 CELLS

Introduction

Breast cancer is known to have a predilection for metastasizing to bone, occurring in over 70% of patients with advanced disease [1]. Patients suffering from bone metastases commonly present with pain, hypercalcemia and pathologic fracture, and the current standard of care focuses primarily on relieving the symptoms of tumor-induced bone disease rather than preventing establishment of the tumor in bone. When tumor cells take hold in the bone microenvironment, they increase expression of parathyroid hormone related protein (PTHrP) [2, 3], which indirectly stimulates osteoclasts to resorb the bone matrix. The consequential release of TGF-β from the bone matrix continues to drive the expression of PTHrP [4, 5]. However, the mechanism behind the initiation of osteolytic gene expression associated with tumor-induced bone disease is not well understood.

Cancer cells are known to respond to mechanical cues in soft tissue [6-8], and we have recently demonstrated that the rigid mineralized bone matrix, which is six orders of magnitude stiffer than soft tissue, is one of the factors driving initiation of PTHrP expression via Rho kinase (ROCK) and TGF-βRII in osteolytic cancer cells [9]. Cells sense matrix rigidity by integrin adhesion sites [10], which results in the activation of focal adhesion kinase (FAK) and Src family kinases (SFKs) to recruit

downstream effectors of cytoskeletal tension such as RhoA and ROCK [11, 12]. Inhibition of ROCK blocks the ability of the cell to respond to mechanical stimuli [6] as well as tumor metastasis to bone [13]. Similarly, inhibition of SFKs, which are required to regulate integrin-cytoskeleton interactions for mechanotransduction, also prevents metastasis to bone [14]. Active Src is known to co-localize with integrins at focal adhesion sites [15], and the relocation of active Src to these focal adhesions has been shown to be RhoA- and ROCK-dependent [15]. FAK is also known to co-localize with integrins at focal adhesions, where its tyrosine phosphorylation and activity are stimulated by integrin binding and thought to be regulated by SFKs [15].

Cross-talk between integrins and growth factor receptors is of known importance in predicting tumor malignancy and invasiveness [16]. TGF-β receptor type II (TGFβRII) interacts physically with $\alpha_v\beta_3$ integrin to enhance TGF-β-mediated stimulation of MAP-kinases (MAPKs) and Smad2/3 mediated gene transcription in mammary epithelial cells (MECs) during epithelial-mesenchymal transition (EMT)[11]. TGFβRII signaling is also implicated in osteoclastogenic gene expression in breast cancer [17]. Integrin $\alpha_v\beta_3$ in tumor cells regulates the early stages of skeletal metastasis in both breast and prostate cancer, where it directly interacts with fibronectin (Fn) in the bone matrix [18]. Furthermore, inhibition of $\alpha_v\beta_3$ in osteoclasts reduces bone loss in models of osteolytic skeletal metastases, where $\alpha_v\beta_3$ integrin is required by osteoclasts to resorb the bone matrix [19].

We hypothesize that the rigid mineralized bone matrix results in the increased clustering of $\alpha_v\beta_3$ integrin and TGFβRII to initiate signaling by SFKs, resulting in the

expression of osteolytic genes in breast via ROCK. To test our hypothesis, we designed hydrogel, polyurethane (PUR) and pyrex monoculture systems to mimic the viscoelastic properties of breast tissue, the basement membrane, and mineralized bone *in vitro*. We then measured changes in osteoclastogenic and integrin gene expression in tumor cells in response to the rigidity of these substrates. To better understand the relative contributions of Src and integrins in the previously reported response of tumor cells to the rigid bone matrix [9], we also employed pharmacological and genetic approaches to selectively stimulate Src and inhibit known integrin associated effectors, such as RhoA/ROCK and TGFβ.

Materials and Methods

Synthesis of in vitro *substrates*

Biocompatible polyester polyurethane (PUR) substrates were synthesized and characterized as described previously [9]. Briefly, an appropriate amount of poly(ε-caprolactone-*co*-glycolide) triol (M_n = 300 or 3000 Da) was mixed with an LDI prepolymer and COSCAT 83 catalyst (Vertellus) for 20s in a Hauschild SpeedMixer™ DAC 150 FVZ-K vortex mixer (FlackTek, Inc, Landrum, SC). The targeted index (ratio of NCO to OH equivalents times 100) was 105. The resultant mixture was poured into the wells of a tissue culture plate and allowed to cure for 24h at 60˚C. Pyrex (67 GPa) was used as a hard tissue control. To facilitate cell adhesion and ensure that the surface chemistry was constant for all substrates tested, fibronectin (Fn) was adsorbed to the surface of the substrates by incubation in a 4 μg/mL solution of Fn in PBS at 4^{o}C overnight. Polyacrylamide (PAA) hydrogels were

synthesized by copolymerizing a 10% solution of acrylamide and bis-acrylamide in water via free-radical polymerization using a redox pair of initiators (tetramethyl ethylene diamine (TEMED) and 10% ammonium persulphate (APS) in water) and conjugated with Fn as described previously [9].

Fibronectin Characterization

To measure the surface concentration of Fn, coated substrates and scaffolds were incubated in a solution of Fn antibody (1:1000) followed by incubation with a secondary HRP-conjugated antibody. The relative amount of adsorbed antibody was then quantified by reaction with 2'- azino-bis(3-ethylbenzthiazoline-6-sulphonic acid) (ABTS) and subsequent optical density reading at 405nm. All PUR and PAA and were prepared at the same surface concentration of Fn (1.9 $\mu g\ cm^{-2}$). All 3D scaffolds were prepared at a surface concentration of 0.5 $\mu g\ cm^{-2}$.

Cell lines

MDA-MB-231 cells were purchased from ATCC (Manassas, VA) and selected for the ability to metastasize to bone [20]. MDA-MB-231 cells stably expressing either a constitutively active (MDA-Δ4) or dominant negative (MDA-KDΔ4) form of ROCK were transfected and maintained as described previously [9]. MDA-231 cells stably expressing a dominant negative form of the TGFβ type 2 receptor (MDA-TβRIIΔcyt) were transfected and maintained as described previously [17].

Cell Culture

Cells were maintained and cultured at 37°C under 5% CO2 in 1x DMEM plus 10% heat inactivated FBS and 1% penicillin/streptomycin. Cells were harvested with trypsin from substrates after 24h in culture for mRNA extraction (Qiagen RNeasy kit).

Quantitative real-time PCR

To measure changes in gene expression, mRNA reverse transcription was carried out using the SuperScript III kit (Invitrogen) per manufacturer's instructions. Briefly, total RNA was extracted using the RNeasy Mini Kit (Qiagen). The Superscript III First Strand Synthesis System for quantitative RT-PCR primed with random hexamers was used to synthesize cDNA using between 1 and 5μg total RNA. The expression of PTHrP, Gli2, integrin β_3 and integrin β_5 subunit was measured in triplicate by quantitative RT-PCR using validated TaqMan primers with the 7300 Real-Time PCR System (Applied Biosciences) using the following cycling conditions: 95°C for 15 seconds and 60°C for 1 minute, preceded by an initial incubation period of 95°C for 10 minutes. Quantification was performed using the absolute quantitative for human cells method using 18S as an internal control. The expression of osteopontin (OPN), interleukin-11 (IL11, CXCR4, connective tissue growth factor (CTGF), and matrix metalloproteinases 2 and 9 (MMP2 and MMP9) was determined using SYBR green primers as described previously [21].

siRNA transfections

MDA-MB-231 cells were transiently transfected with 5 μM of either ON-TARGETplus SMARTpool siRNA for human integrin β3 subunit, cyclophilin B, or non-targeting sequences (Dharmacon) using DharmaFECT4 (Dharmacon) according to manufacturer's instructions. Cells were harvested with trypsin after 24h for RNA extraction and qPCR analysis.

Western Blotting and Immunoprecipitation

Cells cultured as described above were harvested into a radio-immunoprecipitation assay lysis buffer or 1% Nonidet P-40 containing a cocktail of protease inhibitors (Roche, Basel, Switzerland). Equal protein concentrations were prepared for loading with NuPAGE sample buffer (Invitrogen) and separated on a gradient (4%-20%) SDS-PAGE gel (Biorad). After transferring to a PVDF, membranes were blocked with 5% BSA in TBS containing 0.1% Tween-20 for 1h at room temperature, followed by incubation with either phospho-p38MAPK (1:1000, Cell Signaling) or p38MAPK (1:1000, Cell Signaling) antibodies overnight at 4°C. After washing, membranes were blotted with anti-rabbit or anti-mouse IgG (1:5000), and bands were detected by enhanced chemiluminescence. Membranes were then stripped and reprobed using an antibody for β-actin (1:5000) as a loading control. To investigate association of membrane proteins, 400μg total protein lysate per tube was incubated overnight at 4°C under gentle end-over-end mixing with anti-TGFβRII (1 μg, Santa Cruz). Subsequently, the immune complex was captured with protein A/G agarose resin, thoroughly washed with lysis buffer and eluted with

non-reducing sample buffer. Proteins were then separated on an SDS-PAGE gel (7.5%, Biorad) and transferred to a PVDF membrane. Following blocking with 5% milk, membranes were incubated with either anti-integrin β_3 or β_5 antibody (Santa Cruz, 1:1000) at 4°C overnight. After washing, membranes were blotted with anti-rabbit or anti-mouse IgG (1:5000), and bands were detected by enhanced chemiluminescence.

Drug Treatments

Cells were treated with the Src-tyrosine kinase inhibitor PP2 (Calbiochem, 20μM) or the mAB clone LM609 against $\alpha_v\beta_3$ integrin (Millipore, 10μg/mL) for 24 hours before harvesting with trypsin for mRNA extraction. To stimulate TGF-β signaling, cells were treated with either 5 ng/mL TGF-β or TGF-β vehicle (5% BSA-HCL) in serum-free media for 24 h prior to harvesting. To stimulate src phosphorylation, cells were treated with Bombesin (Sigma, 20nm) for 24h before harvesting with trypsin for mRNA extraction [22].

Results

Expression of PTHrP and Gli2 are mediated by integrin and Src-kinase activity

We previously reported that PTHrP and Gli2 expression are regulated by ROCK [9]. As ROCK is a known downstream effector of integrin signaling and a phosphorylation target for Src [23, 24], we sought to determine the relationship between PTHrP/Gli2 expression and integrin signaling activity. We inhibited Src kinases or $\alpha_v\beta_3$ integrin in MDA-MB-231 2D culture *in vitro* using either a small

molecule inhibitor (PP2) or a monoclonal antibody (LM609), respectively. In response to Src kinase inhibition, MDA-MB-231 cells showed a 3-fold decrease in PTHrP expression (Fig 4.1A) and a 15-fold decrease in Gli2 expression (Fig 4.1C). Likewise, $\alpha_v\beta_3$ integrin inhibition produced a 3-fold decrease in PTHrP mRNA (Fig 4.1B) and a 24-fold decrease in Gli2 mRNA (Fig 4.1D). Interestingly, knockdown of β_3 integrin subunit by siRNA did not alter expression of PTHrP or Gli2 (data not shown), suggesting a compensatory mechanism for PTHrP expression.

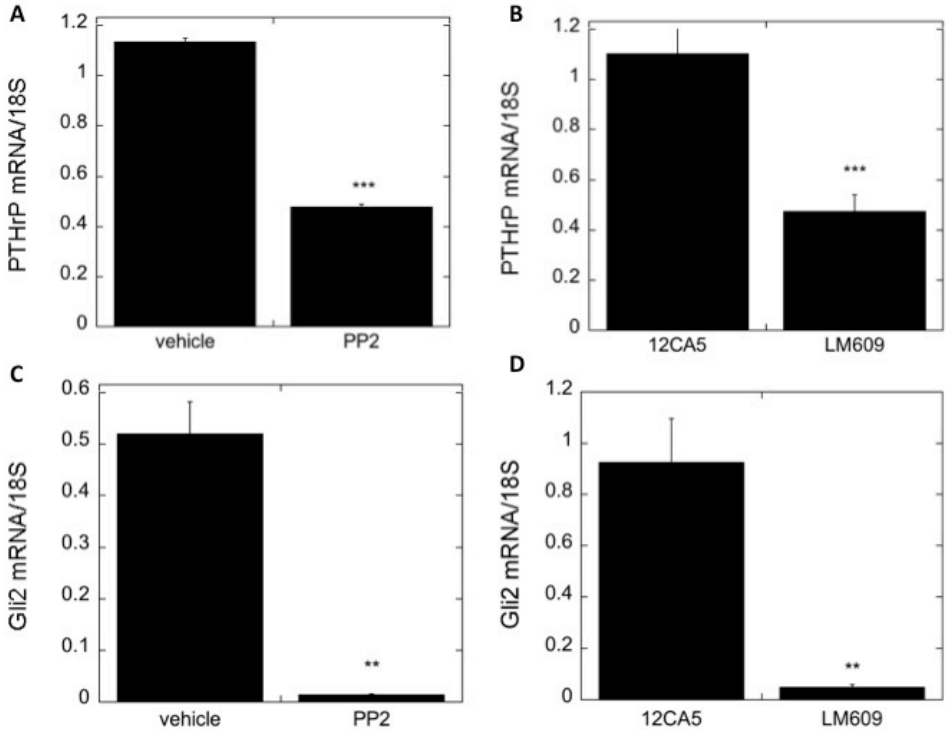

Figure 4.1. Src kinase and integrin $\alpha_v\beta_3$ inhibition reduce expression of PTHrP and Gli2 *in vitro* A) Expression of PTHrP in MDA231 cells in response to Src inhibition with PP2 B) in response to $\alpha_v\beta_3$ inhibition with LM609 C) Gli2 expression in response to PP2 D) in response to LM609. *= $p<0.05$; ** = $p<0.01$; *** = $p<0.005$ compared to vehicle control

To ensure that these changes in gene expression in response to PP2 or LM609 treatment were specific and not the result of an overall down-regulation, we measured changes in a number of other factors of known importance in osteolytic

metastases [21] in response to LM609 and PP2 treatment. Table 4.1 summarizes the fold changes over vehicle control for these genes in MDA-MB-231 cells. We found no significant changes in other genes in response to LM609 treatment, while PP2 treatment resulted in a significant increase in only interleukin 11 (IL11) expression and a decrease in connective tissue growth factor (CTGF) expression.

Table 4.1. Expression of a selected panel of osteolytic genes in response to Src kinase and integrin $\alpha_v\beta_3$ inhibition. Values are fold change over control with $p<0.05$.

Gene/Treatment	LM609	PP2
OPN	1.5	1.5
IL11	-1.1	4.3
CXCR4	1.1	1.8
CTGF	1.1	-4.5
MMP9	1.3	1.1
MMP2	1.0	-1.3

β_3 integrin expression and association with TGFβRII are regulated by rigidity

Since expression of PTHrP and Gli2 appear to be mediated by Src and $\alpha_v\beta_3$ integrin as well as substrate rigidity, we sought to determine whether integrin expression or activity is regulated by the rigidity of the extracellular matrix. When cultured on materials approximating the rigidity of bone, MDA-MB-231 cells showed a 4.5-fold increase in mRNA expression of β_3 integrin subunit as compared to cells grown in a soft matrix (Fig 4.2A). It has previously been reported that Src phosphorylates TGFβRII following clustering with β_3 integrin subunit [11]; thus we specifically examined clustering of membrane proteins by immunoprecipitation in response to substrate rigidity. We found that TGFβRII readily bound to β_3 integrin subunit in MDA-MB-231 cells cultured on rigid, bone like substrates, but not on soft

substrates approximating the elasticity of mammary tissue (Fig 4.2B). Surprisingly, we did not observe a significant decrease in PTHrP expression in response to β_3 siRNA knockdown (Fig 4.2C).

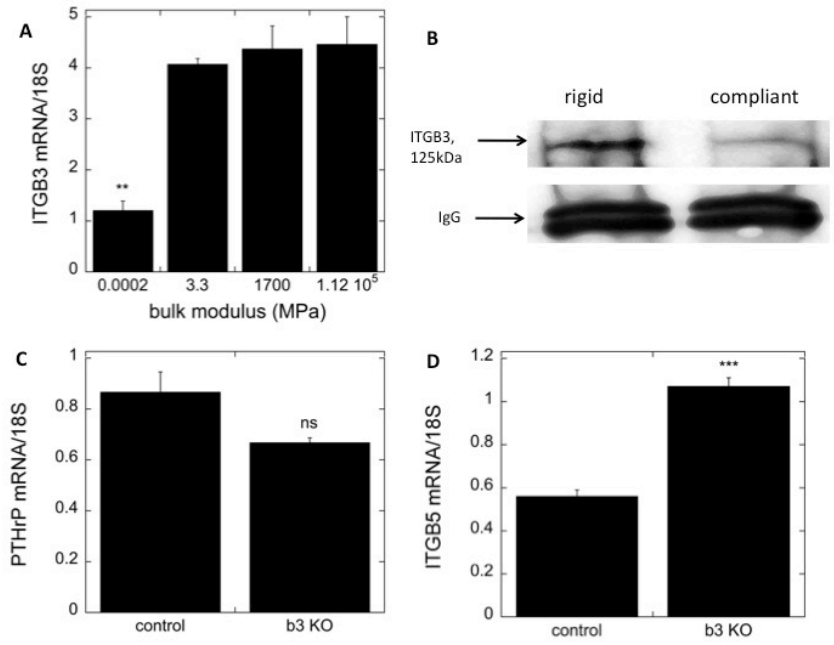

Figure 4.2. Expression of integrin β_3 subunit and its clustering to TGFβRII are a function of rigidity. (A) MDA231 show increased expression of β_3 subunit in response to rigidity *in vitro*. (B) MDA-MB-231 cells show increased physical interaction between integrin β_3 subunit and TGFβRII when cultured on rigid matrices. Nonspecific binding to IgG showed no differences in loading (C) knockout of β_3 subunit does not significantly alter PTHrP expression (D) knockout of β_3 subunit increases expression of β_5 mRNA *= $p<0.05$; ** = $p<0.01$; *** = $p<0.005$ compared to control

β_5 integrin subunit compensates for β_3 integrin subunit during siRNA knockout

Since LM609 is known to inhibit both $\alpha_v\beta_3$ and $\alpha_v\beta_5$ integrin and reduces PTHrP expression (Fig 4.1), we postulated that expression of β_5 integrin subunit compensates for β_3 during siRNA knockdown to rescue PTHrP expression. We examined mRNA expression by quantitative real-time PCR of β_5 integrin subunit in MDA-MB-231 cells transfected with siRNA against β_3 integrin subunit, and found a 2-fold increase in β_5 expression in response to β_3 knockdown (Fig 4.2D). Interestingly, this compensation is not through direct association of the β_5 integrin

subunit with TGFβRII, as the two showed no detectable binding by immunoprecipitation (data not shown).

Exogenous TGFβ stimulation of PTHrP and Gli2 are is Src kinase and $\alpha_v\beta_3$ integrin dependent

It is well known that treatment with exogenous TGFβ stimulates expression of PTHrP and its associated transcription factor, Gli2 [4]. To test whether this stimulation was mediated by integrin activity, we selectively inhibited Src or $\alpha_v\beta_3$ in the presence of exogenous TGFβ in MDA-MB-231 cells. While TGFβ treatment induced 6- and 4- fold increases in PTHrP and Gli2, respectively, it remained at basal levels for PTHrP and was reduced 3-fold for Gli2 when co-treated with PP2 (Fig 4.3 A, C). Similarly, TGFβ treatment was not able to rescue PTHrP or Gli2 expression in MDA-MB-231 cells treated with LM609 (Fig 4.3 B, D).

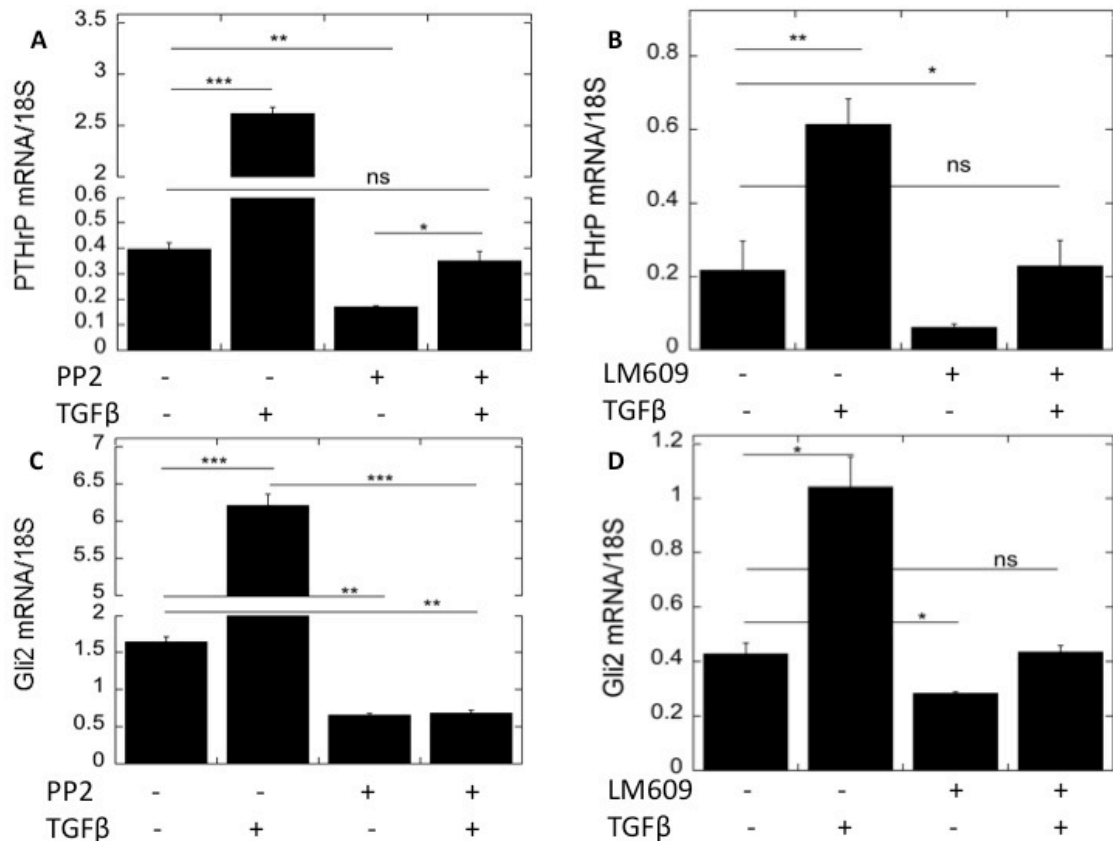

Figure 4.3. Src kinase and integrin $\alpha_v\beta_3$ inhibition suppresses PTHrP expression by exogenous TGF-β treatment. Treatment with PP2 inhibits expression of PTHrP (A) and Gli2 (B). Treatment with 5ng/mL exogenous TGF-β increases expression of PTHrP and Gli2, but this increase is prevented when cells are co-treated with PP2. Similarly, treatment with LM609 inhibits PTHrP (B) and Gli2 (D) and cannot be rescued by co-treatment of TGF-β.

Src induced osteoclastogenic gene expression is mediated by ROCK

We previously reported that ROCK mediates TGFβ-induced PTHrP expression [9], and find here that Src induced β_3 integrin activity is also essential for TGFβ-driven PTHrP expression (Fig 4.3). To test whether Src effects on PTHrP are facilitated by ROCK, we stimulated Src kinase phosphorylation using Bombesin [22] in MDA-MB-231 cells expressing a dominant negative form of ROCK (MDA-KDΔ4) or the TGFβ type II receptor (MDA-TβRIIΔcyt). While Bombesin treatment induced 17- and 3-fold increases in PTHrP and Gli2 expression in MDA-MB-231 cells transfected with an empty vector control, bombesin treatment did not stimulate expression of either gene in MDA-KDΔ4 or MDA-TβRIIΔcyt cells (Fig 4.4).

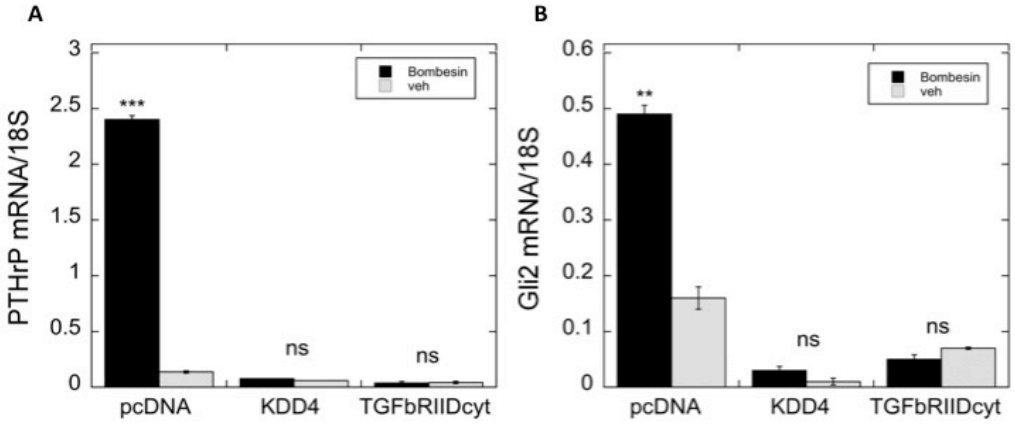

Figure 4.4. ROCK and TGFβRII are required for Src stimulation of PTHrP and Gli2. Treatment with 20nM Bombesin induced significant increases in PTHrP (A) and Gli (B) expression in MDA-MB-231 cells transfected with an empty vector control (pcDNA). Cells expressing a dominant negative form of ROCK (KDD4) or lacking the TGFβ type 2 receptor (TGFβRIIDcyt) did not respond to bombesin treatment.*= $p<0.05$; ** = $p<0.01$; *** = $p<0.005$ compared to vehicle control

Discussion

The rigidity of the extracellular matrix is of increasing interest in the development of new and effective therapies to prevent metastasis, as rigidity has been shown to stimulate Rho-mediated cell contractility to influence a number of cellular outcomes, including motility, morphology and differentiation [24-34]. We have recently demonstrated that Rho-mediated contractility in response to bone-like mechanical properties also contributes to the expression of osteoclastogenic factors in breast cancer, particularly PTHrP and its transcription factor Gli2 [9]. Prior to the generation of cytoskeletal tension, cells need to bind to a solid substratum via integrin clusters, followed by the activation of Src and SFKs to phosphorylate downstream effectors of cytoskeletal tension, such as Rho/ROCK [24]. Integrin $\alpha_v\beta_3$ and Src-mediated phophorylation of TGFβRII have been shown to be of particular interest in breast cancer, where they are implicated in EMT [11], and their inhibition reduces tumor burden and incidence *in vivo* [19, 35]. However, the link between integrin and Src activity and Rho/ROCK dependent cytoskeletal tension in response to substrate rigidity has not been investigated. In this study we show that not only are expression of PTHrP and Gli2 mediated by integrin binding and Src activity, but that this activity is a function of matrix mechanical properties that stimulate Rho-mediated contractility.

Src phosphorylation of TGFβRII in response to TGFβRII and $\alpha_v\beta_3$ clustering is known to activate MAPK signaling [11], an important upstream effector of PTHrP [36]. Specific inhibitors to both Src tyrosine kinases and $\alpha_v\beta_3$ have shown promise in preclinical studies, reducing both tumor burden and incidence in bone [19, 35].

We show here that inhibition of both Src tyrosine kinases and integrin $\alpha_v\beta_3$ specifically reduce the expression of PTHrP and its transcription factor Gli2 by MDA-MB-231 tumor cells. Breast cancer cells require expression of PTHrP to recruit osteoclasts in order to resorb and establish themselves in bone, which releases TGF-β from the bone matrix and serves to further stimulate PTHrP expression by tumor cells [1, 37]. This process is often referred to as the "vicious cycle" of cancer induced bone disease, and is one of the main challenges in the effective treatment of osteolytic metastases. Our finding suggests that Src tyrosine kinase and integrin $\alpha_v\beta_3$ inhibition specifically function to interrupt the vicious cycle and thus prevent the establishment of tumor cells in bone.

Interaction between TGFβRII and $\alpha_v\beta_3$ has also been associated with EMT, a process influenced by tissue rigidity [7, 8]. Previous studies, however, have focused only on the effects of soft tissue ($O(10^3$ Pa)). Since we see that $\alpha_v\beta_3$ integrin activity is important in bone metastases, we wanted to determine whether the mineralized tissue rigidity effects on osteoclastogenic gene expression we have observed [9]. We find that both expression β_3 integrin subunit and its association with TGFβRII increase on substrates with bone-like mechanical properties. These data imply that breast cancer cells specifically change their expression of β_3 integrin subunit in response to bone-like mechanical properties. Furthermore, the increased association of β_3 integrin subunit with TGFβRII suggests that bone-like mechanical properties activate MAPK signaling in MDA-MB-231 cells [11]. Interestingly, knockdown of β_3 integrin subunit does not abrogate PTHrP expression, while treatment with the antibody LM609 does reduce PTHrP expression. It is important

to note that LM609 not only inhibits $\alpha_v\beta_3$, but also $\alpha_v\beta_5$, suggesting a compensatory mechanism between β_3 and β_5 subunit. Indeed, we find that in the absence of β_3 integrin subunit, expression of β_5 subunit is increased. However, the compensation in PTHrP expression does not appear to be mediated by direct binding between β_5 subunit and TGFβRII. It is important to note at this point that Src-kinase activity has been shown to facilitate signaling by $\alpha_v\beta_5$ [38, 39]. Specifically, Src is known to phosphorylate FAK, which is important in mechanotransduction [12], to facilitate signaling through the FAK/$\alpha_v\beta_5$ complex [38]. As such, it is likely that the absence of β_3 integrin subunit induces a compensatory mechanism for PTHrP expression through β_5 subunit and Src, since our data indicate that Src kinase activity affects PTHrP expression. Consequently, effective integrin inhibition therapies for the prevention of bone metastases will likely benefit from cotreatment that also targets downstream effectors such as Src.

Exogenous TGFβ stimulation is known to stimulate PTHrP expression [17], and this stimulation is facilitated in part by ROCK [9]. Since ROCK, Src and integrin binding are all integral parts of the mechanotransduction response, we wanted to determine whether Src and integrin $\alpha_v\beta_3$ are also implicated in TGFβ induced PTHrP expression. We find that blocking signaling of Src and $\alpha_v\beta_3$ prevents any significant stimulation of PTHrP or Gli2 by TGFβ, and that this action is facilitated by ROCK. While TGFβ signaling blockade has been proven effective in reducing bone metastases in animal models [17], its clinical applications are limited due TGFβ's opposing effects on tumor cells at the primary and bone metastatic site. The action of TGFβ is pleiotropic and context dependent; it is generally agreed upon that during

early tumor growth, TGFβ signaling is tumor suppressive, while it furthers malignant conversion and progression in later stage cancers [40-42]. This pleiotropic action complicates the use of TGFβ antagonists in the clinic, suggesting blockade of Src or $\alpha_v\beta_3$ signaling may be a more effective clinical target for the treatment and prevention of bone metastases.

Conclusions

In this study, we have shown that the rigidity of the bone matrix stimulates expression of osteolytic factors *in vitro* through β_3 integrin and Src activity. Specifically, expression of β_3 integrin subunit and its aggregation with TGFβRII, which is known to activate MAPK signaling through Src phosphorylation [11], are stimulated by substrate rigidity. Since MAPK signaling is known to influence PTHrP expression[36], these data suggest that the rigidity of the bone matrix induces PTHrP expression in tumor cells through promoting physical interaction between β_3 integrin subunit and TGFβRII. Additionally, we have demonstrated that the integrin signaling and Src kinase activity are required to induce expression of the osteoclastogenic factor PTHrP and its transcription factor, Gli2, and that this process is mediated by ROCK. Taken together, these data suggest that the rigidity of the bone matrix is involved in in the establishment of osteolytic metastases by stimulating intgrin mediated contractility. This is especially important in breast cancer, as bone metastases are associated with poor patient prognosis. Understanding the mechanisms involved in the establishment of these metastases could ultimately lead to new targeted therapies to improve clinical outcomes.

References

1. Guise, T., et al., *Evidence for a causal role of parathyroid hormone-related protein in the pathogenesis of human breast cancer-mediated osteolysis.* J Clin Invest, 1996. **98**(7): p. 1544-1549.
2. Powell, G.J., et al., *Localization of parathyroid hormone-related protein in breast cancer metastases: increased incidence in bone compared with other sites.* Cancer Res, 1991. **51**(11): p. 3059061.
3. Southby, J., et al., *Immunohistochemical localization of parathyroid hormone-related protein in human breast cancer.* Cancer Res, 1990. **50**(23): p. 7710-6.
4. Sterling, J.A. and B.A. Oyajobi, *The hedgehog signaling molecule Gli2 induces parathyroid hormone-related peptide expression and osteolysis in metastatic human breast cancer cells.* Cancer Res, 2006. **66**(15): p. 7548-7553.
5. Yin, J.J., *TGF-beta signaling blockade inhibits PTHrP secretion by breast cancer cells and bone metastases development.* J Clin Invest, 1999. **103**(2): p. 197-206.
6. Alexander, N.R., et al., *Extracellular matrix rigidity promotes invadopodia activity.* Curr Biol, 2008. **18**(17): p. 1295-1299.
7. Paszek, M.J. and V.M. Weaver, *The tension mounts: mechanics meets morphogenesis and malignancy.* J Mammary Gland Biol Neoplasia, 2004. **9**: p. 325-342.
8. Paszek, M.J., et al., *Tensional homeostasis and the malignant phenotype.* Cancer Cell, 2005. **8**: p. 241-254.
9. Ruppender NS, M.A., Martin TJ, Mundy GR, Sterling JA and Guelcher SA, *Matrix Rigidity Induces Osteolytic Gene Expression of Metastatic Breast Cancer Cells.* PLoS One, 2010. **5**(11): p. e15451.
10. Geiger, B. and A. Bershaksky, *Exploring the neighborhood: adhesion-coupled cell mechanotransducers.* Cell, 2002. **110**: p. 139-143.
11. Galliher AJ, S.W., *Beta3 integrin and Src facilitate transforming growth factor beta mediated induction of epithelial-mesenchumal transition in mammary epithelial cells.* Breast Cancer Research, 2006. **8**(4): p. R42.
12. Cary LA, G.J., *Focal adhesion kinase and integrin-mediated signaling.* Frontiers in Bioscience, 1999. **15**(4): p. D102-113.
13. Liu, S., et al., *Inhibition of rho-associated kinase signaling prevents breast cancer metastasis to human bone.* Cancer Res, 2009. **69**(22): p. 8742-51.
14. Myoui A, N.R., Williams PJ, Hiraga T, Tamura D, Michigami T et. al., *c-Src tyrosine kinase activity is associated with tumor colonization in bone and lung in an animal model of human breast cancer metastasis.* Cancer Research, 2003. **63**(16): p. 5028-5033.
15. Schaller, P.a., *The Interplay between Src and Integrins in Normal and Tumor Biology.* Oncogene, 2004. **23**: p. 7928-7946.
16. Desgrosellier JS, C.D., *Integrins in Cancer: Biological implications and therapeutic opportunities. .* Nature Reviews Cancer, 2010. **10**(1): p. 9-22.
17. JJ Yin, e.a., *TGF beta signaling blockade inhibits PTHrP secretion by breast cancer cells and bone metastases development.* J Clin Invest, 1999. **103**: p. 197-206.

18. Schneider JG, A.S., Weilbaecher KN, *Integrins and Bone Metastasis: Integrating tumor cell and stromal cell interactions.* Bone.
19. Zhao Y, B.R., Treilleux I, Pujuguet P, Peyruchaud O, Baron R *Tumor alphavbeta3 integrin is a therapeutic target for breast cancer bone metastases.* Cancer Research, 2007. **67**(12): p. 5821-5830.
20. Yoneda, T., et al., *A Bone-Seeking Clone Exhibits Different Biological Properties from the MDA-MB-231 Parental Breast Cancer Cells and a Brain-Seeking Clone In Vivo and In Vitro.* Journal of Bone and Mineral Research, 2001. **16**(8): p. 1486-1495.
21. Kang, Y., et al., *A multigenic program mediating breast cancer metastasis to bone.* Cancer Cell, 2003. **3**: p. 537-49.
22. SS Wu, e.a., *Bombesin and angiotensin II rapidly stimulate Src phosphorylation at Tyr-418 in fibroblasts and intestinal epithelial cells through a PP2-insensitive pathway.* Cell Signal., 2005. **17**(193-102).
23. EH Danen, e.a., *Integrins control motile strategy through a Rho-Cofilin Pathway.* J Cell Biol, 2005. **169**(3): p. 515-26.
24. MR Brouns, e.a., *p190 RhoGAP is the principal Src substrate in brain and regulates axon outgrowth, guidance and fasiculation.* Nat Cell Biol, 2001. **3**(4): p. 361-7.
25. McBeath, R., et al., *Cell shape, cytoskeletal tension, and RhoA regulate stem cell lineage commitment.* Dev Cell, 2004. **6**: p. 483-95.
26. Mulder, J., *p116Rip targets myosin phosphatase to the actin cytoskeleton and is essential for RhoA/ROCK-regulated neuritogenesis.* Mol Biol Cell, 2004. **15**: p. 5516-5527.
27. Narumiya, S., M. Tanji, and T. Ishizaki, *Rho signaling, ROCK and mDia1, in transformation, metastasis and invasion.* Cancer Metastasis Rev, 2009. **28**(1-2): p. 65-76.
28. Nishimura, Y., et al., *Overexpression of ROCK in human breast cancer cells: evidence that ROCK activity mediates intracellular membrane traffic of lysosomes.* Pathol Oncol Res, 2003. **9**(2): p. 83-95.
29. Nobes, H., *Rho, rac, and cdc42 GTPases regulate the assembly of multimolecular focal complexes associated witha ctin stress fibers, lamellipodia and filopodia.* Cell, 1995. **81**: p. 53-62.
30. Nobes, H., *Rho GTPases control polarity, protrusion and adhesion during cell movement.* J Cell Biol, 1999. **144**(6): p. 1235-44.
31. Ridley, H., *The small GTP-binding protein rho regulates the assembly of focal adhesions and actin stress fibers in response to growth factors.* Cell, 1992. **70**(3): p. 389-399.
32. DE Discher, e.a., *Tissue cells feel and respond to the stiffness of their substrate.* Science, 2005. **310**(5751): p. 1139-43.
33. Engler, A.J., et al., *Matrix Elasticity Directs Stem Cell Lineage Specification.* Cell, 2006. **126**: p. 677-689.
34. Wells, R.G. and D.E. Discher, *Matrix elasticity, cytoskeletal tension, and TGF-beta: the insoluble and soluble meet.* Science Signaling, 2008. **1**(10).

35. Harms, e.a., *A small molecule antagonist of the alphavbeta3 integrin suppresses MDA-MB-435 skeletal metastasis.* Clin Exp Met, 2004. **21**: p. 119-128.
36. SM Kakonen, e.a., *Transforming growth factor beta stimulates parathyroid hormone related protein an dosteolytic metastases via Smad and MAPK signaling pathways.* J Biol Chem, 2005. **227**(24571-78).
37. TA Guise, e.a., *PTHrP expression by breast cancer cells enhance osteolytic bone metastases in vivo.* J Bone Min R, 1994. **9**: p. S128.
38. BP Eliceiri, e.a., *Src-mediated coupling of focal adhesion kinase to integrin alphavbeta5 in vascular endothelial growth factor signaling.* J Biol Chem, 2002. **157**(1): p. 149-60.
39. M Leifheit-Nestler, e.a., *Overexpression of integrin beta 5 enhances the paracrine properties of circulating angiogenic cells via Src kinase mediated activation of STAT3.* Arterioscler Thromb Vasc Biol, 2010. **30**(7): p. 1398-406.
40. W Cui, e.a., *TGFb1 inhibits the formation of benign skin tumors, but enhances progression to invasive spindle carcinomas in transgenic mice.* Cell, 1996. **86**: p. 531-542.
41. R Derynck, e.a., *TGFb signaling in tumor suppression and cancer progression.* Nat Genet, 2001. **29**: p. 117-129.
42. PM Siegel, e.a., *Transforming growth factor beta signaling impairs Neu-induced mammary tumorigenesis while promoting pulmonary metastasis.* PNAS, 2003. **100**: p. 8430-8435.

CHAPTER V

FUTURE DIRECTIONS IN THREE DIMENSIONAL CELL CULTURE

Introduction

In the past 10 years it has become increasingly evident that mechanisms of cellular migration and mechanotransduction play a vital role in cell differentiation and the progression of many diseases, including cancer[1-7]. While 2D *in vitro* culture is a valuable tool in beginning to understand cell behavior, cells grow within a 3D matrix in most physiological conditions, where they can experience matrix rigidities ranging from 10^3 – 10^{10} Pa [8]. Since both fibroblast and epithelial cell polarity, morphology and migration differ when grown in 2D and 3D culture [9-11], it becomes important to compare 2D and 3D *in vitro* models used to study cell-matrix interactions, especially in cancer where abnormal polarity and cell architecture are associated with carcinogenesis [12, 13]. We have previously succeeded in generating 2D *in vitro* culture systems to study the effects of a wide range if substrate rigidities on invadopodia formation [14], intracellular signaling and gene expression [15], implicating cellular processes involved in polarity, morphology and migration. In light of the known differences observed in these processes in 2D and 3D culture [9-11], we sought to explore the influences of a 3D microenvironment on our findings of rigidity and cancer invasiveness. To do so, we compared the gene expression of MDA-MB-231 cells cultured on the 2D substrates described in chapter III to 3D substrates ranging in rigidity from 25 kPa to 115 GPa.

Materials and Methods

Materials Synthesis

To span a wide range of rigidities, we employed the use of hydrogels and polyurethanes, as well as hydroxyapatite substrates as a hard tissue control. 3D collagen hydrogels were prepared with the Chemicon 3D collagen gel culture system per manufacturer's instructions with the addition of fibronectin at an equal concentration to that adsorbed to the hydroxyapatite and PUR scaffolds (see *Fibronectin Characterization,* chapter III). Hydroxyapatite scaffolds were provided by Interpore Cross. Methyl 2,6-diisocyanatohexane (lysine methyl ester diisocyanate, LDI) was purchased from Kyowa Hakko USA (New York, NY). Coscat 83, an organobismuth urethane catalyst, was supplied by ChasChem, Inc. (Rutherford, NJ). Stannous octoate, glycerol, poly(e-caprolactone) triol (300 Da), and e-caprolactone were purchased from Aldrich (St. Louis, MO), and glycolide was purchased from Polysciences (Warrington, PA). Glycerol was dried at 10 mm Hg for 3 hours at 80^{o}C and e-caprolactone was dried over anhydrous magnesium sulfate prior to use. All other materials were used as received.

Quasi-prepolymer was synthesized by charging poly(e-caprolactone) (PCL, 300 g mol^{-1}) to a flask fitted with a reflux condenser and heated to 60^{o}C in an oil bath. Lysine diisocyanate methyl ester (LDI, Kyowa Hakko) was then charged, the reactor immersed in an oil bath maintained at 90^{o}C, and Coscat 83 was added while stirring under dry argon. The reaction was allowed to proceed for three hours under vacuum at 90^{o}C, at which time the reactor was purged with dry argon and the quasi-prepolymer was poured into a vessel stored at 4^{o}C. Structure was verified by nuclear magnetic

resonance spectroscopy (NMR, Bruker, 300 MHz), molecular weight was measured by GPC, and % free NCO was measured by titration.

Polyester triols ranging from 300 to 3000 g mol^{-1} (100 – 1000 g eq^{-1}) were synthesized from a glycerol starter, 70% e-caprolactone and 30% glycolide monomers, and stannous octoate catalyst as described previously [16]. Briefly, the appropriate amounts of dried glycerol, dried e-caprolactone, glycolide, and stannous octoate (0.1 wt-%) were mixed in a 100-ml flask and heated under an argon atmosphere with mechanical stirring to 135°C. The mixture was allowed to react for ~30 h and subsequently removed from the oil bath. NMR was used to verify the structure of the polyester triols, with deuterated dichloromethane (DCM) as a solvent. The hydroxyl (OH) number was measured by titration (Metrohm 798 MPT Titrino) according to ASTM D-4662-93 as described [17].

2D substrates were synthesized by mixing an appropriate amount of poly(e-caprolactone-*co*-glycolide) triol with LDI quasi-prepolymer, and COSCAT 83 catalyst (Vertellus) for 20s in a Hauschild SpeedMixer™ DAC 150 FVZ-K vortex mixer (FlackTek, Inc, Landrum, SC). The targeted index (ratio of NCO to OH equivalents times 100) was 105. The resultant mixture was poured into the wells of a tissue culture plate and allowed to cure for 24h at 60°C. To facilitate cell adhesion and ensure that the surface chemistry was constant for all substrates tested, fibronectin (Fn) was adsorbed to the surface of the substrates by incubating them in a 4μg/mL solution of Fn in PBS at 4°C overnight.

3D PUR scaffolds were prepared by combining polyol, isocyanate and catalyst as described above, with the addition of crystalline NaCl at a ratio of 8 parts salt to 1 part

total polymer. The mixture was then poured into a Teflon mold and allowed to cure for 24h at 60°C, followed by porogen leaching in distilled water overnight. Scaffolds were vacuum dried at 80°C overnight, followed by ethylene oxide sterilization prior to cell culture. Structure and pore connectivity was verified by SEM. To facilitate cell adhesion and ensure that the surface chemistry was constant for all scaffolds tested, Fn was adsorbed to the scaffolds by incubating them in a 50 μg/mL solution of Fn in PBS at 4°C overnight and coverage was detected by ELISA (described in chapter III).

Mechanical Properties of 3D Scaffolds and 2D Substrates

Tensile modulus and strength of the PUR films were measured at 37°C for 3×15×1mm films using a TA Instruments Q800 DMA (controlled force displacement ramp, 1 N min^{-1} to 18 N min^{-1}) [16]. Storage and loss moduli for the polyacrylamide gels under shear conditions were measured using a TA Instruments AR-G2 Rheometer (TA Instruments, New Castle, DE) at 37°C, using a 20-mm circular head as described previously [1, 18]. Gels were compressed between a heated Peltier plate and a 20-mm upper plate and subjected to an oscillating (0.1 – 10 Hz) shear strain that was validated to be in the linear range by strain sweep tests.

Compression moduli of the PUR scaffolds were measured at 37°C for 4x4mm disks using a TA Instruments Q800 DMA (controlled force displacement ramp, 1 N min^{-1} to 18 N min^{-1}). This modulus is related to Young's modulus of the bulk polymer E_s, analogous to the tensile modulus for the nonporous materials, by the following equation [19]:

$$\frac{E^*}{E_s} = C_1\left(\frac{\rho^*}{\rho_s}\right)^2 \qquad (5.1)$$

where ρ^* = scaffold density, ρ_s = bulk polymer density, and the constant $C_1 \cong 1$ includes the geometric constants of proportionality. For brittle materials, the bulk and scaffold moduli were related by [19]

$$\frac{\sigma^*}{\sigma_{fs}} \approx 0.2\left(\frac{\rho^*}{\rho_s}\right)^{\frac{3}{2}} \qquad (5.2)$$

where σ^* is the stress in the scaffold at brittle collapse and σ_{fs} is the tensile stress at failure of the bulk material. σ_{fs} was determined by tensile testing (controlled force displacement ramp, 1 N min^{-1} to 18 N min^{-1}) and recording the stress at failure. The elastic modulus of the brittle scaffold can then be calculated using

$$E^* = \frac{2\sigma^* l^2}{3\delta t} \qquad (5.3)$$

where l is the length of the beam, δ is the deflection of the beam at failure and t is the thickness of the beam as determined by 3-point bend testing.

Cell Culture

MDA-MB-231 cells were maintained and cultured at 37°C under 5% CO_2 in 1x DMEM plus 10% heat inactivated FBS and 1% penicillin/streptomycin. PUR and HA scaffolds were incubated in a solution of MDA-MB-231 cells ($1x10^6$ cells/mL) on a shaker for 1h. Scaffolds were then transferred into a tissue culture plate and maintained at 37°C under 5% CO_2 in 1x DMEM plus 10% heat inactivated FBS and 1% penicillin/streptomycin.

Cells were harvested with trypsin and centrifugation from scaffolds after 24h in culture for mRNA extraction (Qiagen RNeasy kit). Cells were embedded in the 3D collagen gels by addition of 10% by volume of a $3x10^5$ cells/mL solution prior to polymerization. The gels were then maintained for 24h at the conditions mentioned above. Cells were harvested by incubating the gels in a solution of collagenase in PBS (1000 u/mL) for 30 min.

Quantitative Real Time PCR

To measure changes in gene expression, mRNA reverse transcription was carried out using the SuperScript III kit per manufacturer's instructions. Briefly, total RNA was extracted using the RNeasy Mini Kit. The SuperScript III First Strand Synthesis System for quantitative RT-PCR primed with random hexamers was used to synthesize cDNA using between 1 and 5μg total RNA. The expression of PTHrP and Gli2 was measured by quantitative RT-PCR using validated TaqMan primers with the 7300 Real-Time PCR System (Applied Biosciences). Assays were performed in triplicate on the RealPlex Machine (Eppendorf) under the following cycling conditions: 95°C for 15 seconds, 58°C for 30 seconds, and 68°C for 30 seconds. Quantification was performed using the absolute quantitative for human cells method using 18S as an internal control.

Results

We observed similar increases in both PTHrP and Gli2 mRNA expression in response to increased substrate and scaffold modulus in both 2D and 3D culture at lower elastic moduli, suggesting that cells in the bone microenvironment experience 2D-like conditions on scaffolds up to 10^9 Pa (Fig 5.1 A-D).

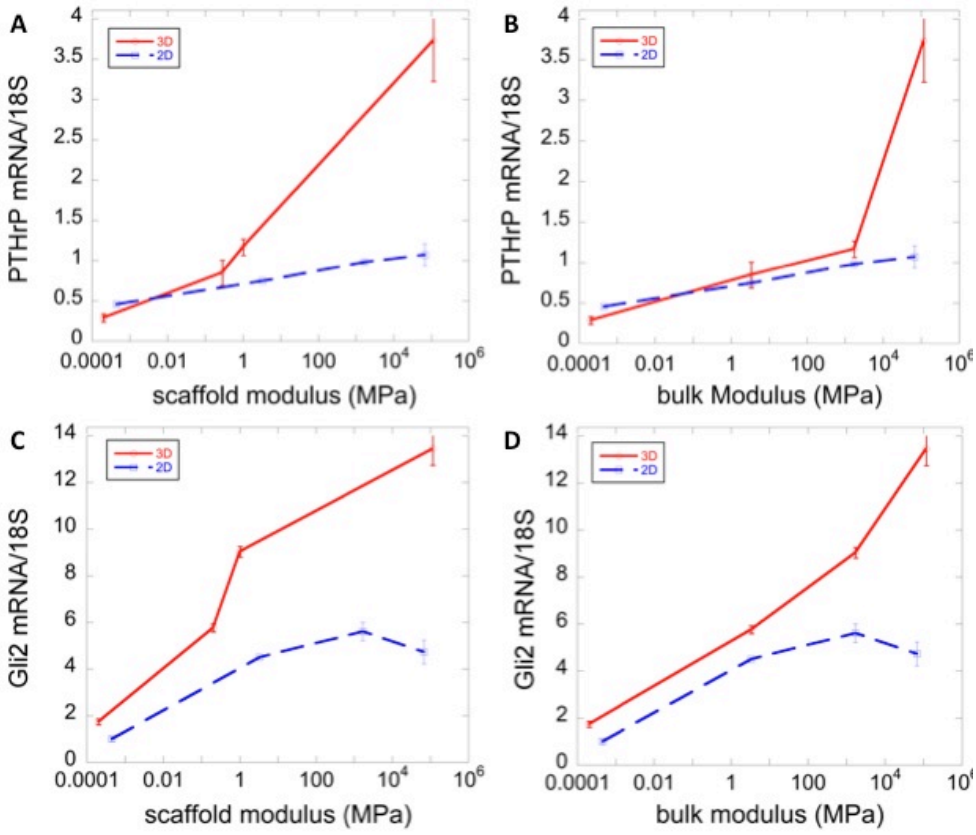

Figure 5.1. Expression of PTHrP and Gli2 by MDA-MB-231 cells in 2D and 3D culture as a function of scaffold and bulk modulus. MDA-MB-231 cells showed increased expression of PTHrP and Gli2 in both 2D and 3D culture. This effect appeared to be enhanced when examining expression of PTHrP (A) and Gli2 (C) as a function of scaffold modulus. Closer agreement, however, was revealed when examining PTHrP (B) and Gli2 (D) expression as a function of bulk modulus.

We also examined the effects of rigidity in 3D as a function of bulk modulus. Equations 5.1-3 define the relationship between Young's modulus of the scaffold, E^*, and that of the bulk polymer, E_s. A summary of comparisons between measured and calculated scaffold and bulk moduli is given in table 5.1.

Table 5.1 Measured, calculated and bulk moduli for 3D PUR scaffolds

Modulus (MPa)/Material	T3000	PCL300
E^* (measured)	0.26	0.90
E^* (calculated)	0.21	1.4
E_s	3.3	1700

Analysis of gene expression as a function of bulk modulus, which is analogous to the tensile moduli measured for the 2D films, revealed a closer agreement of values for lower moduli. This suggests that cells may be experiencing an environment similar to that of a 2-dimensional surface in the pore of the 3D scaffold, and are able to deform the softer materials in the x-y plane. This is to be expected, as cells are on the order of 10 μm, whereas pore size in the 3D scaffold is approximately 350 μm in diameter (Fig 5.2A). Furthermore, this situation is representative of the trabecular bone microenvironment (a site for early metastases), where the trabecular network size ranges from 75 to 500μm (Fig 5.2B). Nevertheless, there remained a difference between the hard control substrates, suggesting that at high rigidities, cell experience the 2D and 3D environment differently.

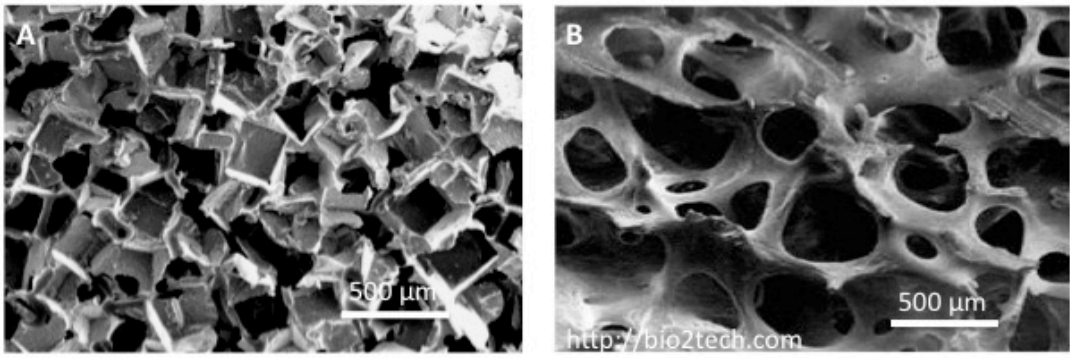

Figure 5.2. SEM images of salt-leached PUR scaffold and trabecular bone. PUR scaffolds show interconnected pores and an average pore size of approximately 350 μm (A). Scanning electron micrographs of trabecular bone show similar average pore size, ranging from approximately 75 to 500 μm (B).

Discussion

While these data are compelling, they warrant further study into the effects of 2D and 3D culture with respect to cancer-induced bone destruction. While we have demonstrated a clear rigidity mediated effect, the three dimensional spatial organization of cancer cells in bone remains the subject of further study. Cell behavior – from division through proliferation, migration and apoptosis-- is tightly regulated by the cell's spatial and temporal organization. With respect to cancer, cell polarity, migration and proliferation—the hallmarks of abnormal morphogenesis -- are all known to be dependent on 3D spatial organization[9-11]. Thus, physiologically relevant *in vitro* synthetic replicates of tissues will need to be controlled for pore size, architecture and surface chemical composition to account for mechanical cues, cell-matrix communication and cell-cell interactions. As such, PUR scaffolds with alternative pore geometries should be tested for synthetically replicating bone *in vitro*. This could be achieved with either an alternative porogen (such as spherical paraffin microbeads) or gas foaming, as described previously [16]. It is also important to note that cells embedded within a hydrogel matrix likely differ in their spatial organization and polarity than those seeded within a porous 3D scaffold such as the polyurethanes and hydroxyapatite scaffolds described in this chapter. As such, the porosity of the scaffold and tissue in question must be considered when designing biomimetic 3D *in vitro* scaffolds. Cells in soft tissue are embedded within the extracellular matrix [14], thus embedding cells within a hydrogel presents an appropriate simulation of this native environment. Conversely, tumor cells in bone grow in the marrow cavity and fill the trabecular space, and thus a porous scaffold approximating the porosity of bone,

such as the PUR scaffolds described in this chapter, appropriately mimic this environment. Interestingly, when examining PTHrP and Gli2 expression as a function of 3D scaffold modulus, we observe the most significant increases in gene expression when drastically increasing scaffold modulus (1MPa for PCL300 to 115 GPa for HA, Figure 5.1) and not when changing scaffold architecture (collagen, 0.002 MPa to T3000, 0.2MPa, Figure 5.1), suggesting that the rigidity of the scaffold is the primary influence on expression of PTHrP and Gli2 by MDA231.

To promote native-tissue like properties in a synthetic scaffold, micron length scales must be considered in its construction. The tissue type in question can direct architecture of the scaffold; parallel fibers have been shown to promote peripheral nerve reconstruction [20], while random non-woven networks aid in skin repair [21, 22]. Thus, indentation techniques may be considered for determining mechanical properties on the length scale of the cell for the tissue of interest and associated synthetic replicate. While this may appear to be a more appropriate technique for measuring mechanical properties of a substrate given the length scale of the cell, it is important to consider both the nature of the material itself as well as the mode of deformation. Since many synthetic materials used *in vitro* are affine crosslinked polymer networks and only experience small deformations, it can be assumed that these deformations are distributed homogeneously throughout the material and strain is constant on all length scales. As such, the bulk material properties are relevant to determine forces experienced by the cell. When examining gene expression as a function of scaffold modulus, we see early divergence between the 2D and 3D data (Figure 5.1A, C). However, when these same 3D data are analyzed as a function of bulk

modulus calculated from either equation 5.1 (for non-brittle polymers such as the T3000) or equations 5.2 and 5.3 (for brittle materials such as hydroxyapatite and PCL300), we see much closer agreement between the 2D and 3D curve (Figure 5.1 B, D). Interestingly, there remained a significant increase for the extremely rigid hydroxyapatite material (Figure 5.1 B, D). This could be indicative of either a differential spike in PTHrP and Gli2 expression at extremely high rigidities or an effect of the spatial organization of the cells within the pore of the scaffold. MDA-MB-231 cells have been shown to exhibit tissue tropism [23], with subclones that preferentially metastasize to bone (such as the one employed in this work) proliferating more rapidly on rigid matrices than on soft ones. This could result in increased proliferation of the cancer cells within the hydroxyapatite scaffold as compared to the PUR scaffold, resulting in cell packing and thus a differing spatial organization that could affect gene expression. Nevertheless, further studies need to be performed to conclusively determine the cause of the observed increase in PTHrP on the hydroxyapatite scaffolds.

Furthermore, design of accurate *in vitro* replicates of tissues must take into consideration the organization of a cell within the native tissue. Depending on tissue type, cells could be attached to a 2D surface within a 3D matrix, or be anchored on more than two planes, which determines whether the scaffold or bulk modulus is relevant to cell behavior. This distinction between E_s and E^* is particularly interesting when considering a single cell attached within the pore of a scaffold as opposed to a cell attached to a 2-dimensional flat surface. While a cell generates contractile forces in the x-y plane in 2D culture, it could potentially generate forces in all 3 dimensions when embedded within a scaffold, depending on the size and shape of the pore. Additionally,

pore walls are much thinner than 2D surfaces for cell culture, which affects the cell's ability to deform its surroundings. Thus, it is vital to consider length scales in the design and characterization of any material used for studying cell behavior.

Ultimately, the goal is to recreate the structure of the native tissue completely, taking into account tissue organization and mechanics. Irrespective of tissue type, scaffolds must feature pore size, connectivity and geometry to allow for mass transport and nutrient exchange, as well as control of macromechanical properties. Surface concentration and distribution of adhesion-mitigating proteins (such as those containing the RGD sequence) can also affect cell behavior. It has been demonstrated that a minimum spacing of 440nm is required to facilitate cell attachment, and that a further increase in surface concentration (<140nm spacing) promoted formation of stress fibers and focal adhesions [24]. Thus, the *in vitro* model of the future should be able to accurately modulate the surface concentration and distribution of tissue relevant matrix proteins independent of bulk material composition.

Studies of tissue rigidity and architecture in disease progression will ideally lead to preclinical models for the development of new therapies. While animal models are the current standard for preclinical models, study of tissue mechanics on cell behavior is complicated in native tissues due to different growth factors, cytokines, ECM proteins and tissue architecture. It thus becomes desirable to create an artificial tissue-like environment within the animal, where the biochemical makeup as well as the architecture can be controlled. The polyurethane materials described in chapters II-IV have shown *in vivo* biocompatibility [16, 25, 26], and 3D porous scaffolds fabricated by either gas foaming or porogen leaching can be implanted subcutaneously in an animal

to generate a mechanically tunable *in vivo* system for the study of cell-matrix interactions. Such a model could definitively answer questions about tissue rigidity effects *in vivo* and allow for testing of drugs that specifically target only mechanotransduction.

Taken together, these findings demonstrate the need for more accurate *in vitro* models if we are to advance the field of molecular biology to develop new therapies for current clinical problems. Given the complexity of both native tissue and the resultant manufacturing of structurally and biochemically controlled synthetic scaffolds, such studies require new collaborative approaches that likely overlap the fields of biology and engineering.

References

1. Alexander, N.R., et al., *Extracellular matrix rigidity promotes invadopodia activity.* Curr Biol, 2008. **18**(17): p. 1295-1299.
2. Butcher, D.T., T. Alliston, and V.M. Weaver, *A tense situation: forcing tumour progression.* Nat Rev Cancer, 2009. **9**(2): p. 108-22.
3. Paszek, M.J., et al., *Tensional homeostasis and the malignant phenotype.* Cancer Cell, 2005. **8**: p. 241-254.
4. Yeung, T., et al., *Effects of Substrate Stiffness on Cell Morphology, Cytoskeletal Structure, and Adhesion.* Cell Motil. Cytoskeleton, 2005. **60**: p. 24-34.
5. DE Discher, e.a., *Tissue cells feel and respond to the stiffness of their substrate.* Science, 2005. **310**(5751): p. 1139-43.
6. Engler, A.J., et al., *Matrix Elasticity Directs Stem Cell Lineage Specification.* Cell, 2006. **126**: p. 677-689.
7. Wells, R.G. and D.E. Discher, *Matrix elasticity, cytoskeletal tension, and TGF-beta: the insoluble and soluble meet.* Science Signaling, 2008. **1**(10).
8. E Cukierman, e.a., *Taking Cell-Matrix Adhesions to the Third Dimension.* Science, 2001. **294**(5547): p. 1708-12.
9. Bissell, C.R.a.M., *Dynamic reciprocity revisited: a continuous, bidirectional flow of information between cells and the ECM regulates mammary epithelial cell function.* Biochem Cell Biol, 1995. **78**(7-8): p. 391-7.
10. Bard, T.E.a.J., *Collagen substrata for studies on cell behavior.* J Cell Biol, 1972. **54**(3): p. 626-37.
11. Broecker, P.F.a.E., *The biology of cell locomotion within three-dimensional extracellular matrix.* Cellular and Molecular Life Sciences, 2000. **57**(1): p. 41-64.
12. Weitzman, B.a., *Culture of normal and malignant primary epithelial cells in a physiological manner simulates in vivo patterns and allows discrimination of cell type.* Cancer Research, 1993. **53**: p. 2644-54.
13. Taylor-Papadimitrou, D.A.a.J., *Cell adhesion molecules in the normal and cancerous mammary glad.* J Mam Gland Biol Neoplasia, 1996. **1**: p. 207-18.
14. Parekh A, R.N., et al., *Sensing and Modulation of Invadopodia Across a Wide Range of Rigidities.* Biophys J., 2011. **100**(3): p. 573-82.
15. Ruppender NS, M.A., Martin TJ, Mundy GR, Sterling JA and Guelcher SA, *Matrix Rigidity Induces Osteolytic Gene Expression of Metastatic Breast Cancer Cells.* PLoS One, 2010. **5**(11): p. e15451.
16. Hafeman, A., et al., *Injectable biodegradable polyurethane scaffolds with release of platelet-derived growth factor for tissue repair and regeneration.* Pharm Res, 2008. **25**(10): p. 2387-99.
17. Guelcher, S.A., et al., *Synthesis, mechanical properties, biocompatibility, and biodegradation of polyurethane networks from lysine polyisocyanates.* Biomaterials, 2008. **29**(12): p. 1762-1775.
18. Enderling, H., et al., *Dependence of invadopodia function on collagen fiber spacing and crosslinking: computational modeling and experimental evidence.* Biophys J, 2008. **95**(5): p. 2203-2218.
19. Ashby, L.G.a.M., *Cellular Solids: Structure and Properties*. 2nd ed1997, Cambridge, UK: Cambridge University Press.

20. T Sun, e.a., *Development of a bioreactor for evaluating novel nerve conduits.* Biotechnol. Bioeng, 2008. **99**: p. 1250-1260.
21. T Sun, e.a., *Self organization of skin cells in a three dimensional electrospun polystyrene scaffold.* Tissue Eng, 2005. **11**: p. 1023-1033.
22. KA Blackwood, e.a., *Development of biodegradable electrospun scaffolds for dermal replacement.* Biomaterials, 2008. **29**: p. 3091-3104.
23. Kostic A, e.a., *Differential Matrix Rigidity Response in Breast Cancer Cell Lines Correlates with the Tissue Tropism.* PLoS One, 2009. **4**(7): p. e6361.
24. Hubbell, S.M.a.J., *An RGD spacing of 440 nM is sufficient for integrin alphavbeta3 mediated fibroblast spreading and 140nm for focal contact and stress fiber formation.* J Cell Biol, 1991. **114**: p. 1089-1100.
25. Hafeman, A.E., et al., *Local delivery of tobramycin from injectable biodegradable polyurethane scaffolds.* J Biomater Sci, Polym Ed, 2008. **In Press**.
26. Li, B., et al., *The effects of rhBMP-2 released from biodegradable polyurethane/microsphere composite scaffolds on new bone formation in rat femora.* Biomaterials, 2009. **30**(35): p. 6768-79.

CHAPTER VI

THE FUTURE OF CANCER TREATMENT: TARGETED THERAPIES FOR BONE METASTASES

With a survival rate of less than 30% [1], the need for more effective therapies for osteolytic bone metastases is clear. While the current standard of clinical care focuses on slowing progression of bone destruction in combination with cytotoxic agents to eradicate the cancer, future therapies will consist of targeted treatments – drugs that selectively target signaling pathways used by the cancer cells to home to and establish themselves in bone. Several targets have previously been identified in successful preclinical trials (such as TGFβ and MMP blockade), but have achieved little success in a clinical setting due to complex pleiotropic and mechanistic challenges [2]. In the past 5 years, the fields of biophysics and mechanotransduction have become increasingly relevant in terms of cell fate and behavior, particularly with respect to cancer. Increased tissue rigidity is one of the first signs of breast cancer [3] – women with breast cancer present in the clinic with suspicious lumps in the breast – and this increased rigidity has been found to promote abnormal cell morphogenesis and cancer invasiveness [4-6]. This concept has to date not been clearly translated to bone, in part because previous studies had suggested that cells cannot distinguish and are thus unaffected by the rigidity of bone [7, 8]. Nevertheless, some preclinical studies for antagonists of various mechanotransduction effectors have shown promise in the prevention and

reduction of cancer induced osteolytic lesions, but the exact mechanisms behind this efficacy are not well understood [9, 10].

This lack of understanding is, in part, due to the fact that it is technically challenging to accurately study the effects of tissue rigidity both *in vitro* and *in vivo*. Studying the effects of tissue mechanics *in vivo* is challenging because of the different biochemical makeup of the tissue itself. The growth factor and cytokine makeup of bone, for example, vastly differs from that of breast tissue, making it impossible to separate rigidity effects from biochemical effects in native tissue. Thus, the need for mechanically tunable biocompatible synthetic materials is clear. Tissues in the body range from 10^3 – 10^{10} Pa [11], and generating materials to synthetically replicate these conditions and studying their effects on cell behavior requires knowledge of both materials science and molecular biology, demonstrating the increasing need for cross-discipline collaboration to advance our understanding of biological processes.

The need for more effective cancer therapies is clear: large scale randomized clinical studies of chemotherapy efficacy have only shown a 2% increase in 5-year survival rates, calling into question the justification of chemotherapy as the current standard of clinical care [12]. Furthermore, bisphosphonates, which are commonly co-prescribed for the treatment of osteolytic metastases, do not target the tumor itself and only serve to slow cancer associated bone destruction. Past studies have identified both proteases and growth factors as clinical targets to prevent the progression of cancer, but targeting these molecules has, as of yet, shown little success in the clinic.

Preclinical trials of MMP inhibitors (MPI) were promising, leading to further evaluation in clinical trials. Unfortunately, results of phase I and II clinical trials have been disappointing due to a number of reasons. Patients reported musculoskeletal pain and inflammation with broad spectrum MPI treatment, a complication not observed in the preclinical trials [13]. In response, Agouron and Bayer developed selective MPIs (prinomastat and tanomastat), but these were also plagued with the same side effects [13]. Clinical efficacy of MPIs has also come under scrutiny, as their action is cytostatic (slows cell growth) rather than cytotoxic. Phase III clinical trials attempted to examine the benefit of MPIs over the current standard of care, and unfortunately led to the conclusion that MPIs are of little benefit in the treatment of human cancer. One reason for this may be that MPIs were administered to patients with advanced disease, while in the preclinical mouse models they were given at early stages of disease and administered throughout tumor progression[13]. This early stage treatment is of course an unrealistic condition in the clinic and also suggests that MPIs are unsuitable for the treatment of metastatic disease.

TGFβ signaling blockade has also shown great promise in preclinical animal models of metastatic breast cancer, reducing both tumor burden and growth of breast cancer in bone [14], but its clinical use is complicated due to TGFβ's pleiotropic effects. Not only does TGFβ suppress tumor growth in early stage cancer while promoting invasion in late stage cancer, but it is also known to affect the tumor microenvironment by upregulating protease and ECM production while decreasing immune activity [2]. A patient may undergo a mastectomy to remove a

primary malignancy but has subsequently developed osteolytic metastases to be treated with anti-TGFβ therapy. While this course of action may treat the metastases, it could potentially stimulate cells at the primary site to become invasive and proliferate, thus restarting the process of invasion. TGFβ signaling is also implicated cell cycle regulation, proliferation and immune function for many cell types, further complicating its clinical use. Given its complexity, the biological target for TGFβ related therapies may be stromal, immune, vascular or a combination of all of these. Additionally, given TGFβ's involvement in numerous normal cellular functions, long term effects of anti-TGFβ therapy are required before any viable clinical therapies can be developed.

Considering the increasing body of evidence implicating mechanotransduction responses in cancer progression, future clinical trials will likely focus on new targets, such as ROCK, $\alpha_v\beta_3$, and Src. A novel preclinical model of breast cancer metastasis to human bone showed that the specific small molecule antagonist to ROCK, Y27632, reduced the presence of metastatic lesions, but was not clear in demonstrating a pathway by which ROCK promotes breast cancer metastasis [10]. Furthermore, the $\alpha_v\beta_3$ antagonist PSK1404 has shown promise in the prevention of bone metastasis in preclinical models, yet its exact role in the prevention of lesions is not well understood [9, 15]. Similarly, although PTHrP has been identified as a target in osteolytic tumor progression some time ago, the mechanisms behind its initiation are not well understood[16, 17]. Furthermore, although PTHrP inhibition has been shown successful in the prevention of bone metastases in animal models [18], clinical trials using an anti-PTHrP antibody have

shown little success. Guanosine nucleotides, including the chemotherapeutic 6-thioguanine, have also shown promise in inhibiting PTHrP [19], however their clinical use is complicated due to cytotoxicity and lack of bioavailability in bone. However, our data suggest that Rho mediated contractility is central to breast cancer induced bone destruction. Furthermore, it has recently been established that Rho-mediated contractility is part of a feed-forward signaling loop that drives contractility and promotes invasiveness [20]. Specifically, increased ECM crosslinking in soft tissue (due to tumor-secreted lysyl oxidase) stimulates cell contraction through sites of integrin adhesion via Rho/ROCK. This resultant tension leads to further matrix stiffening and continued signaling by ROCK to drive expression of genes to promote an invasive phenotype (Fig 6.1). Since bone is a rigid, mineralized tissue, it presents an environment that facilitates a constitutive activation of this loop. Furthermore, our data show that disrupting key components of this loop (Src, $\alpha_v\beta_3$, or ROCK) block the expression of osteoclastogenic genes.

These findings suggest that targeting components of the mechanotransduction signaling loop could present viable targets for clinical trials in the treatment of bone metastases. While we and others have shown clear rigidity mediated effects on mechanotransduction processes involving integrin and Rho mediated contractility [5-8, 21-27], these processes are also known to be dependent on spatial organization of the cell within the matrix [26, 28-31]. As such, future models of ECM influences on disease progression must take into account the organization of normal and malignant cells within the native tissue. Given the complexity of cellular and tissue architecture, development of such models will

likely involve concepts of polymer science, tissue engineering, physiology and molecular biology. It is our hope that overlap and collaboration in these fields will lead to the development of new *in vitro* and *in vivo* models for the study of cell-matrix interactions and new insights into the progression of metastatic disease to ultimately generate targeted cancer cures.

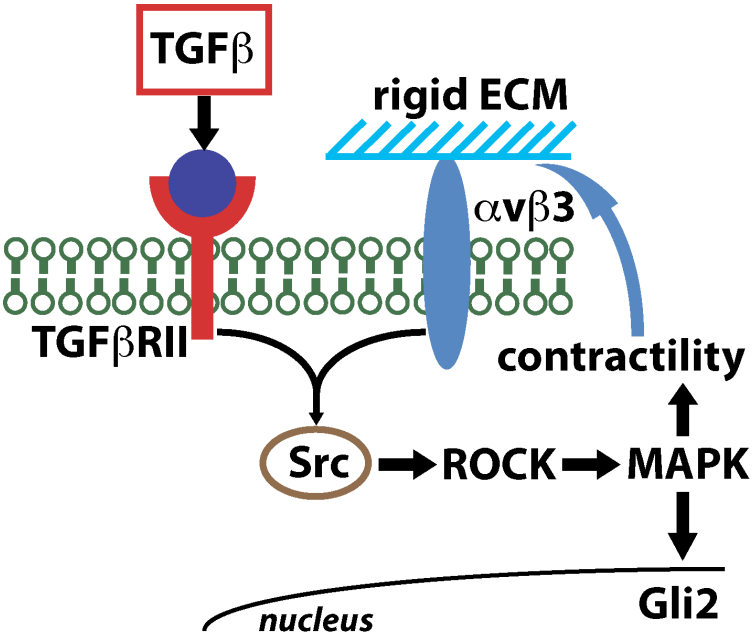

Figure 6.1. Mechanotransduction feed-forward loop involved in cancer progression. ROCK, stimulated by matrix rigidity, drives integrin and Src mediated contractility. This in turn further stimulates ROCK to facilitate expression of osteoclastogenic factors.

References

1. American Cancer Society. *Cancer Facts and Figures*. 2010.
2. R Derynck, e.a., *TGFb signaling in tumor suppression and cancer progression.* Nat Genet, 2001. **29**: p. 117-129.
3. MW Beckmann, D.N., HG Schnurch, BA Gusterson, HG Bender, *Multistep carcinogenesis of breast cancer and tumor heterogeneity.* Journal of Molecular Medicine, 1997. **75**: p. 429-439.
4. Paszek, M.J. and V.M. Weaver, *The tension mounts: mechanics meets morphogenesis and malignancy.* J Mammary Gland Biol Neoplasia, 2004. **9**: p. 325-342.
5. Paszek, M.J., et al., *Tensional homeostasis and the malignant phenotype.* Cancer Cell, 2005. **8**: p. 241-254.
6. Alexander, N.R., et al., *Extracellular matrix rigidity promotes invadopodia activity.* Curr Biol, 2008. **18**(17): p. 1295-1299.
7. DE Discher, e.a., *Tissue cells feel and respond to the stiffness of their substrate.* Science, 2005. **310**(5751): p. 1139-43.
8. Engler, A.J., et al., *Matrix Elasticity Directs Stem Cell Lineage Specification.* Cell, 2006. **126**: p. 677-689.
9. Zhao Y, B.R., Treilleux I, Pujuguet P, Peyruchaud O, Baron R *Tumor alphavbeta3 integrin is a therapeutic target for breast cancer bone metastases.* Cancer Research, 2007. **67**(12): p. 5821-5830.
10. Liu, S., et al., *Inhibition of rho-associated kinase signaling prevents breast cancer metastasis to human bone.* Cancer Res, 2009. **69**(22): p. 8742-51.
11. SW Moore, e.a., *Stretchy proteins on stretchy substrates: the important elements of integrin-mediated rigidity sensing.* Dev Cell, 2010. **19**: p. 194-206.
12. G Morgan, e.a., *The contribution of cytotoxic chemotherapy to 5-year survival in adult malignancies.* Clin Oncol, 2004. **16**(8): p. 549-60.
13. Coussens, L.M., B. Fingleton, and L.M. Matrisian, *Matrix metalloproteinase inhibitors and cancer: trials and tribulations.* Science, 2002. **295**(2387-2392).
14. JJ Yin, e.a., *TGF beta signaling blockade inhibits PTHrP secretion by breast cancer cells and bone metastases development.* J Clin Invest, 1999. **103**: p. 197-206.
15. A Gnoni, e.a., *Dasatinib: An anti-Tumour Agent via Src Inhibiton.* Curr Drug Targets, 2011. **ePub ahead of print**.
16. Powell, G.J., et al., *Localization of parathyroid hormone-related protein in breast cancer metastases: increased incidence in bone compared with other sites.* Cancer Res, 1991. **51**(11): p. 3059061.
17. Southby, J., et al., *Immunohistochemical localization of parathyroid hormone-related protein in human breast cancer.* Cancer Res, 1990. **50**(23): p. 7710-6.
18. Guise, T., et al., *Evidence for a causal role of parathyroid hormone-related protein in the pathogenesis of human breast cancer-mediated osteolysis.* J Clin Invest, 1996. **98**(7): p. 1544-1549.
19. WE Gallwitz, T.G.a.G.M., *Guanosine nucleotides inhibit different syndromes of PTHrP excess caused by human cancers in vivo.* J Clin Invest, 2002. **110**(10): p. 1559-1572.

20. Huang, S.J. and D.E. Ingber, *Cell tension, matrix mechanics, and cancer development.* Cancer Cell, 2005. **8**: p. 175-6.
21. Parekh A, R.N., et al., *Sensing and Modulation of Invadopodia Across a Wide Range of Rigidities.* Biophys J., 2011. **100**(3): p. 573-82.
22. Ruppender NS, M.A., Martin TJ, Mundy GR, Sterling JA and Guelcher SA, *Matrix Rigidity Induces Osteolytic Gene Expression of Metastatic Breast Cancer Cells.* PLoS One, 2010. **5**(11): p. e15451.
23. Wells, R.G. and D.E. Discher, *Matrix elasticity, cytoskeletal tension, and TGF-beta: the insoluble and soluble meet.* Science Signaling, 2008. **1**(10).
24. Butcher, D.T., T. Alliston, and V.M. Weaver, *A tense situation: forcing tumour progression.* Nat Rev Cancer, 2009. **9**(2): p. 108-22.
25. Enderling, H., et al., *Dependence of invadopodia function on collagen fiber spacing and crosslinking: computational modeling and experimental evidence.* Biophys J, 2008. **95**(5): p. 2203-2218.
26. Wang, F., et al., *Reciprocal interactions between β1-integrin and epidermal growht factor receptor in three-dimensional basement membrane breast cultures: a different perspective in epithelial biology.* Proc Natl Acad Sci USA, 1998. **95**: p. 14281-14286.
27. Yeung, T., et al., *Effects of Substrate Stiffness on Cell Morphology, Cytoskeletal Structure, and Adhesion.* Cell Motil. Cytoskeleton, 2005. **60**: p. 24-34.
28. Broecker, P.F.a.E., *The biology of cell locomotion within three-dimensional extracellular matrix.* Cellular and Molecular Life Sciences, 2000. **57**(1): p. 41-64.
29. Dhimolea, E., et al., *The role of collagen reorganization on mammary epithelial morphogenesis in a 3D culture model.* Biomaterials.
30. Wozniak, M.A., *ROCK-generate contractility regulates breast epithelial cell differentiation in response to the physical properties of a three-dimensional collagen matrix.* J Cell Biol, 2003. **163**(583-595).
31. P Panorchan, J.L., TP Kole, Y Tseng and D Wirtz, *Microrheology and ROCK signaling of Human Endothelial Cells Embedded in a 3D Matrix* Biophys J., 2006. **91**: p. 3499-3507.